Title
Imaging Genetics of Functional and Structural Connectivity in Children with Autism

Author
Rudie, Jeffrey David

Publication Date
2012

Peer reviewed|Thesis/dissertation

UNIVERSITY OF CALIFORNIA

Los Angeles

Imaging Genetics of Functional and Structural Connectivity in Children with Autism

A dissertation submitted in partial satisfaction of the

requirements for the degree Doctor of Philosophy

in Neuroscience

by

Jeffrey David Rudie

2012

ABSTRACT OF THE DISSERTATION

Imaging Genetics of Functional and Structural Connectivity in Children with Autism

By

Jeffrey David Rudie

Doctor of Philosophy in Neuroscience

University of California, Los Angeles, 2012

Professor Mirella Dapretto, Chair

Autism spectrum disorders (ASD) are heterogeneous yet highly heritable neurodevelopmental disorders characterized by atypical social behavior, delayed and/or abnormal verbal and nonverbal communication, as well as unusual repetitive behaviors and restricted interests. In vivo neuroimaging studies have consistently reported reductions in functional and structural connectivity of large-scale brain networks and recent genetic and neurobiological work suggests that ASD are related to altered synaptic and local-circuit connectivity. This dissertation seeks to provide insight into the neurobiological basis of ASD by using a network approach and by characterizing risk factors to ultimately aid in the development of more effective diagnostic tools and biologically-based treatments and interventions.

In chapter 1, we examine functional connectivity of brain systems involved in social and emotional processing in ASD during an emotion-processing task. We use the amygdala and right inferior frontal gyrus, pars opercularis, as seeds in whole-brain functional connectivity analyses. We show that ASD is related to reduced integration *within* and segregation *between* distinct functional systems, which indicates that brain networks may partially reflect immature patterns of connectivity

In chapter 2, we examine intrinsic functional connectivity with resting-state fMRI (rsfMRI) and structural connectivity with diffusion tensor imaging (DTI) using a complex network approach. Using graph theoretical methods, we show that pairwise differences in functional connectivity are reflected in network level reductions in modularity and local efficiency, yet higher global efficiency. Structural networks displayed lower levels of white matter integrity and atypical age-related changes in global efficiency. By combining functional and structural network properties we further show that there is an age-related imbalance between structure and function in ASD.

In chapter 3 we examine the neural correlates of an established autism risk polymorphism in Met receptor tyrosine kinase (*MET*). We show that this polymorphism is a potent modulator of key social brain circuitry in children and adolescents with and without ASD as *MET* risk genotype was associated with atypical fMRI activation and deactivation patterns to social stimuli (i.e., emotional faces), as well as reduced functional and structural connectivity in temporo-parietal regions known to have high MET expression, particularly within the DMN.

The dissertation of Jeffrey David Rudie is approved.

Daniel H. Geschwind

Susan Y. Bookheimer

Paul M. Thompson

Mirella Dapretto, Committee Chair

University of California, Los Angeles

2012

TABLE OF CONTENTS

LIST OF FIGURES

Chapter 1

Chapter 2

Chapter 3

LIST OF TABLES

Chapter 1

Chapter 2

Chapter 3

ACKNOWLEDGMENTS

This work would not have been possible without the love and support of my family and friends, in particular my parents Dave and Kathy Rudie, my sister Coral, and my girlfriend Vanessa Franca. My mentor Mirella Dapretto provided me with crucial guidance throughout my time as a graduate student, including teaching me how to conduct research, give a clear presentation, write a manuscript and ultimately succeed in academia. Additionally, I am grateful for the mentorship I received from Pat Levitt and my committee members Dan Geschwind, Susan Bookheimer and Paul Thompson. I wish to thank all of the children and families who graciously participated in the studies as well as my cousin Andrew for inspiring me to study autism.

I also wish to thank current and previous Dapretto Lab members including Jennifer Pfiefer, Kristin McNeally, Larissa Borofsky, Susan Lee, Mari Davies, Ashley Scott, Natalie Colich, Leanna Hernandez, Devora Beck-Pancer, Alia Martin, and Zarrar Shehzad for help with experimental design and data collection, Steve Petersen, Bradley Schlaggar and Jonathan Power for initial guidance on graph theory methods, as well as Jesse Brown, Zarrar Shehzad, and John Colby for technical guidance and Salvatore Torrisi, Brett Abrahams and Elizabeth Losin for reading and commenting of text included in this dissertation.

The research presented in this dissertation was funded by various sources including grants from the National Institute of Child Health and Human Development (PO1 HD055784), the National Institute of Mental Health (1R01 HD065280-01) and Autism Speaks. Graduate student support was provided through training grants from UCLA's Medical Scientist Training Program (T32 GM008044) as well as UCLA's Training Program in Neurobehavioral Genetics (T32 MH073526-05). This project was also, in part, supported by grants (NIMH 1R01 MH080759, RR12169, RR13642, and RR00865) from the National Center for Research Resources, a component of the National Institutes of Health (NIH). For generous support, we

also wish to thank the Brain Mapping Medical Research Organization, Brain Mapping Support Foundation, Pierson-Lovelace Foundation, Ahmanson Foundation, William M. and Linda R. Dietel Philanthropic Fund at the Northern Piedmont Community Foundation, Tamkin Foundation, Jennifer Jones-Simon Foundation, Capital Group Companies Charitable Foundation, Robson Family, and North-star Fund.

Chapter 1 is a version of an article published in the journal *Cerebral Cortex, 22*, 1025-037, **Rudie J.D.,** Shehzad Z., Hernandez L.M., Colich N., Iacoboni M., Bookheimer S.Y., Dapretto M., (2012*). Reduced Functional Integration and Segregation of Distributed Neural Systems Underlying Social and Emotional Information Processing in Autism Spectrum Disorders*, with permission from Oxford publishers and all authors.

Chapter 2 is a version of an article currently under review at *Journal of Neuroscience*: **Rudie J.D**., Brown J.A., Beck-Pancer D., Hernandez L.M., Dennis E.L., Thompson P.M., Bookheimer S.Y., Dapretto M., *Altered Functional and Structural Brain Network Organization in Autism*.

Chapter 3 is a version of an article currently in revision at *Neuron*: **Rudie J.D.,** Hernandez L.M., Brown J.A., Beck-Pancer D., Colich N., Gorrindo P., Geschwind D.H., Bookheimer S.Y., Levitt P., Dapretto M. *Autism Risk Variant in MET Impacts Functional and Structural Brain Networks*.

VITA

August 2003	Millstone Family Scholarship, Washington Univeristy
May 2006	Graduated Washington University, B.A, Major in Biology and Psychology, Summa Cum Laude
July 2007	Entered Medical Scientist Training Program at David Geffen School of Medicine, Los Angeles, California
June 2009	FSL and Freesurfer Neuroimaging Course, San Francisco, California
June 2009	Cold Springs Harbor Workshop On Autism Spectrum Disorders, Cold Springs Harbor, New York
July 2009	UCLA Neuroimaging Training Program Advanced Summer School, Los Angeles, California
March 2010	SPM Functional Connectivity Workshop, Boston, Massachusetts
June 2010	Neurobehavioral Genetics Training Grant Recipient
December 2010	Advancement to Candidacy
November 2011	BRI/Semel Neuroscience Graduate Student Travel Award
May 2012	IMFAR 2012 Student Travel Award

PUBLICATIONS

Scott-Van Zeeland, A.A., Abrahams, B.S., Alvarez-Retuerto, A.I, Sonnenblick, L.I., **Rudie, J.D**., Ghahremani D., Mumford, J., Poldrack, R.A., Dapretto, M., Geschwind, D.H., Bookheimer, S.Y. (2010). Altered Functional Connectivity Associated with Variation in CNTNAP2. *Science Translational Medicine*: *2, 56ra80*

Masten, C.L., Colich, N.L., **Rudie, J.D.**, Bookheimer, S., Eisenberger, N.I., & Dapretto, M. (2011). An fMRI investigation of responses to peer rejection in adolescents with autism spectrum disorders. *Developmental Cognitive Neuroscience*. Volume 1(3), 250-270.

Rudie J.D., Shehzad Z., Hernandez L., Colich, N., Iacoboni M., Bookheimer, S.Y., Dapretto M., (2012). Reduced Functional Integration and Segregation of Distributed Neural Systems Underlying Social and Emotional Information Processing in Autism Spectrum Disorders. *Cerebral Cortex*: *22*, 1025-037.

Colich, N.L., Wang, A.T., **Rudie, J.D.,** Hernandez, L.H., & Dapretto, M. (2012). Atypical Neural Processing of Ironic and Sincere Remarks in Children and Adolescents with Autism Spectrum Disorders. *Metaphor and Symbol,* 27:70-92.

Roussotte, F.F., **Rudie J.D**., Smith L., O'Connor M.J., Bookheimer S.Y., Narr K.L., Sowell E.R. (2012) Fronto-striatal connectivity in children during working memory and the effects of prenatal methamphetamine and polydrug exposure. *Developmental Neuroscience*, in press.

Dennis, E.L., Jahanshad, N., **Rudie, J.D**., Brown, J.A., Johnson, K., McMahon, K.L., de Zubicaray, G.I., Montgomery, G., Martin, N.G., Wright, M.J., Bookheimer, S.Y., Dapretto, M., Toga, A.W. & Thompson, P.M. (2012). Altered structural brain connectivity in healthy carriers of the autism risk gene, *CNTNAP2*. *Brain Connectivity*, in press.

Vizueta, N., **Rudie, J.D**., Townsend, J.D., Torrisi, S., Moody, T.D., Bookheimer, S.Y., Altshuler, L.L. (2012). Regional fMRI Hypoactivation and Altered Functional Connectivity During Emotion Processing in Unmedicated Bipolar II Depressed Subjects. *American Journal of Psychiatry*, in press.

Rudie J.D., Hernandez L.M., Brown J.A., Beck-Pancer D., Colich, N., Gorrindo P., Geschwind D.H., Bookheimer, S.Y., Levitt P., Dapretto M., (In Revision at *Neuron*). Autism Risk Variant in MET Impacts Functional and Structural Brain Networks.

Rudie J.D., J.A. Brown. D. Beck-Pancer, Hernandez L.M., Dennis E.L., Thompson P.M., Bookheimer, Dapretto M., (Under Review at *Journal of Neuroscience*). Altered Functional and Structural Brain Network Organization in Autism.

ABSTRACTS

Rudie, J. D., Martin A., Borofsky L. A., Scott A. A., Bookheimer S. Y., Iacoboni M. and Dapretto M. (2009) Neural Activity in Mirror Neuron and Reward Circuitry While Viewing Emotional Expressions Relates to Core Deficits in Autism. Poster Presented at the International Meeting for Autism Research, Chicago, IL.

Rudie, J. D., Shehzad, Z., Colich, N., Bookheimer S. Y., Iacoboni M. and Dapretto M. (2010) Disrupted Long-Range Connectivity in the Mirror Neuron System in Children with Autism Spectrum Disorders. Poster presented at the International Meeting for Autism Research, Philadelphia, PA.

Rudie, J. D., Shehzad, Z., Pfeifer, J., Colich, N., Iacoboni M., Bookheimer S. Y., and Dapretto M. (2010) Reduced Functional Connectivity Between Fusiform Face Area and Amygdala in Adolescents with Autism. Poster presented at the International Meeting of the Organization for Human Brain Mapping, Barcelona, Spain.

Rudie, J. D., Hernandez, L., Shehzad, Z., Colich, N., Bookheimer S. Y., and Dapretto M. (2010) Reduced coherence of intrinsic connectivity networks in children with autism spectrum disorders. Abstract accepted for **oral presentation** at the Society for Neuroscience Meeting, San Diego, CA.

Rudie, J. D., L. M. Hernandez, D. Shirinyan, N. L. Colich, P. Gorrindo, D. H. Geschwind, P. Levitt, S. Y. Bookheimer and M. Dapretto (2011). ASD Risk Polymorphism in MET is Associated with an Aberrant Pattern of Functional Activity Across Regions of High MET Expression. Abstract accepted for **oral presentation** at the International Meeting for Autism Research, San Diego, CA.

Rudie, J. D., Brown J.A, Hernandez L.M., Bookheimer, S.Y., Dapretto, M (2011). Whole Brain Structural and Functional Connectivity Networks in Autism. Abstract accepted for a poster presentation at the International Meeting of the Organization for Human Brain Mapping, Quebec City, Canada.

Rudie, J. D., Hernandez L.M., Brown J.A., Geschwind D.H., Levitt P., Bookheimer, S.Y., Dapretto, M. (2011) A common variant in the autism risk gene *MET* moderates aberrant structural and functional connectivity in children with and without ASD. Abstract accepted for **oral presentation** for the Society for Neuroscience Meeting in Washington DC.

Rudie J. D., Colby J. B., Shehzad Z., Douglas P. M., Brown J. A., Beck-Pancer D., Hernandez L. M., Geschwind D. H., Thompson P. M., Cohen M. S., Bookheimer S. Y., and Dapretto M. (2012). Autism Classification Using Local, Global, and Connectome-Wide Measures of Functional Connectivity. Abstract accepted for **oral presentation** at the International Meeting for Autism Research, Toronto, Canada.

INTRODUCTION

Autism is a pervasive neurodevelopmental disorder that affects one in 88 individuals (CDC report, 2012). A variety of overlapping heritable disorders, including autism, Asperger's syndrome and PDD-NOS, fall under the umbrella classification of autism spectrum disorder (ASD). Kanner (1943) originally described three core features that are still used in current autism diagnosis: impaired reciprocal social interactions, abnormal language acquisition and usage, as well as restricted interests and repetitive behaviors. Beyond these core features, there is significant clinical heterogeneity, particularly with variable onset and progression of symptoms, comorbidity with other neurologic and psychiatric disorders, and response to interventions (Dawson et al., 2002). Despite these deficits, evidence suggests that individuals with ASD have preserved or enhanced processing in certain domains such as sensory perception (Jones et al., 2009; Ashwin et al., 2009), increased attention to details (Smith et al., 2009), and an enhanced ability to analyze rule-based systems for predicting the behavior of inanimate objects (Baron-Cohen et al., 2002; 2009). In contrast, individuals with ASD show impairments in executive processes and in synthesizing complex sensory input to arrive at a "big picture" understanding of their environment, likely contributing to the classical deficits in social communication and reciprocal social interactions. While dysfunctional reciprocal interactions are the core behavioral manifestations of ASD, clinical heterogeneity as well as enhanced cognitive functioning in particular domains should be accounted for in any complete etiologic and neurodevelopmental account of ASDs.

A comprehensive model, explaining all core deficits of ASD and accounting for the broader autism phenotype, is not fully developed. Yet, an emerging hypothesis, based on multi-dimensional research spanning genes to behavior, posits that deficits in reciprocal social behavior may result from dysfunctional long-range connections between brain regions that are highly evolved in humans (Just et al., 2004; Courchesne & Pierce, 2005; Geschwind & Levitt,

2007; Mundy et al., 2009). From a developmental perspective, this model suggests that disruption in the initial architecture and connectivity of local circuits constrains the experience-dependent changes that normally allow for the reorganization of connections, to create stable long-range connections during development. This “developmental disconnection” model also provides an explanation for the preservation or enhancement of certain cognitive functions, such as enhanced visual and auditory discrimination. This enhanced function could be the result of increased local network connectivity stemming from both faulty initial circuitry and inefficient long-range connectivity. For example, disconnection of dorsolateral prefrontal and anterior cingulate cortex from sensory association areas – necessary for joint attention early in infancy – may lead to a cascade of events preventing the development of language and typical social behavior (Mundy et al., 2009). The failure to establish normative connections between these regions may simultaneously allow for increased connectivity within sensory association cortices, leading to enhanced sensory discrimination and increased attention to detail. While this model serves as an initial framework for understanding autistic symptomatology it is clear that much more work needs to be done to bridge the gaps between different levels of autism research.

Task Based fMRI and Functional Connectivity Studies

Functional MRI (fMRI) studies of high-functioning individuals with ASD have consistently reported hypoactivation in brain regions involved in a variety of tasks that tap into social cognition (see Pelphrey and Carter, 2008, for review). Abnormal activity has been reported in specialized regions such as the amygdala (e.g. Dalton et al., 2005), fusiform gyrus (e.g., Schultz et al., 2005), inferior frontal gyrus (e.g., Dapretto et al., 2006) and medial prefrontal cortex (e.g., Castelli et al., 2002). Individuals with autism also fail to show normal deactivation patterns in networks such as the default mode network (DMN; Kennedy et al., 2006; Di Martino et al., 2009), which is implicated in social cognitive and theory of mind processes (Raichle et al., 2001;

Andrews-Hanna et al., 2010). This array of findings in different brain regions highlights the need for characterization of ASD as a disorder involving the interactions of multiple brain systems, as ASD is not likely to be understood in terms of disruption in a single brain region or system.

Multiple neuroimaging studies of autism have examined functional connectivity (i.e., correlated activity) between different brain regions in ASD, finding functional underconnectivity between brain regions during the performance of a variety of different cognitive tasks, including language processing (Just et al., 2004), emotion processing (Kleinhans et al., 2008), working memory (Koshino et al., 2007; Kana et al., 2007), motor function (Mostofsky et al., 2009), or visuospatial processing (Villalobos et al., 2005). Just et al. (2004) suggested that widespread underconnectivity could be related to all higher-level cognitive deficits observed in autism. However, other studies have characterized ASD as a disorder of "altered" or "abberant" connectivity, given findings of overconnectivity within thalamo-cortical (Mizuno et al., 2006) and striato-cortical circuits (Turner et al., 2006; Di Martino et al., 2011) suggesting a more complex pattern. These findings support network dysfunction, yet highlight the need to examine connectivity within and between different systems.

Intrinsic Functional Connectivity

Functional brain imaging studies have demonstrated that, even in the absence of an overt cognitive task, there exist synchronized low frequency spontaneous fluctuations in neuronal activity across different brain networks (Biswal et al., 1995; see Fox and Raichle, 2007, for review). These networks undergo increasing integration (i.e. increasing long-range within network connectivity) and segregation (i.e. reduced connectivity between networks) across typical development (TD; Fair et al., 2007a, 2008, 2009; Kelly et al., 2009; Supekar et al., 2009; Stevens et al., 2009; Dosenbach et al., 2010). Recent studies characterizing intrinsic

fluctuations in ASD have consistently found that task-independent (i.e., intrinsic) functional connectivity, including interhemispheric (Anderson et al., 2010; Dinstein et al., 2011) and DMN connectivity is reduced in ASD (Cherkassky et al., 2006; Kennedy, 2008; Weng et al., 2010; Assaf et al., 2010). Thus evidence suggests that intrinsic connectivity networks in autism show an altered pattern of connectivity that may reflect an "immature" development of these networks.

Structural Connectivity

Diffusion tensor imaging (DTI) measures the axonal architecture of the brain indirectly by measuring the diffusion of water. DTI can be used to quantify white matter integrity by characterizing the shape and direction of diffusion in the brain. Several studies have used DTI to examine white matter microstructure in individuals with ASD. Barnea-Gorealy et al. (2004) first reported reduced white matter integrity as measured by decreased fractional anisotropy (FA) in frontal and temporal regions, while additional studies have subsequently reported reduced FA in individuals with ASD in the corpus callosum (Alexander et al., 2007; Keller et al., 2007; Shukla et al., 2010), internal capsule (Keller et al., 2007; Cheng et al., 2010; Shukla et al., 2010), frontal (Sundaram et al., 2008) and temporal regions (Lee et al., 2007). Increasing FA has been consistently observed across typical development (e.g., Lebel et al., 2008), again suggesting that the aberrant pattern of connectivity observed in individuals with ASD may reflect less 'mature' (or delayed) development.

Complex Network Science

Recent developments in the quantitative analysis of complex networks have been applied to brain network organization (see Bullmore and Sporns, 2009, for review). Graph theory, which describes complex systems as a set of "nodes" (i.e., brain regions) and "edges"

(i.e., connections between brain regions) has characterized the brain as a complex hierarchical modular network exhibiting robust levels of local and global efficiency (i.e., small-world properties; Watts and Strogatz, 1998) that can be quantitatively characterized using graph theoretical methods (Rubinov et al., 2009). Despite the array of regional and systems level findings in ASD, it is unclear how these alterations influence the entire brain when conceived of as a network of several hundred interacting regions composing multiple integrated and segregated systems since no studies have used graph theory to examine functional or structural brain networks in ASD.

Combining Structure and Function

Recent work in neurotypical adults has begun to directly relate structural and functional connectivity between brain regions. Defining structural connectivity through fiber tracts between brain regions and functional connectivity as timeseries correlations between brain regions, Hagmann et al. (2008) found a strong correspondence between structural connectivity and rs-fcMRI in the same participants. While functional connectivity is more variable and can be detected for brain regions that are not structurally connected, it appears as though functional connectivity is somewhat constrained by anatomical structure. Recent studies found that during typical development, measures of functional connectivity and structural connectivity become more correlated within the default mode network (Supekar et al., 2010) and across the entire brain (Hagmann et al., 2010). No studies to date have used DTI and rs-fMRI to compare connectivity across both modalities in ASD, or to compare structural and functional network properties.

Genetics of ASD

Several lines of evidence suggest that ASDs are among the most heritable of all neuropsychiatric disorders. Twin studies show 50 to 90 percent concordance in monozygotic twins and 1 to 30 percent in dizygotic twins (Bailey et al., 1995; Le Couteur et al., 1996; Hallmayer et al., 2011). Sibling recurrence risk is at least 25 times the population risk (Fombonne et al., 2003). There is a consistent segregation of quantitative sub-threshold traits (i.e., the broader autism phenotype) in family members similar to that found in probands (Bishop et al., 2004). This occurrence in family members of probands and within the general population has been termed the broader autism phenotype. Despite this clear heritability, finding the genes involved has been a relatively arduous process, hampered by clinical heterogeneity, complex genetics, and gene-environment interactions. The current understanding of autism genetics points to a combination of multiple rare duplications, deletions, mutations, common variants and environmental factors accounting for ASD symptomatology and heterogeneity. Defined mutations, genetic syndromes, and *de novo* copy-number variations (CNVs) are believed to have large effects and to account for 10 to 20 percent of ASD cases (Abrahams & Geschwind, 2008). Common inherited functional variants in a variety of genes are believed to have smaller additive effects (Levitt & Campbell, 2009). Pathway analyses suggest that proteins involved in neuronal migration, cellular adhesion, synaptogenesis and intracellular signaling are implicated in autism risk. The neural pathways forged by these candidate genes indicate that dysfunction in neural connectivity and activity-dependent synaptic plasticity underlies the etiology of ASDs.

Imaging Genetics

Imaging genetics research, which links genetic variation to functional and structural characteristics of the brain (i.e., endophenotypes), has begun to shed insight on neurobiological

disorders such as Alzheimer's disease and schizophrenia (Hariri & Weinberger, 2003; Roffman et al., 2006; Stein et al., 2010). An endophenotype is a feature that is associated with illness in a population, is heritable, is primarily state-independent, and co-segregates with illness in families (Gottesman et al., 2003). Low frequency spontaneous fluctuations measured from resting state functional connectivity MRI (rs-fcMRI) in the DMN and measures of fractional anisotropy were found to be heritable (Glahn et al., 2010; Chiang et al., 2010; Kochunov et al., 2010), suggesting these are good endophenotypes.

An array of neuroimaging studies linking genetic variants with regional activity and functional integration in genes such as ApoE (Bookheimer et al., 2000; Brown et al., 2011), 5HTTLPR (Hariri et al., 2002; Pezawas et al., 2005), and COMT (Egan et al., 2001; Buckholtz et al., 2007) have given insight into the biological basis of these neuropsychiatric disorders. These candidate risk genes, as well as newly discovered candidate ASD risk genes, have relatively well-known neurobiological mechanisms of action and gene expression patterns. Therefore, specific predictions about candidate risk genes' role in neural pathways can be made prior to *in vivo* imaging studies. Given the vast clinical heterogeneity, and only recent identification of common variants linked to ASD, it is not surprising that few imaging studies to date have focused on ASD risk genes (Raznahan et al., 2009; Meyer-Lindenberg et al., 2008; Scott-Van Zeeland et al., 2010). For heritable neuropsychiatric disorders, ASD in particular, an approach that relates common risk variants to structural and functional connectivity is ideal, not only because it gives us insights into the neurobiological basis of the disorder, but also because it can lead to the establishment of intermediate phenotypes, potentially aiding in new gene discovery and valid sub-groups for targeted and biologically-based treatments.

MET Receptor Tyrosine Kinase (*MET*) as an ASD Candidate Gene

One of the most well characterized molecular signaling pathways implicated in autism is the ERK/PI3K signaling pathway. This pathway signals through the Met Receptor Tyrosine Kinase (*MET*) and has pleiotropic roles in multiple organ systems including the gastrointestinal, immune and central nervous systems (Levitt and Campbell, 2009). In the brain, *MET* regulates multiple downstream signaling pathways that are crucial for neuronal processes such as axonal guidance, neuronal migration and activity-dependent synapse formation (Bill and Geschwind, 2009). In addition to *MET*, this signaling pathway includes multiple autism candidate genes such as *PTEN* and the genes responsible for Neurofibromatosis and Tuberous Sclerosis, which are syndromic disorders that have high rates of ASD diagnoses.

In the primate, MET is enriched in excitatory neurons and their axons projecting from subcortical limbic forebrain structures, including the amygdala (Judson et al., 2009), as well as from temporal and parieto-occipital cortices to target regions during synaptogenesis and axon outgrowth (Judson et al., 2010; Eagleson et al., 2011). MET displays a strong differential expression pattern between tempero-parieto-occipital and frontal cortex (Judson et al., 2010). Interestingly, *MET* transcript and protein expression in temporal cortex is reduced in individuals with ASD (Campbell et al., 2007) and MET's fronto-temporal differential expression pattern is diminished in individuals with ASD (Voineagu et al., 2011). In order to characterize MET's role in local neuronal circuits, Met was conditionally knocked out in a mouse model of ASD (Judson et al., 2009, 2010; Qiu et al., 2011). In these cKO mice, neuronal morphology and activity in layer 2/3 pyramidal cortical neurons is altered. Basal dendritic spine volume is increased (Judson et al., 2009) and local connectivity in specific subcortico-cortical circuits is upregulated two fold in both cKO and heterozygote mice relative to wild type (Qiu et al., 2011).

Common and rare variants in *MET* have been associated with ASD in multiple independent cohorts (Campbell et al., 2006, 2008; Jackson et al., 2009; Sousa et al., 2009;

Marshall et al., 2008; Thanseem et al., 2010; Pinto et al., 2010). A common variant (rs1858830) in the promoter region of MET associated with autism risk (Campbell et al., 2006, 2008; Jackson et al., 2009) was shown to reduce MET mRNA in vitro (Campbell et al., 2006). Similar to individuals with ASD, healthy control subjects who carry this risk allele have lower levels of the MET protein in their temporal cortices (Campbell et al., 2007). Furthermore, this promoter variant has been shown to moderate autism phenotypes, whereby individuals with ASD who carry this risk allele have more severe social and communication phenotypes than those who do not (Campbell et al., 2009). These convergent genetic, clinical, and developmental neurobiology findings make the *MET* promoter variant a well-poised candidate for investigation by *in vivo* human brain imaging studies.

CHAPTER 1: Altered Integration and Segregation of Distributed Neural Systems Underlying Social and Emotional Information Processing

Abstract

A growing body of evidence suggests that autism spectrum disorders (ASDs) are related to altered communication between brain regions. Here we present findings showing that ASD is characterized by a pattern of reduced functional integration as well as reduced segregation of large-scale brain networks. Twenty-three children with ASD and 25 typically-developing matched controls underwent fMRI while passively viewing emotional facial expressions. We examined whole-brain functional connectivity of two brain structures previously implicated in emotional face processing in autism: the amygdala bilaterally and the right pars opercularis of the inferior frontal gyrus (rIFGpo). In the ASD group, we observed reduced functional integration (i.e., less long-range connectivity) between amygdala and secondary visual areas, as well as reduced segregation between amygdala and dorsolateral prefrontal cortex. For the rIFGpo seed, we observed reduced functional integration with parietal cortex and increased integration with right frontal cortex as well as right nucleas accumbens. Finally, we observed reduced segregation between rIFGpo and the ventromedial prefrontal cortex. We propose that a systems-level approach – whereby the integration and segregation of large-scale brain networks in ASD is examined in relation to typical development – may provide a more detailed characterization of the neural basis of ASD.

Introduction

Autism spectrum disorders (ASDs) are pervasive neurodevelopmental disorders characterized by atypical social behavior, delayed and/or abnormal verbal and nonverbal communication, as well as unusual patterns of repetitive behaviors and restricted interests. While the neurobiological basis for ASD remains largely unknown, it has been hypothesized that disruption of the initial architecture and connectivity of local circuits in individuals with ASD may alter the experience-dependent maturation of large-scale brain networks required for integrative processing (Belmonte et al. 2004; Just et al. 2004; Courchesne and Pierce 2005; Geschwind and Levitt 2007; Mundy et al. 2009). Thus, developmental abnormalities in ASD may prevent the typical reorganization of neuronal connections into functionally integrated networks that are crucial for facilitating complex social behavior.

Functional neuroimaging studies have generally focused on differences in regional brain activation among individuals with ASD while processing social and emotional stimuli. More specifically, abnormal activity has been reported in specialized regions or networks such as the amygdala (emotion processing; e.g., Baron-Cohen et al. 1999; Dalton et al. 2005), fusiform gyrus (face processing; e.g., Schultz et al. 2005. Pierce et al. 2004), superior temporal sulcus (biological motion; e.g., Pelphrey and Carter 2008), inferior frontal gyrus (mirror neuron system; e.g., Dapretto et al. 2006; Oberman and Ramachandran 2007), medial prefrontal cortex (theory of mind; e.g., Castelli et al. 2002; Wang et al. 2007), and precuneus (default mode network; e.g., Kennedy and Courchesne 2008b). A recent meta-analysis of functional activation studies in ASD identified areas consistently hypoactivated during social and emotional information processing which included amygdala, inferior frontal gyrus, and higher order association areas such as medial prefrontal cortex (Di Martino et al. 2009). Additionally, the meta-analysis found that individuals with ASD tended to hyperactivate primary sensory areas such as postcentral

gyrus, superior temporal gyrus and inferior occipital gyrus. Hyperactivation of primary sensory areas and hypoactivation of association areas may reflect a bottleneck of information flow that prevents appropriate integration of incoming sensory information important for social behavior. While regional characterizations of brain dysfunction in ASD have informed our initial understanding of the neurobiological underpinnings of this disorder, a systems-level approach that characterizes communication within and between different brain networks should provide further insight.

In recent years, neuroimaging studies of autism have begun to focus on functional connectivity between different brain networks. In an early baseline glucose metabolism study using Positron Emission Tomography (PET), Horwitz et al. (1988) first reported reduced correlations among frontal and parietal cortices in individuals with autism. Later, in a theory of mind PET study involving mental attributions of animated shapes, Castelli et al. (2002) found reduced connectivity between extrastriate visual cortex and the superior temporal sulcus in adults with ASD. They suggested that dysfunction in the interaction between higher and lower order perceptual processes may be related to the behavioral manifestations of autism. In a later fMRI study, Just et al. (2004) found reductions in connectivity strengths between higher-level association areas engaged during a sentence comprehension task in high-functioning individuals with ASD. Although their analyses found reduced connectivity in relatively few of the many pairwise connections examined, the authors proposed that the underdevelopment of integrative circuitry as indexed by widespread anterior-posterior underconnectivity could be responsible for all higher-level cognitive deficits in autism. Further studies in individuals with ASD have supported this claim, reporting evidence of underconnectivity between task activated regions, particularly for fronto-parietal connections, during tasks involving working memory (Koshino et al. 2005), visuomotor coordination (Villalobos et al. 2005), visual imagery (Kana et

al. 2006), executive functioning (Just et al. 2007), response inhibition (Kana et al. 2007), face processing (Kleinhans et al. 2008), and theory of mind (Kana et al. 2009).

Recent imaging studies performed in the absence of an overt cognitive task (i.e., during "resting-state") have established that synchronized, low frequency (<0.1 Hz) spontaneous fluctuations in neuronal activity are present across different brain regions (Biswal et al. 1995; see Fox and Raichle 2007, for review). These findings suggest that the brain is intrinsically organized into several large-scale interactive functional networks during both rest and task conditions (Calhoun et al. 2008, Smith et al. 2009). A growing number of resting-state studies examining the default mode network (DMN; Raichle et al. 2001) have reported reduced connectivity in this network in individuals with ASD (Cherkassky et al. 2006; Kennedy and Courchesne 2008; Monk et al. 2009; Weng et al. 2010; Assaf et al. 2010). Dysfunction of the DMN in ASD is consistent with the social deficits observed in ASD and the DMN's known role in social cognition (e.g. Iacoboni et al. 2004, Andrews-Hanna et al. 2010). However, the DMN does not function independently of other systems and is unlikely to be the only affected system in autism given the array of both social and cognitive impairments as well as non-DMN brain regions implicated in the disorder.

Although there have been consistent reports of reduced fronto-parietal connectivity in ASD during both rest and task (e.g. Just et al. 2007; Kennedy and Courshesne 2008), other studies have found evidence of overconnectivity within thalamo-cortical (Mizuno et al. 2006) and striato-cortical circuits (Turner et al. 2006; Di Martino et al. 2010), as well as greater cortico-cortical connectivity (Noonan et al. 2009; Shih et al. 2010). Thus, in contrast with a general underconnectivity theory, it has been argued that underconnectivity is likely not a general feature of the autistic brain; rather, it may depend on the specific regions and networks being examined as well as the networks engaged by the task being performed.

In parallel with reports of altered functional connectivity in autism, investigators have begun to map the typical development of functional brain networks (see Uddin et al. 2010, for review). Using a variety of methodological approaches, several groups have reported that during development, functional brain networks show increases in long-range functional connectivity among nodes of a given network (i.e. functional integration) as well as reduced local (i.e. intralobar) positive connectivity among nodes in different networks (i.e. functional segregation; Fair et al. 2007a, 2008, 2009; Kelly et al. 2009; Supekar et al. 2009; Stevens et al. 2009; Dosenbach et al. 2010). Studies in neurotypical individuals have also highlighted the role of functional segregation as measured through anticorrelations between distinct brain networks (Fox et al. 2005, 2009; Fransson et al. 2005; Kelly et al. 2008; Stevens et al. 2009). Most prominently, the internally-directed default mode or "task negative" network has been shown to display an anticorrelated relationship with the externally-directed "task positive" or attentional control network. Increased anticorrelations (i.e., reduced connectivity), interpreted as increasing segregation, between these networks have been observed across typical development (Stevens et al. 2009) and in adults who displayed superior behavioral performance (Kelly et al. 2008; Hampson et al. 2010). Despite recent controversy regarding the proper interpretation of anticorrelations (Murphy et al 2009, Fox et al. 2009; see a discussion of this issue in **Supplemental Materials**) it has been suggested that investigating functional segregation, as measured by antagonistic relationships between large-scale networks, such as the default mode and task positive networks, may provide a better understanding of the neural basis of social communication deficits in ASD than functional integration alone (Uddin and Menon 2009). However, this hypothesis has largely been unexplored (Kennedy and Courchesne, 2008).

Although resting state studies have become the standard way to probe functional connectivity, examining connectivity of networks engaged during cognitive tasks should provide information about network functioning that is complementary to resting state and task activation

studies (Stevens 2009). In the present study, we sought to examine functional integration and segregation of large-scale brain networks involved in social and emotional information processing in children and adolescents with ASD by performing whole brain connectivity analyses of fMRI data acquired during an emotion processing task using seed regions that have previously been reported to display aberrant activation during socially relevant tasks.

It is well established that the amygdala plays a central role in emotion processing (LeDoux 2000). Findings of dysfunctional emotional face processing (Baron-Cohen et al. 2000, Adolphs et al. 2001), as well as diminished amygdala functional activation (Baron-Cohen et al. 1999; Critchley et al. 2000) led to an early theory of amygdala dysfunction in autism (Baron-Cohen et al. 2000). Although initial studies documented amygdala hypoactivation, later functional studies have found amygdala hyperactivation (Dalton et al. 2005; Monk et al. 2010), which was related to eye fixation patterns (Dalton et al. 2005). Additional studies have documented structural abnormalities (Munson et al. 2006, Nacewicz et al. 2006; Schumann et al. 2009) as well as reduced functional connectivity between the amygdala and both the fusiform face area (Kleinhans et al. 2008) and the anterior insula (Ebisch et al. 2010). Thus, further characterization of amygdala connectivity may be useful for understanding emotion processing deficits in ASD.

In addition to the amygdala's role in emotion processing, it is known that higher order networks, including the mirror neuron system (MNS) and the salience network, are involved in social and emotional information processing. The salience or cingulo-opercular network (Seeley et al. 2007; Dosenbach et al. 2007) is a task positive network that includes the anterior cingulate and anterior insula, and has been described as being involved in regulating behavior through monitoring homeostatic and sensory stimuli (Craig 2009; Seeley et al. 2007). The MNS, which includes the inferior frontal gyrus, pars opercularis (IFGpo) and inferior parietal lobule (IPL), is believed to allow for simulation of shared motor representations between self and others (see

Rizzolati and Fabbri-Destro 2010, for review). Consistent with the hypothesized role of the salience network, the MNS has been hypothesized to connect higher-level association areas with the limbic system (including the amygdala) through the anterior insula (Jabbi et al. 2008), allowing for an intuitive understanding of one's own and others' emotions (Carr et al. 2003; Leslie et al. 2004). Measures of empathetic behavior and interpersonal competence have been found to positively correlate with activity in the IFGpo, anterior insula and amygdala (Pfeifer et al. 2008). Numerous studies have reported structural and functional abnormalities in these higher order networks in individuals with ASD (e.g., Villalobos et al. 2005; Dapretto et al. 2006; Hadjikani et al. 2006; Hadjikani et al. 2007; Ebisch et al. 2010).

Given the known roles of the amygdala and IFGpo in social and emotional information processing, as well as consistent reports of dysfunction of these regions and associated systems in ASD (Di Martino et al. 2009), we used these structures as seeds for whole-brain connectivity analyses in children and adolescents with ASD. We chose to examine connectivity during an emotional face processing task known to engage these networks in order to further tap into the functioning of this circuitry. We predicted that children and adolescents with ASD would show reduced long-range functional connectivity/integration of networks examined using these seed regions. We also predicted that there would be reduced segregation between distinct functional networks in individuals with ASD as measured by increased local connectivity as well as reduced anticorrelations.

Materials and Methods

Participants

High-functioning children and adolescents with autism spectrum disorders and typically developing (TD) children and adolescents were recruited through referrals from the UCLA Autism Evaluation Clinic and/or through flyers posted throughout the greater Los Angeles area.

Six subjects (20% of the total sample) with ASD and three TD subjects (10% of the total sample) were scanned but not included in analyses due to excessive head motion (>3mm maximum relative head motion and/or no activation in primary visual cortices). The final matched groups consisted of 23 high-functioning children and adolescents (two females) with ASD and 25 TD children and adolescents (three females). The groups did not differ significantly in age, head motion, Full Scale IQ, Verbal IQ, or Performance IQ as assessed by the Wechsler Abbreviated Scale of Intelligence - Revised (Wechsler et al. 1999) or Wechsler Intelligence Scale for Children - Third Edition (see **Table 1.1** for sample characteristics). Although the groups did not significantly differ by age or IQ, these variables were included as covariates in additional between-group analyses to examine how they may have affected our results; these analyses showed that covarying for age or IQ did not alter any of the observed between-group differences, thus these results are not reported. For the ASD group, prior clinical diagnosis of autism or autism spectrum disorder was confirmed by the *Autism Diagnostic Observation Scale* (ADOS-G) and/or *Autism Diagnosis Interview* (ADI-R; Lord et al. 2000; Lord et al. 1994). Nineteen of the children with ASD met criteria for autism as defined by the ADI-R and all children in the ASD group met criteria for autism or autism spectrum disorder as defined by the ADOS. Seventeen participants with ASD and all TD participants reported no current medication use. For the remaining six participants with ASD, medication use was unknown. All participants reported no history of neurologic disorders (including head injury, stroke, tumor, seizures), psychiatric disorders (e.g. schizophrenia, attention-deficit/hyperactivity disorder) or other brain abnormalities. Subjects and parents provided written consent according to the guidelines specified by the Institutional Review Board at the University of California, Los Angeles.

Experimental Design

Participants underwent a rapid event-related fMRI paradigm in which faces with different emotional expressions were displayed. Subjects were asked to “just look at the expression on

each face." The experimental design was the same as the observation run used in our previous studies in children with ASD (Dapretto et al. 2006) and typically developing children (Pfeifer et al. 2008; Pfeifer et al. 2011). Ten of the children with ASD and five of the TD children from Dapretto et al. (2006) overlapped with subjects used in this study. Subjects were presented with 80-full color faces from the NimStim facial expressions stimulus set (Tottenham et al. 2009). The scan consisted of 96 events whereby each emotion (neutral, happy, sad, fearful and angry) as well fixation crosses (null events) were displayed for 2s with an average inter-trial interval of 3s. The fixation crosses were displayed at eye level in order to direct attention to the eyes as this has previously been shown to increase fixation to the eyes and normalize activity in both amygdala and fusiform gyrus (e.g., Hadjikhani et al. 2004). The order of presentation of all events was optimized and jittered (jitter ranging from 500ms to 1500ms in 125ms increments) to maximize contrast detection efficiency (Wager and Nichols 2003).

The patterns of regional activity observed in both TD and ASD children (**Figure 1.2**) closely resembled those previously obtained in prior studies using the same activation paradigm (Dapretto et al. 2006; Pfeifer et al. 2008; Pfeifer et al. 2011), including robust activity in visual cortices, amygdala, IFG, and hippocampus.

Data Acquisition

The MRI data were acquired on a Siemens 3.0 T Allegra MRI scanner. Stimuli were presented through a computer connected to a high-resolution magnet-compatible audio and goggle system (Resonance Technology, Inc). A 2D spin-echo scout localizing scan (TR=4000ms, TE=40ms, matrix size 256 by 256, 4mm thick, 1mm gap) was acquired and used for graphic prescription. A matched bandwidth T2-weighted high-resolution echo planar scan (TR=5000ms, TE=33ms, matrix size 128 by 128, FoV=20cm, 36 slices, yielding an in plane voxel dimension of 1.5x1.5mm, with 4mm thick slices) was acquired co-planar to the functional scan in order to ensure identical distortion characteristics to the fMRI scan. The functional

BOLD MRI scan lasted 4min 54s (TR=3000ms, TE=28ms, matrix size 128 by 128, FoV=20cm, 36 slices yielding an in plane voxel dimension of 3x3mm with 4mm thick axial slices).

Functional Connectivity MRI Data Analysis

Data were analyzed using FSL version 4.1.4 (FMRIB's Software Library, www.fmrib.ox.ac.uk/fsl; Smith et al. 2004) and AFNI (Analysis of Functional NeuroImages; Cox 1996). Structural and functional images were skull-stripped using AFNI (3dskullstrip and 3dautomask, respectively). Functional volumes were motion-corrected to the average functional volume with MCFLIRT using a normalized correlation ratio cost function and sinc interpolation (Jenkinson et al. 2002). Translations and rotations in the x, y, and z dimensions were calculated from volume to volume then collapsed into mean absolute (compared to the average functional volume) and relative (compared to the previous volume) displacements. Images were spatially smoothed (FWHM 5mm) and temporally high pass filtered (t > 0.01 Hz).

Time-series statistical analysis was carried out according to the general linear model using FEAT (FMRI Expert Analysis Tool), Version 5.98. For each subject, we first regressed out nuisance covariates, including 6 rigid body motion parameters and average white matter (WM), cerebrospinal fluid (CSF) and global time-series. The WM and CSF time-series reflected signal from subject-specific regions of interest (ROIs) created using FAST (FSL's Automatic Segmentation Tool). The residuals from the previous step were aligned to high-resolution coplanar images via an affine transformation with 6 degrees of freedom and then aligned to the standard Montreal Neurological Institute (MNI) average of 152 brains using an affine transformation with 12 degrees of freedom using FMRIB's Linear Image Registration Tool (FLIRT). In order to examine whole brain connectivity with nodes of interest, we used anatomically-based ROIs from the Harvard-Oxford probabilistic atlas (thresholded at 25% probability): the bilateral amygdala (**Figure 1.1 top panel, A**) and the right pars opercularis, inferior frontal gyrus (rIFGpo, BA 44; **Figure 1.1 bottom panel, A**). We chose to focus on the

right IFGpo given that previous studies on the processing of facial affect reported greater activity and/or more robust group differences in this region (Dapretto et al. 2006; Hadjikhani et al. 2007; Uddin et al. 2008). We extracted time-series from our ROIs for each subject and correlated them with every voxel in the brain to generate connectivity maps for each subject and ROI. Individual correlation maps were converted into z-statistic maps using Fischer's *r* to *z* transformation and then combined at the group level using the ordinary least squares method. For a complete list of anatomical regions positively and negatively connected to the seeds, as well as the peak voxel in MNI coordinates and *Z*-statistics, see **Table 1.2** and **Table 1.3.**

Analyses Without Global Signal Regression and With Task Regression

To address the methodological concern related to anticorrelations and using global signal regression as a preprocessing step (see Murphy et al. 2009; Jones et al. 2010), we performed all analyses with and without global signal regression. Each of the major patterns of between-group differences was also present when global signal regression was not used (see **1.3**, **1.4** and **Supplemental Materials** for a more thorough discussion of the analysis without global signal regression).

Additionally, we wanted to examine whether we could isolate connectivity differences that were task-dependent versus those that were due to underlying intrinsic connectivity. In order to do this, we ran all analyses using residuals from a general linear model (GLM) that included task stimulus timings for each type of emotional expression convolved with 4 basis functions generated with FLOBS (FSL's Linear Optimal Basis Function) and by applying a low pass filter (t<0.1 Hz; Fair et al. 2007b; Jones et al. 2010). Again, we did not observe substantial qualitative differences with this approach (see **Figure 1.5**), which may reflect the fact that this method does not completely remove task effects and/or that measured connectivity may largely be due to intrinsic connectivity (see **Supplemental Materials**). Given that the results may be partially driven by the task regardless of this approach, we present all results without task

regression or low pass filtering (and global signal regression) and discuss group differences as a combination of task-related and intrinsic connectivity.

Thresholding and Visualization of Segregated Networks

All within- and between-group connectivity maps were thresholded at $Z > 2.3$ ($p < 0.01$) and corrected for multiple comparisons at the cluster level ($p < 0.05$) using Gaussian random field theory. For between-group comparisons of connectivity maps, ASD>TD for positive connectivity is the same as TD>ASD for negative connectivity. Therefore, in order to identify and interpret four potential types of group differences (TD>ASD for regions of positive connectivity, TD>ASD for regions of negative connectivity, ASD>TD for regions of positive connectivity, ASD>TD for regions of negative connectivity), we masked the group difference maps by the respective TD and ASD within-group positive and negative connectivity maps.

Results

Bilateral Amygdala Seed

Within-Group Positive Connectivity

In the TD group, activity in bilateral amygdala was positively correlated with activity in portions of the temporal lobe including the hippocampus, inferior temporal gyrus and fusiform gyrus as well as basal ganglia and thalamus (**Figure 1.1** top panel, B; **Table 1.2**)**.** Bilateral amygdala activity was also correlated with activity in frontal regions including the orbitofrontal gyrus and IFG pars orbitalis, as well as occipital regions including the lingual gyrus, occipital poles and MT/V5 complex (**Figure 1.1** top panel, B; **Table 1.2**). For the ASD group, activity in bilateral amygdala was positively correlated with a similar network as the TD group except for the bilateral occipital poles and left fusiform gyrus (**Figure 1.1** top panel, C; **Table 1.2**). The ASD group also displayed positive connectivity between the bilateral amygdala and the left

middle temporal gyrus (**Figure 1.1** top panel, C; **Table 1.2**).

Within-Group Negative Connectivity

In the TD group, activity in bilateral amygdala was negatively correlated with posterior regions including the precuneus/posterior cingulate, inferior and superior parietal lobules and frontal regions including dorsolateral prefrontal frontal cortex (DLPFC), and dorsal ACC (**Figure 1.1** top panel, B; **Table 1.2**). For the ASD group, activity in the bilateral amygdala was negatively correlated with a less extensive network that included the same regions as the TD group except the DLPFC and dorsal ACC (**Figure 1.1** top panel, C; **Table 1.2**).

Between-Group Analyses

The TD group showed significantly more positive connectivity with bilateral MT/V5 complex and inferior temporal/fusiform cortex (red circles in **Figure 1.1** top panel, D; **Table 1.2**). The TD group also showed greater negative connectivity with DLPFC and dorsal ACC (blue circles in **Figure 1.1** top panel, D; **Table 1.2**). Relative to the TD group, the ASD group did not show stronger positive or negative connectivity with any regions.

Right Inferior Frontal Gyrus, Pars Opercularis* (rIFGpo) *Seed

Within-Group Positive Connectivity

In the TD group, activity in the rIFGpo was positively correlated with activity in other frontal regions, including the precentral gyrus, medial superior frontal gyrus, anterior insula, and anterior cingulate cortex (ACC), as well as with activity in the inferior and superior parietal lobules (**Figure 1.1** bottom panel, B; **Table 1.3)**. Activity in the rIFGpo was also correlated with activity in the caudate and putamen. In the ASD group, activity in the rIFGpo was positively correlated with a similar network as the TD group that did not include the left inferior and superior parietal lobules (**Figure 1.1** bottom panel, C; **Table 1.3)**. In the ASD group, activity in the rIFGpo was also positively correlated with activity in right lateral frontal regions as well as the right nucleus accumbens and thalamus (**Figure 1.1** bottom panel, C; **Table 1.3)**.

Within-Group Negative Connectivity

In the TD group, activity in the rIFGpo was negatively correlated with activity in regions including the ventral medial prefrontal cortex (VMPFC), precuneus/posterior cingulate, left angular gyrus, left middle temporal gyrus and left parahippocampal gyrus (**Figure 1.1** bottom panel, B; **Table 1.2**). For the ASD group, activity in rIFGpo was negatively correlated with a similar but less extensive network of regions that did not include the VMPFC (**Figure 1.1** bottom panel, C; **Table 1.2**).

Between-Group Analyses

The TD group showed significantly more positive connectivity with the left inferior and superior parietal lobules (red circles in **Figure 1.1** bottom panel, D; **Table 1.3**). The ASD group showed significantly more positive connectivity with right frontal regions and right nucleus accumbens (purple circles in **Figure 1.1** bottom panel, D; **Table 1.3**). The TD group showed greater negative connectivity with regions in the VMPFC (blue circles in **Figure 1.1** bottom panel, D; **Table 1.3**). There were no regions showing greater negative connectivity in the ASD group.

Discussion

Here we examined the functional organization of brain networks in children and adolescents with ASD, as compared with matched controls, during a passive emotional face processing task. We used the bilateral amygdala and the right pars opercularis as seed regions for whole-brain connectivity analyses since these areas have been implicated in atypical socioemotional and face processing in ASD. Overall, the pattern of altered connectivity we observed in ASD for both seeds suggest that ASD is characterized by reduced functional integration and segregation of large-scale brain networks. Specifically, the ASD group showed reduced integration between amygdala and secondary visual areas and between rIFGpo and

parietal cortex as well as increased positive connectivity between rIFGpo and several regions in right frontal cortex. Additionally, the ASD group displayed weaker negative correlations (i.e. reduced functional segregation) between amygdala and dorsal anterior cingulate/dorsolateral prefrontal cortex as well as between rIFGpo and ventromedial prefrontal cortex.

We interpret these findings in accordance with recent studies that have begun to chart the typical maturation of functional brain networks across development as well as in terms of the known functional roles of the regions/networks positively and negatively connected with each of our seed regions. Additionally, given that group differences may be due to a combination of intrinsic and task-driven connectivity, we interpret our results in the context of previous studies that have carefully characterized differences in intrinsic connectivity as well as differences in task-related regional activation and connectivity in ASD during emotional face processing.

Bilateral Amygdala Seed

Positive Connectivity

Consistent with prior reports (Pezawas et al. 2005; Stein et al. 2007; Roy et al. 2009), using the bilateral amygdala as a seed region for a whole-brain functional connectivity analysis, we found that, in typically-developing children, the bilateral amygdala was positively connected to a network of regions which included the hippocampus/parahippocampal gyrus, basal ganglia, thalamus, fusiform gyrus, orbitofrontal gyrus and ventral ACC (**Figure 1.1** top panel, B). In the TD group, the amygdala was also positively connected with visual regions including the lingual gyrus, occipital poles and V5/MT complex. Although the first set of regions listed above was functionally connected with the amygdala in a resting state study of neurotypical adults (Roy et al. 2009), visual regions reported here were not correlated with amygdala activity in that study (in fact, they were found to be mostly anticorrelated with amygdala activity). This difference may reflect co-activation between the amygdala and visual areas induced by the task, considering

that these regions are strongly engaged by the emotional faces presented in this study (Dapretto et al. 2006; Pfeifer et al. 2008; see **Supplemental Materials**).

Children with ASD displayed connectivity between the bilateral amygdala and each of the same regions as the TD group, except that they exhibited reduced connectivity with secondary visual areas including bilateral V5/MT complex and the right fusiform gyrus (see red circles in **Figure 1.1** top panel, D). Reduced connectivity between secondary visual areas and amygdala in the ASD group is consistent with reduced connectivity between fusiform face area and amygdala found by Kleinhans and colleagues (Kleinhans et al. 2008). In previous face processing activation studies, hypoactivation of the amygdala (Critchley et al. 2000; Wang et al. 2004;) as well as fusiform gyrus (e.g. Schultz et al. 2000; Pierce et al. 2001) have been consistently reported. However, amygdala and fusiform hypoactivation have been shown to be highly dependent on task demands (Hadjikhani et al. 2004; Wang et al. 2004), familiarity (Pierce et al. 2004), or time fixating on eyes (Dalton et al. 2005). In the present study (**Figure 1.2**), typically-developing children showed heightened activity in the fusiform gyrus and amygdala; however, post hoc analyses found no correlations between task-related activation in either the fusiform gyrus or amygdala and the level of fusiform-amgydala connectivity. Furthermore, reduced amygdala-V5/MT/fusiform connectivity was still observed in analyses where task-related activity was regressed out (see **Supplemental Materials, Figure 1.5**). Thus, it is unlikely that between-group differences in task-related activity is driving the observed connectivity effect. Reduced connectivity between amygdala and secondary visual areas fits well with the general underconnectivity theory (Just et al. 2004) and highlights a pattern of reduced functional integration in a distributed network involved in processing facial affect.

Negative Connectivity

A network of regions was found to be negatively correlated (i.e. segregated) with activity in the amygdala. In the TD group, this network largely overlapped with regions previously

reported to be anticorrelated with activity in the amygdala (Pezawas et al. 2005; Stein et al. 2007; Roy et al. 2009; **Figure 1.1** top panel, B) including the precuneus/posterior cingulate, dorsal ACC, and DLPFC. Frontal regions including the dorsal ACC and DLPFC have been associated with cognitive processes (e.g., reasoning and rationalizing) that are deemed important for regulating emotional reactions stemming from the amygdala and limbic system (e.g. Hariri et al. 2000, 2003; Phillips et al. 2003). In a structural equation modeling study performed during an emotion processing task, the precuneus/anterior cingulate and dorsal ACC were shown to have a negative influence on amygdala activity (Stein et al. 2007). Reduced negative connectivity between these frontal regions and the amygdala has been found in affective disorders such as major depression and bipolar disorder (Almeida et al. 2009; Chepenik et al. 2010).

Interestingly, while children with ASD did show a similar, although relatively weaker, network of regions anticorrelated with amygdala activity, they did not show anticorrelated activity between the bilateral amygdala and the dorsal ACC and DLPFC (see blue circles in **Figure 1.1** top panel, D). This between-group difference remained in analyses conducted without global signal regression (see **Supplemental Materials, Figures 1.3** and **1.4**). Although stronger negative connectivity for the typically-developing group could also be interpreted as stronger positive connectivity for the ASD group, given the previous literature on frontal regulation of the limbic system (e.g., Hariri et al. 2003; Stein et al 2007), we take this difference to more likely reflect stronger fronto-limbic decoupling in typically-developing children. Future studies using methods better suited for capturing regulatory interactions (such as psychophysiological interaction, PPI) may be able to more definitively address these competing accounts.

Right Pars Opercularis (rIFGpo) Seed

Positive Connectivity

Using the rIFGpo as a seed region of interest for whole-brain functional connectivity, we found that, in the TD group, the rIFGpo was positively connected to a network of regions largely resembling the task positive network that has been associated with externally directed, attentionally demanding tasks (Fox et al. 2005; **Figure 1.1** bottom panel, B). This network includes the precentral gyrus, anterior insula, anterior cingulate, medial superior frontal gyrus, inferior/superior parietal lobule and lateral occipital gyrus. Although a finer classification of the task positive network might place the rIFGpo into the salience/cingulo-opercular subnetwork, as opposed to the fronto-parietal executive subnetwork (Seeley et al. 2007; Dosenbach et al. 2007), our seed-based approach, using the rIFGpo as a seed region, generated connectivity maps resembling the entire task positive network.

While children with ASD also displayed connectivity between the rIFGpo and a similar network as observed in the TD group, there was notably decreased connectivity with regions increasingly distant from the seed (**Figure 1.1** bottom panel, C). Group differences were significant for regions in the contralateral parietal lobe, which included the inferior and superior parietal lobules (see red circles in **Figure 1.1** bottom panel, D). This finding is consistent with multiple task-based studies (e.g. Just et al. 2004; Koshino et al. 2005; Kana et al. 2007) which reported reduced connectivity between frontal and parietal regions in individuals with ASD, supporting the underconnectivity theory (e.g. Just et al. 2004, 2007) as well as dysfunction of the canonical MNS (Nishitani et al. 2004; Dapretto et al. 2006; Oberman and Ramachandran 2007). Reduced connectivity along this anterior-posterior axis is also strongly associated with an immature pattern of functional integration in neurotypical individuals (Fair et al. 2007a, 2008, 2009; Kelly et al. 2009; Dosenbach et al. 2010). Given that the IFGpo is part of the functionally significant cingulo-opercular/salience network (Dosenbach et al. 2007; Seeley et al. 2007), our findings provide support for the notion that this network may be a hub of dysfunction in autism

(Uddin and Menon 2009; Ebisch et al., 2010) and, more specifically, that altered connectivity within this network may be related to socio-emotional functioning.

The ASD group showed a pattern of greater intralobar or 'local' connectivity with frontal regions relatively proximal to the seed that included right superior frontal cortex and right lateral orbital cortex (see purple circles in **Figure 1.1** bottom panel, D). Greater connectivity between the rIFGpo and other right frontal regions fits well with theoretical accounts of greater local connectivity in ASD (Belmonte et al. 2004; Courchesne and Pierce 2005; Geschwind and Levitt 2007), as well as empirical findings of cortico-cortical overconnectivity in adults with ASD (Welchew et al. 2005; Noonan et al. 2009; Shih et al. 2010). Consistent with our findings, Shih et al. (2010) examined connectivity in the imitation network (Iacoboni et al. 1999; Nishitani et al. 2004) and found aberrantly stronger connectivity between IFGpo and superior frontal cortex. They discussed aberrantly increased cortico-cortical connectivity as either reflecting a compensatory mechanism in ASD or being related to early brain growth anomalies that lead to aberrant segregation of functional networks. In studies of typical development, increased functional segregation between networks as measured by reduced local connectivity has been consistently found in adults compared to children (e.g. Kelly et al. 2008; Fair et al. 2009; Dosenbach et al. 2010). Moreover, weakening connections between nodes of different networks were found to be twice as powerful at predicting brain maturity than increasing functional integration within networks (Dosenbach et al. 2010).

In addition to greater local frontal connectivity, the ASD group also showed greater connectivity than the TD group between the rIFGpo and right nucleus accumbens (see purple circle in **Figure 1.1** bottom panel, D). Greater striato-cortical (Turner et al. 2006; Di Martino et al. 2010) and thalamo-cortical (Mizuno et al. 2006; Di Martino et al. 2010) connectivity have previously been found in adults with ASD. Thus, greater cortico-subcortical connectivity appears to be a robust finding in ASD that does not fit with a pattern of local/intralobar overconnectivity.

Turner et al. (2006) hypothesized that increased connectivity in basal ganglia-cortical circuits in ASD is related to executive impairments and may also reflect a compensatory mechanism associated with repetitive and stereotypic behaviors. Mizuno et al. (2006) speculated that increased thalamo-cortical connectivity in ASD might be related to increased arousal and sensory hypersensitivity as well as reduced sensory gating, although there is little evidence directly relating these alterations to specific ASD symptomatology. Interestingly, a recent developmental connectivity study found that subcortical-cortical connectivity is stronger in children compared to adults (Supekar et al. 2009). Thus, a parsimonious, although not mutually exclusive, explanation for each of the major patterns of aberrant connectivity reported in the literature, including the present study, is that they may altogether reflect the relatively "immature" integration and segregation of functional brain networks in ASD. While increased subcortico-cortical connectivity has been found in typical children compared with adults, it is still unclear to what extent increased subcortical-cortical connectivity in ASD may reflect immature vs. aberrant patterns of connectivity (Di Martino et al. 2010).

Negative Connectivity

A network of regions that closely resembles the task negative or default mode network (Raichle et al. 2001; Greicius et al. 2003) was found to be anticorrelated (i.e. functionally segregated) with the rIFGpo. In typically-developing children, the network of regions anticorrelated with activity in the rIFGpo included the precuneus/posterior cingulate, left angular gyrus, left parahippocampal gyrus, and VMPFC. The DMN and task positive network have been shown to consistently display an anticorrelated relationship (Fox et al. 2005, 2009; Fransson et al. 2005; Chang & Glover 2010) and despite the controversy regarding global signal regression and anticorrelated networks (Murphy et al 2009; Fox et al. 2009; see **Supplemental Materials**) recent work has suggested that the degree of anticorrelation between these networks is biologically meaningful (Kelly et al. 2008; Whitfield-Gabrieli et al. 2009; Hampson et al, 2010).

Children with ASD showed a similar, albeit weaker, network of regions anticorrelated with the right IFGpo, which included the posterior components of the DMN. In particular, the ASD group lacked a significant negative relationship between activity in the rIFGpo and VMPFC (see blue circles in **Figure 1.1** bottom panel, D). Reduced anticorrelation (or increased positive correlation) between the task positive network and the DMN is consistent with reduced functional segregation between these two networks. In a developmental study, Stevens et al. (2009) found reductions in positive interactions between a task-positive executive control network and the default mode network in children as compared to adults. The authors suggested that increased segregation between these two networks might allow for more flexible processing as a function of development. Therefore, reduced segregation between these networks found here in ASD is also consistent with the notion that ASD is characterized by an "immature" pattern of functional segregation between major cognitive networks. It is interesting to note that Iacoboni (2006) and Uddin et al. (2007) have previously discussed how the MNS and DMN are "two sides of the same coin," whereby the MNS is involved with simulation of physical and external aspects of self (and others) whereas the DMN is related to more internal and higher level mental-state attribution aspects of self (and others). Reduced segregation between these systems reported here in ASD and during typical development (Stevens et al., 2009) may therefore reflect immature development of one's internal and external representations of self and others.

Our finding that the ASD group showed an anticorrelated relationship between the rIFGpo and the posterior portion of the DMN but not the VMPFC also suggests that the DMN itself is not as well connected in the ASD group. In fact, post hoc analyses (not shown) that used the VMPFC as an additional seed region confirmed that there was reduced functional integration between this frontal DMN region and the posterior parietal components of the DMN in our sample. In line with recent resting state studies (Kennedy and Courchesne 2008; Monk et

al. 2009; Weng et al. 2010; Assaf 2010), our results provide additional evidence of dysfunction within the DMN in ASD and further suggest that the frontal cortex may be the most immature link of this network in ASD.

Conclusions and Future Directions

By using a seed-based connectivity approach to examine communication between brain regions implicated in the processing of facial affect, we found several patterns of altered connectivity suggesting that brain networks in ASD are characterized by reduced functional integration and segregation. To our knowledge, this is the first study to report both decreased long-range connectivity and reduced functional segregation as indexed by increased local connectivity and reduced anticorrelations, respectively. Our findings fit well with theoretical accounts of altered connectivity in ASD and provide a framework whereby connectivity disturbances in ASD can be understood in terms of multiple interacting systems across development. By carefully considering methodological concerns and characterizing connectivity both in terms of integration and segregation, our study may help explain previously conflicting reports of decreased (e.g., Just et al. 2004; Weng et al. 2010) but also increased connectivity in autism (e.g., Noonan et al. 2009; Shih et al. 2010). More generally, our findings suggest that measuring connectivity of neural systems – during task performance and/or resting state – may provide a more sensitive marker of abnormalities in brain function in autism than focusing exclusively on regional activation patterns.

Reduced functional integration and segregation of cortico-cortical and cortico-subcortical networks in ASD are perhaps not surprising given that ASD is a neurodevelopmental disorder associated with reduced engagement in social interactions. However, the extent to which reduced functional integration and segregation may simply reflect immature or delayed connectivity, as opposed to, altered connectivity that is specific to autism and/or related to compensatory mechanisms, remains to be determined. A recent basal ganglia resting state

study in ASD found that although some increased cortico-subcortical connectivity in ASD appeared “immature”, most of the altered connectivity appeared to reflect “developmental derangement” or aberrantly high subcortico-cortical connectivity (Di Martino et al. 2010). Future experiments, including longitudinal studies, should also focus on disentangling how a history of altered engagement with the environment may affect connectivity versus how early brain abnormalities may directly lead to altered connectivity patterns.

A more careful examination of how cortico-cortical and cortico-subcortical connectivity changes across typical development as compared to ASD is also needed. The majority of previous connectivity studies in ASD were performed with adults with ASD, whereas our sample consisted of children and adolescents. A greater reduction in connectivity for adolescents with ASD as compared to adults with ASD has recently been observed in the DMN (Monk et al. 2009; Weng et al. 2010), suggesting that the development of intrinsic connectivity networks shows a more protracted development in ASD and that differences may become subtler by adulthood. Future studies should more carefully investigate this possibility as well as focus on typical and atypical development in even younger populations, given that measures of connectivity can easily be acquired during resting state scans with little concern about adequate task performance. Importantly, resting state connectivity could also be examined in lower functioning individuals, a highly understudied population in the existing neuroimaging literature.

One limitation of the present study, as well as of prior work, is the difficulty of teasing apart the relative contributions of task-related and intrinsic connectivity in determining the observed between-group differences. Although we attempted to control for attention and alertness, we cannot completely rule out the possibility that subtle differences in these behavioral variables may have contributed to the connectivity differences observed between typically-developing children and children with ASD. It should also be noted that, although resting state studies minimize task-induced connectivity, differences in covert cognition might

partially drive group differences (Kennedy and Courchesne 2008). Future studies that directly compare measures of connectivity acquired during resting state versus task performance should prove useful in this respect. Furthermore, the extent to which aberrant functional connectivity in ASD is related to underlying cortical development such as synaptic pruning, myelination or other processes remains largely unknown. Despite growing evidence that predisposing genetic and environmental factors may lead to altered neuronal migration and synaptic formation (Betancour et al. 2009), dysfunctional microcircuitry (Casanova et al. 2002), early brain overgrowth (Courchesne et al. 2003) and disordered structural connections (e.g. Herbert et al. 2004; Sundaram et al. 2008), little work thus far has directly linked any of these findings with altered functional connectivity in ASD (Scott-Van Zeeland et al. 2010). Finally, and perhaps most importantly, future studies in this line of research should also strive to be directly relevant to clinical outcomes (Fox and Greicius 2010). For example, characterizing functional brain networks in individuals at risk for ASD may eventually be used for earlier diagnosis or for developing individualized behavioral and pharmacological interventions.

Supplemental Materials

Given the somewhat conflicting findings in the autism connectivity literature, we paid careful attention to methodological concerns including global signal regression (Murphy et al. 2009; Jones et al. 2010) and task regression (Fair et al. 2007; Jones et al. 2010) by analyzing the data with and without these options in order to determine how they affected the overall patterns of results.

Global Signal Regression

Physiological noise, such as cardiac and respiratory signals, can confound measures of functional connectivity (Birn et al. 2006). Thus, many groups have included the average signal

of the whole brain as a nuisance regressor in order to reduce the effects of non-neuronal fluctuations. This preprocessing step is not commonly used for task-related fMRI because it has been shown to produce artifactual deactivations (Aguirre et al. 1998). However, without the use of global signal regression (GSR), every brain region can be significantly positively correlated with every other brain region (Fox et al. 2009; Van Dijk et al. 2010). In seed-based connectivity analyses, GSR is essentially a partial correlation between brain regions that accounts for this global confound. However, GSR mathematically causes a shift in the distribution of correlations as it mandates there be an equal distribution of positively and negatively correlated voxels (Murphy et al. 2009; Fox et al. 2009). In seed-based connectivity analyses, GSR commonly produces maps with regions displaying significant negative correlations (i.e. anticorrelations). Recently, it has been suggested that anticorrelations should be interpreted with caution, as they may not necessarily reflect an antagonistic or inhibitory relationship between regions (such as between the task positive and task negative networks; Murphy et al. 2009). However, anticorrelations are still observed when utilizing methods that do not involve GSR (e.g., Independent Components Analysis, Beckmann et al. 2005; physiological correction; Chang and Glover 2009), and anticorrelations have been found to be reliable across subjects and over time (Shehzad et al. 2009). Additionally, anticorrelations have been shown to spontaneously emerge in computer simulations of brain networks (Izhikevich and Edelman 2008), and electrophysiological work in cats has shown anticorrelated gamma power fluctuations in homologues of the task-positive and task-negative systems (Popa et al. 2009). Although a recent study suggested that the magnitude of anticorrelations between the task positive and negative networks were artifacts of GSR and network size (Anderson et al. 2010), another recent study found that even without GSR, lower connectivity between task positive and negative regions during rest was associated with better working memory performance (Hampson et al. 2010). Thus, while it is still unclear whether a global signal masks a true

antiphase relationship between task positive and negative brain networks, it appears as though connectivity between these networks is relevant to cognitive functioning.

Despite this controversy regarding anticorrelated brain regions, most groups (e.g. Di Martino et al. 2010, Dosenbach et al. 2010) continue to use GSR because it has been shown to maximize the specificity of positive resting-state correlations in real and simulated data (Weissenbacher et al. 2009), as well as improve localization of known anatomical connections between cortical and subcortical regions (Fox et al. 2009). However, it was also recently shown that the global signal is not entirely composed of non-neuronal fluctuations (Schölvinck et al. 2010), so it is unclear to what extent artifacts are being removed vs. introduced when regressing out the global signal. This may be of particular concern if the global signal is distributed differentially between groups. For these reasons, we decided to perform all analyses with and without GSR and carefully interpret group differences in regions that display anticorrelations upon implementation of GSR.

In our data, the within-group positive connectivity maps without GSR looked qualitatively similar to the within-group connectivity maps with GSR, albeit at a much higher threshold (**Figure 1.3,** A and B). However, no regions were significantly anticorrelated with the seeds for either group without GSR. These findings are consistent with previous reports examining the use of GSR (Murphy et al. 2009; Fox et al. 2009; Weissenbacher et al. 2009; Van Dijk et al. 2010). Interestingly, the between-group results were qualitatively similar to the maps generated when using global signal regression and all of the major patterns of group differences were still observed (**Figure 1.3**, C). Furthermore, many of the group differences in both analyses (i.e., with and without GSR) were found in regions that displayed anticorrelations with the seed regions for analyses with GSR (or displayed the lowest correlations with the seed regions for analyses without GSR).

Although functional segregation can refer to different phenomenon depending on the exact literature, in the context of functional connectivity MRI, functional segregation can be defined as the tendency for region A and B to be not correlated with each other and to be correlated with different regions (i.e., region A's friends are not the same as region B's friends). Thus, one way to determine if an area is functionally segregated from a seed region is to see whether it has lower connectivity with the seed than the seed has with the entire brain. In additional post hoc analyses, regardless of whether GSR was used, the TD group displayed significantly lower amygdala-DLPFC/ACC connectivity compared to amygdala-whole-brain connectivity (**Figure 1.4**, A and B), as well as significantly lower rIFGpo-MPFC connectivity compared to rIFGpo-whole-brain connectivity (**Figure 1.4**, C and D). The ASD group did not show this pattern of functional segregation. Furthermore, the TD group displayed significantly stronger segregation (lower amygdala-DLPFC/ACC and rIFGpo-MPFC connectivity) than the ASD group regardless of whether GSR was used (**Figure 1.4**, A, B, C and D). Therefore, our interpretation of reduced functional segregation between these networks in ASD is supported by analyses with and without GSR.

However, the analyses performed without global signal regression were not *exactly* the same and it is still not completely clear how many artifacts were introduced versus removed by this preprocessing step. The analysis with GSR did find stronger group differences than without GSR, and it is unclear to what extent this is related to improved signal to noise ratio versus an artifact of GSR. Another notable difference in results between the two methods is the absence of increased subcortico-cortical connectivity for the ASD group when GSR was not applied. We speculate that this null finding may be due to increased anatomic specificity for subcortico-cortical connectivity when using global signal regression (Fox et al. 2009). Additionally, although both increased positive connectivity or reduced negative connectivity between different networks is consistent with reduced functional segregation, the analyses with GSR helped

visualize regions that were segregated (i.e. anticorrelated) from the seed regions. For these reasons, we opted to report regions that displayed anticorrelations upon GSR in the results and discussion.

Task Regression

An additional source of controversy in the connectivity literature has to do with teasing apart how the observed altered connectivity in ASD is driven by task-induced connectivity versus intrinsic connectivity. Intrinsic connectivity networks comprise a large amount of variance in fMRI data during rest and task (Fox et al. 2006; Toro et al. 2008), persist during sleep and anesthesia (Horovitz et al. 2009; Greicius et al. 2008), and are differentially attenuated depending on the task being performed (Fransson et al. 2006). However, experimental stimuli will induce coactivation or connectivity in two or more regions making it difficult to determine the extent to which connectivity differences are driven by intrinsic or task-related connectivity. A recent methodological investigation concluded that estimates of disrupted functional connectivity in ASD were largely driven by intrinsic neuronal fluctuations (Jones et al., 2010). Some of the previously mentioned studies (Villalobos et al. 2005; Turner et al. 2006; Mizuno et al. 2006; Noonan et al. 2009; Shih et al. 2010) were performed in the context of a visuomotor task and the authors attempted to control for task-related contributions to functional connectivity by including nuisance regressors to model out task-induced covariation as well as a low pass filter. The authors of these studies have argued that this may be one of the reasons why they generally found overconnectivity in autism whereas other studies found mostly underconnectivity (e.g. Just et al. 2004; Just et al. 2007). A previous comparison between true resting state data and data from an event-related fMRI task where the task was “regressed out” showed that this latter approach did not yield the exact same findings as pure resting state data (Fair et al. 2007). While regressing out the task has been shown to change connectivity patterns and reduce task related effects (Jones et al. 2010), the findings of Fair et al. (2007) suggests

that there are nonlinear, unmodeled task effects that affect signal covariation between regions. Thus, regardless of whether task regression is applied, group differences in connectivity are likely due to a combination of intrinsic and task-related connectivity. This is also a concern in resting state studies, where group differences in connectivity may, in part, be related to differences in spontaneous cognition (Kennedy and Courchesne 2008).

Our analyses performed with a low pass filter and with the convolved stimuli timings included as nuisance regressors showed that, qualitatively, these steps minimally affected our between- and within-group connectivity maps (**Figure 1.5**). This suggests that intrinsic connectivity accounts for the majority of observed functional connectivity and/or that task regression does not fully remove signal covariation due to the task. Our within group connectivity maps for the rIFGpo seed largely matched the task positive and task negative networks identified in previous resting state studies (e.g. Fox et al. 2005, 2009). This further suggests that intrinsic connectivity largely contributed to our connectivity results for the IFGpo seed, which although it is hypothesized to play a role in face processing, it is not robustly engaged by the passive version of this task (Dapretto et al. 2006; Pfeifer et al. 2008; Pfeifer et al. 2011). While the connectivity maps generated from the amygdala seed also closely match the networks identified in a prior amygdala resting state study (Roy et al. 2009), areas known to be strongly engaged by this task (i.e. amygdala and visual areas) did not show positive connectivity in the resting state (Roy et al. 2009) although they were strongly connected in the present study even when we modeled out task effects. Although non task regressed analyses were associated with stronger connectivity between visual cortex and amygdala for the TD group, both analyses still found strong connectivity between the amygdala and visual cortex (**Figure 1.5**, A). Therefore, we speculate that although intrinsic connectivity contributes to a large portion of connectivity for the amygdala seed, there are nonlinear task-related contributions to connectivity that the task regression and low pass filtering could not remove.

Accordingly, we interpret our findings as being related to intrinsic connectivity as well as task-related connectivity.

Table 1.1 Mean, Standard Deviation, and Range of Sample Descriptives

Characteristic	Typically Developing	Autism Spectrum	*p* value
Age	13.3+/-0.96, 10.8-15.7	12.6+/-2.83, 8.2-17.4	0.28
Verbal IQ	105.6+/10.5, 89-126	97.5+/-20.9, 69-138	0.09
Performance IQ	105.9+/-10.3, 88-121	105.6+/-15.9, 75-142	0.94
Full Scale IQ	106.4+/-8.2, 92-116	100.7+/-18.6, 70-134	0.19
Mean Relative Head Motion (mm)	0.12+/-0.10, 0.03-0.27	0.15+/-0.10, 0.05-0.41	0.38
Maximum Relative Head Motion (mm)	0.97+/-0.85, 0.07-2.83	0.97+/-0.73, 0.09-2.89	1
Social Responsiveness Scale Total	17+/-12, 3-51	109+/-30, 60-162	<0.00
ADOS (Comm+Soc)	N/A	12.9+/-4.1, 7-20	N/A
ADI Total	N/A	47.0+/-11.2, 23-62	N/A

Table 1.2 Bilateral Amygdala	TD				ASD				TD>ASD				ASD>TD			
	MNI peak (mm)			Max Z	MNI peak (mm)			Max Z	MNI peak (mm)			Max Z	MNI peak (mm)			Max Z
	x	y	z		x	y	z		x	y	z		x	y	z	
Positive Connectivity																
R Amygdala	30	-8	-16	8.2	14	-4	-18	7.54								
L Amygdala	-16	-10	-16	7.7	-18	-10	-16	7.52								
R Hippocampus	26	-14	-18	7.3	28	-16	-18	6.45								
L Hippocampus	-20	-18	-18	6.6	-24	-12	-26	6.79								
R Putamen	30	-14	-8	4.8	30	-6	-8	4.73								
L Putamen	-32	-12	-10	3.6	-20	2	-8	5.14								
R Pallidum	22	-10	-6	4.1	22	-12	6	3.87								
L Pallidum	-16	-8	-8	4.2	-16	0	-8	4.47								
R Accumbens	6	8	-4	4.9	6	6	-6	4.40								
L Accumbens	-8	10	-4	3.7	-6	6	-6	4.02								
R Thalamus	24	-30	0	5.8	8	-30	2	5.14								
L Thalamus	-22	-34	-2	4.2	-24	-26	2	4.14								
Hypothalamus	4	-6	-4	5.3	-4	-10	2	4.67								
R Parahippocampal Gyrus	18	-16	-22	5.3	22	-32	-20	5.90								
L Parahippocampal Gyrus	-16	-14	-24	5.1	-20	-14	-26	6.48								
R Insula	34	8	-16	4.9	30	10	-16	5.19								
L Insula	-38	0	-14	5.2	-38	2	-18	4.46								
Ventral Anterior Cingulate					0	18	-8	4.15								
Frontal Medial Gyrus	4	60	-14	3.6	4	68	-6	3.56								
Medial Orbital Gyrus	0	34	-18	4.9	-2	40	-20	4.65								
R Inferior Frontal Gyrus, Pars Orbitalis	38	26	-18	3.96	44	38	-18	4.53								
L Inferior Frontal Gyrus, Pars Orbitalis	-44	20	-14	3.54	-46	22	-10	3.87								
R Temporal Pole	54	10	-34	3.05	28	12	-36	5.40								
L Temporal Pole	-32	26	-34	3.56	-24	4	-40	5.15								
R Fusiform	28	4	-38	5.55	38	-44	-16	4.73	40	-44	-6	5.13				
L Fusiform	-34	-50	-12	5.43												
R Middle Temporal Gyrus	66	-12	-22	5.07	62	-4	-14	3.06								
L Middle Temporal Gyrus					-62	-18	-18	4.51								
R Inferior Temporal Gyrus	48	-46	-26	4.27	48	-18	-28	4.33								
L Inferior Temporal Gyrus	-48	-44	-26	3.48	-44	-26	-22	4.99								
R Lingual Gyrus	26	-48	-12	4.81	8	-86	-4	3.89								
L Lingual Gyrus	-16	-70	-10	4.09	-28	-42	-8	4.25								
R Middle Occipital Gyrus	40	-68	-10	5.12	24	-44	-14	4.07	50	-68	4	4.26				
L Middle Occipital Gyrus	-32	-78	2	5.32	-32	-88	-14	3.38	-32	-78	2	4.69				
R Occipital Pole	8	-98	0	4.23												
L Occipital Pole	-14	-98	16	4.84					-6	-92	22	3.38				
L Cerebellum	-4	-52	-18	4.33	-26	-54	-26	3.09								
Negative Connectivity																
Precuneus	0	-52	56	5.61	-12	-62	42	5.07								
Posterior Cingulate	6	-34	46	4.40	8	-40	44	3.22								
R Supramarginal Gyrus	66	-34	42	3.52	64	-36	32	4.55								
L Supramarginal Gurus	-48	-52	36	4.98	-62	-50	34	4.10								
R Angular Gyrus	44	-46	38	5.36	58	-52	46	4.45								
L Angular Gyrus	-42	-56	56	5.17	-44	-54	56	4.57								
R Superior Parietal Lobule	44	-48	58	3.52	32	-46	54	3.98								
L Superior Parietal Lobule	-24	-46	46	2.43												
R Superior Occipital Gyrus	50	-70	36	3.80	42	-72	38	3.05								
L Superior Occipital Gyrus	-40	-84	32	4.55	-38	-76	48	2.84								
Superior Frontal Gyrus, Medial	-2	32	36	5.29					-10	32	26	4.24				
R Superior Frontal Gyrus	18	8	58	5.39	20	56	22	4.89	18	8	62	4.35				
L Superior Frontal Gyrus	-18	10	62	3.49												
R Inferior Frontopolar Gyrus	20	60	0	5.04	32	60	6	2.79								
L Inferior Frontopolar Gyrus	-22	64	-4	3.53												
R Middle Frontal Gyrus	34	24	38	5.36	50	20	36	3.41	28	22	38	4.06				
L Middle Frontal Gyrus	-38	34	36	5.33					-32	28	44	3.77				
Anterior Cingulate	10	34	16	4.22					10	26	22	4.02				
R Precentral Gyrus	36	4	36	3.23												
L Precentral Gyrus	-50	0	36	3.62												
R Postcentral Gyrus					54	-20	24	3.71								

Table 1.3 Right Pars Opercularis	TD				ASD				TD>ASD				ASD>TD			
	MNI peak (mm)			Max Z	MNI peak (mm)			Max Z	MNI peak (mm)			Max Z	MNI peak (mm)			Max Z
	x	y	z		x	y	z		x	y	z		x	y	z	
Positive Connectivity																
R Inferior Frontal Gyrus, Pars Opercularis	58	16	14	8.72	56	14	16	8.85								
L Inferior Frontal Gyrus, Pars Opercularis	-56	10	18	6.33	50	8	4	5.94								
R Precentral Gyrus	50	4	42	7.45	50	6	40	6.74								
L Precentral Gyrus	-52	4	42	4.61	-40	0	30	5.58								
R Inferior Frontal Gyrus, Pars Orbitalis	46	44	-4	5.91	50	30	-6	6.63					30	24	-16	3.72
L Inferior Frontal Gyrus, Pars Orbitalis	-44	40	18	5.91												
R Middle Frontal Gyrus	38	40	28	5.73	50	32	26	6.18								
L Middle Frontal Gyrus	-26	-2	54	4.02	-42	40	20	4.96								
R Anterior Insula	38	20	-2	6.56	36	14	6	6.14								
L Anterior Insula	-32	22	2	7.11	-32	22	2	5.47								
Superior Frontal Gyrus, Medial part	4	14	50	6.65	-2	16	50	3.89								
R Superior Frontal Gyrus, Lateral part					16	4	62	4.54					22	36	40	4.64
Anterior Cingulate Cortex	10	18	30	4.88	10	18	32	5.81					4	28	2	3.97
R Supramarginal Gyrus	64	-32	30	5.73	44	-42	44	4.95								
L Supramarginal Gyrus	-50	-42	52	4.80					-62	-32	42	3.99				
R Superior Parietal Lobule	26	-52	50	3.95	30	-56	44	4.33								
L Superior Parietal Lobule	-30	-48	42	4.88					-30	-48	54	3.95				
R Middle Occipital Gyrus	34	-80	24	4.60	30	-68	36	3.27								
L Middle Occipital Gyrus	-36	-88	20	4.41												
R Superior Occipital Gyrus	16	-78	54	3.96	32	-62	46	3.85								
L Superior Occipital Gyrus	-22	-60	46	5.35					-14	-62	46	3.47				
R Superior Temporal Gyrus	54	-44	10	5.69	48	-32	2	4.13								
R Middle Temporal Gyrus	48	-24	-6	5.49	64	-48	-6	4.33								
R Inferior Temporal Gyrus	44	-50	-10	3.18												
R Lateral Orbital Gyrus					30	52	-10	4.59					36	46	-4	3.07
R Medial Orbital Gyrus	16	42	-18	3.37												
R Caudate	18	0	14	4.75	16	2	14	4.82								
R Putamen	20	2	8	4.13	22	10	-8	4.30					20	10	-2	2.79
L Putamen	-18	-2	6	2.89												
R Accumbens					12	12	-8	3.08					12	14	-6	3.42
R Thalamus					6	-18	10	3.41								
Negative Connectivity																
Precuneus	-4	-54	10	6.30	-6	-66	14	5.06								
Posterior Cingulate	-2	-48	32	6.71	-4	-40	34	4.66								
L Angular Gyrus	-42	-64	32	5.10	-44	-60	34	4.18								
L Parahippocampal Gyrus	-22	-26	-26	4.35	-24	-26	-26	4.25								
L Middle Temporal Gyrus	-56	-14	-18	5.50	-50	-12	-22	3.62								
L Middle Frontal Gyrus	-32	24	52	4.26												
L Temporal Pole	-42	20	-36	4.06												
L Cerebellum	-20	-52	-30	3.37	-14	-58	-18	4.26								
R Cerebellum					20	-58	-28	3.31								
Ventral Anterior Cingulate	-2	32	-4	4.34					0	30	4	4.14				
Middle Frontopolar Gyrus	-24	60	4	3.72					-4	60	14	2.75				
Frontal Medial Gyrus	0	60	-2	5.17					6	54	-4	3.84				

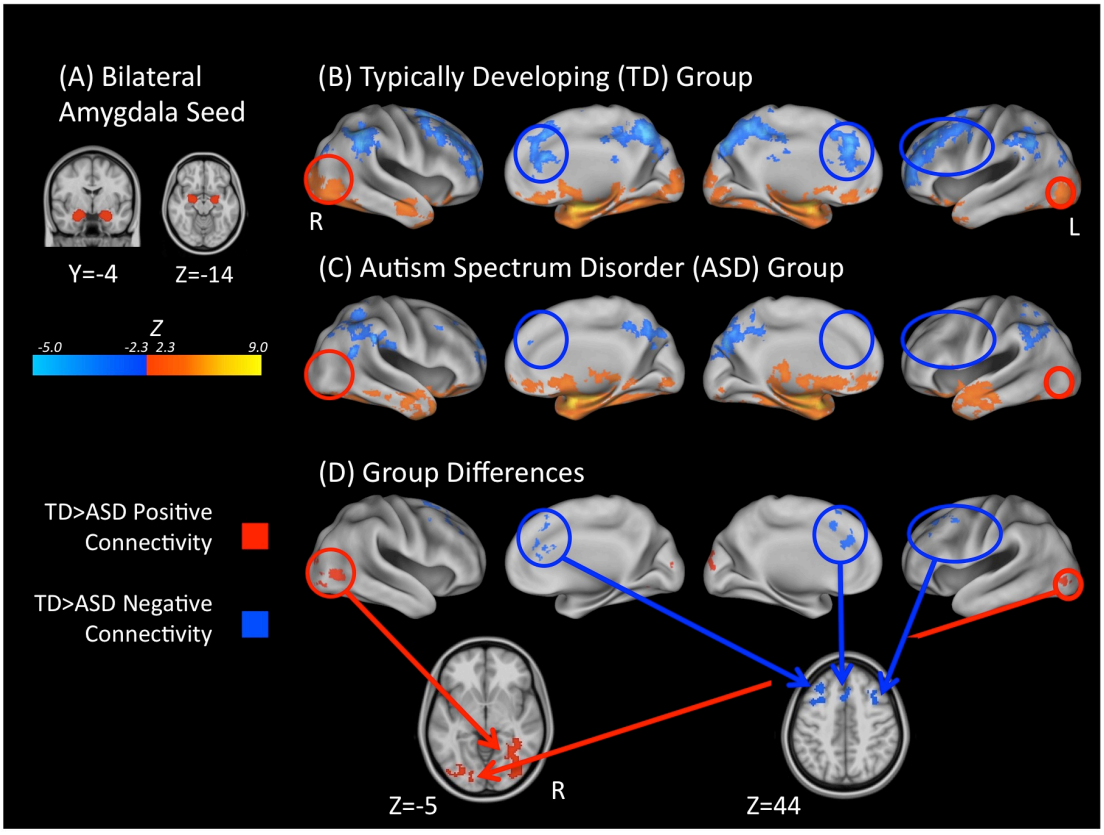
(A) Bilateral Amygdala Seed
Y=-4
Z=-14
Z
-5.0
-2.3
2.3
9.0
TD>ASD Positive Connectivity
TD>ASD Negative Connectivity
(B) Typically Developing (TD) Group
R
L
(C) Autism Spectrum Disorder (ASD) Group
(D) Group Differences
Z=-5
R
Z=44

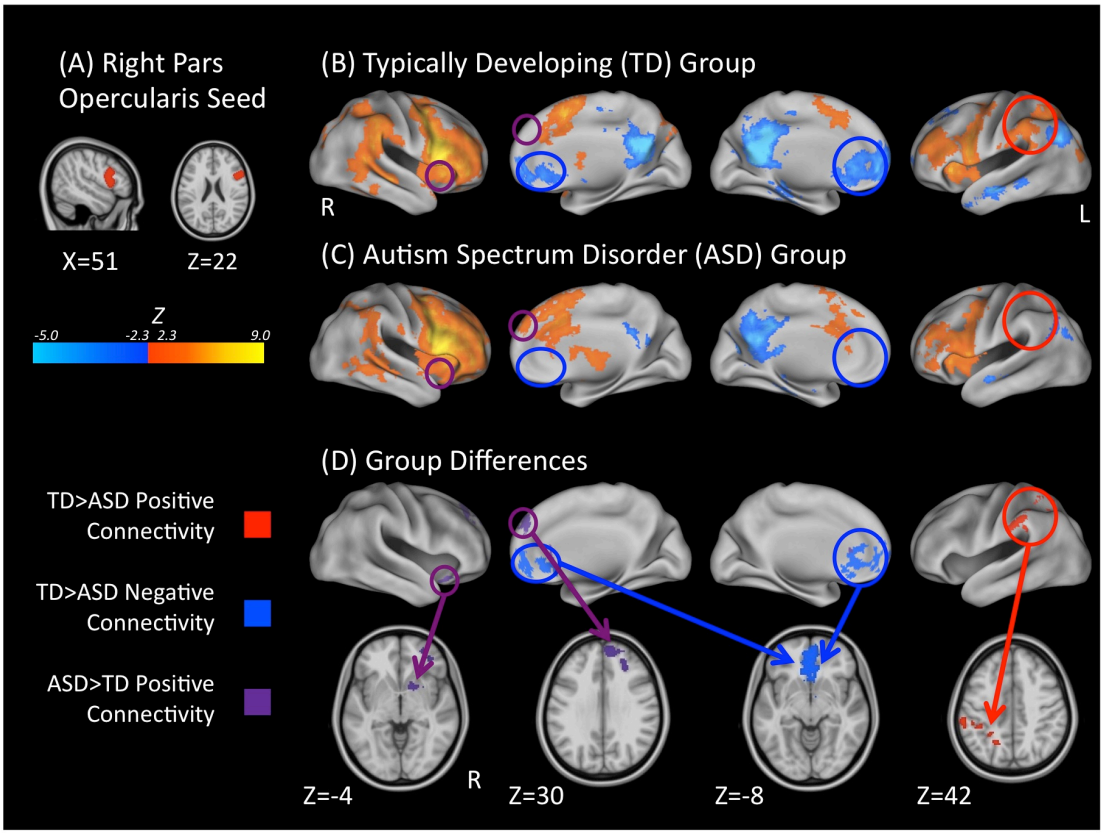
(A) Right Pars Opercularis Seed
X=51
Z=22
Z
-5.0
-2.3
2.3
9.0
TD>ASD Positive Connectivity
TD>ASD Negative Connectivity
ASD>TD Positive Connectivity
(B) Typically Developing (TD) Group
R
L
(C) Autism Spectrum Disorder (ASD) Group
(D) Group Differences
Z=-4
R
Z=30
Z=-8
Z=42

Figure 1.1. Bilateral amygdala (top panel) and right Inferior frontal gyrus, pars opercularis (rIFGpo; bottom panel) connectivity. (A) The Harvard Oxford bilateral amygdala (25% probability) and rIFGpo (25% probability) used as seed regions and displayed on the 1 mm MNI152 T1 standard brain. (B) Typically-developing (TD) within-group connectivity maps, (C) autism spectrum disorder (ASD) within-group connectivity maps, and (D) direct between-group contrasts rendered on the Inflated PALS B12 brain using CARET and on the 1 mm MNI152 T1 standard brain using AFNI. Maps are thresholded at $Z > 2.3$ ($p < 0.01$) with correction for multiple comparisons applied at the cluster level ($p < 0.05$). Red circles highlight areas of greater positive connectivity with the seed region for the TD group. Blue circles highlight areas of greater negative connectivity with the seed region for the TD group. Purple circles highlight areas of greater positive connectivity with the seed region for the ASD group.

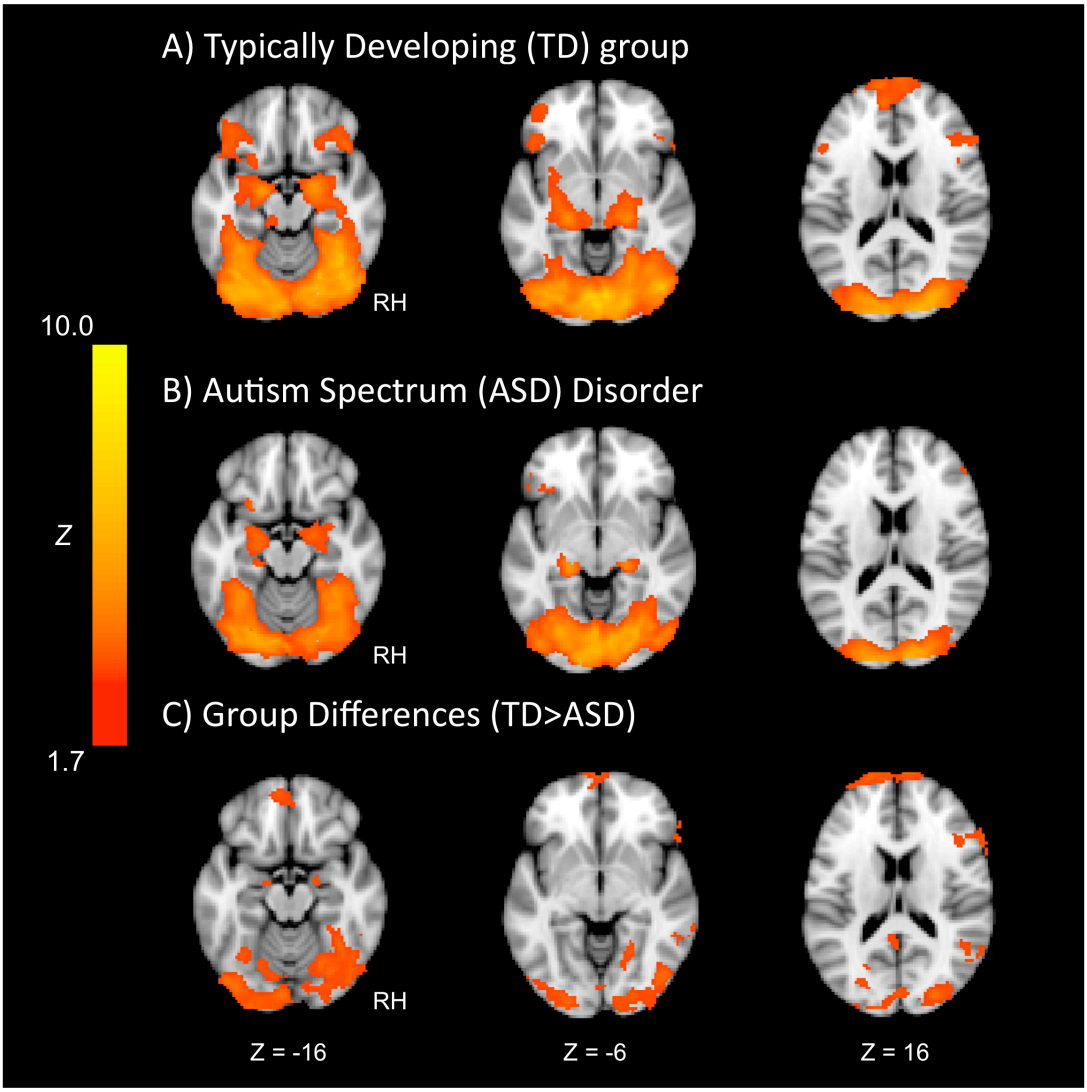

Figure 1.2. fMRI Activation maps. Using FSL's FEAT, the five sets of emotional faces and null events were modeled with a convolved double gamma HRF according to the GLM. The contrast of all emotional faces vs. null event was brought to the group level using a mixed effects analysis with FLAME (FMRIB's Local Analysis of Mixed Effects). The typically developing group (A) and Autism Spectrum Disorder group (B) robustly activated visual areas, thalamus, basal ganglia, hippocampus and amygdala as well as smaller clusters in the inferior frontal gyrus (IFG) and medial prefrontal cortex (MPFC). (C) Some group differences in activation were observed in secondary visual areas including fusiform gyrus, amygdala, IFG and MPFC. All Activation maps are thresholded at Z > 1.7, corrected for multiple comparisons except within the IFG and amygdala.

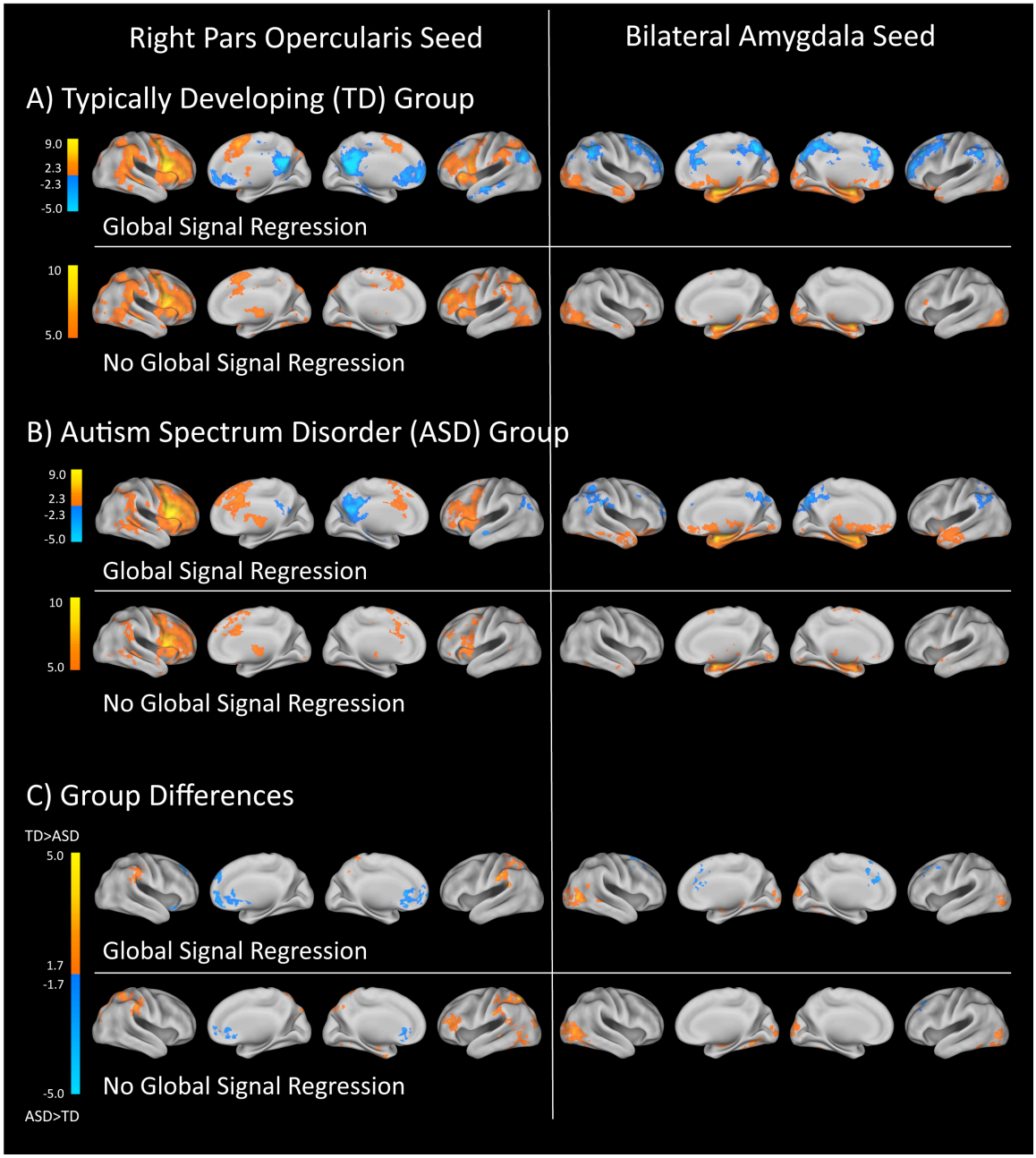

Figure 1.3. Whole brain connectivity analyses performed with and without global signal regression (GSR). Connectivity maps for global signal regression and no global signal regression for A) typically developing within group B) Autism Spectrum Disorder within group and C) direct between group contrasts. Z-statistics we rendered on the Inflated PALS B12 brain using CARET. Within group maps are thresholded at $Z > 2.3$ for within group maps with global signal regression, $Z > 5.0$ ($p < 0.0000003$) for within group maps without global signal regression, $Z > 1.7$ ($p < 0.05$) for between group contrasts, and corrected for multiple comparisons at the cluster level ($p < 0.05$).

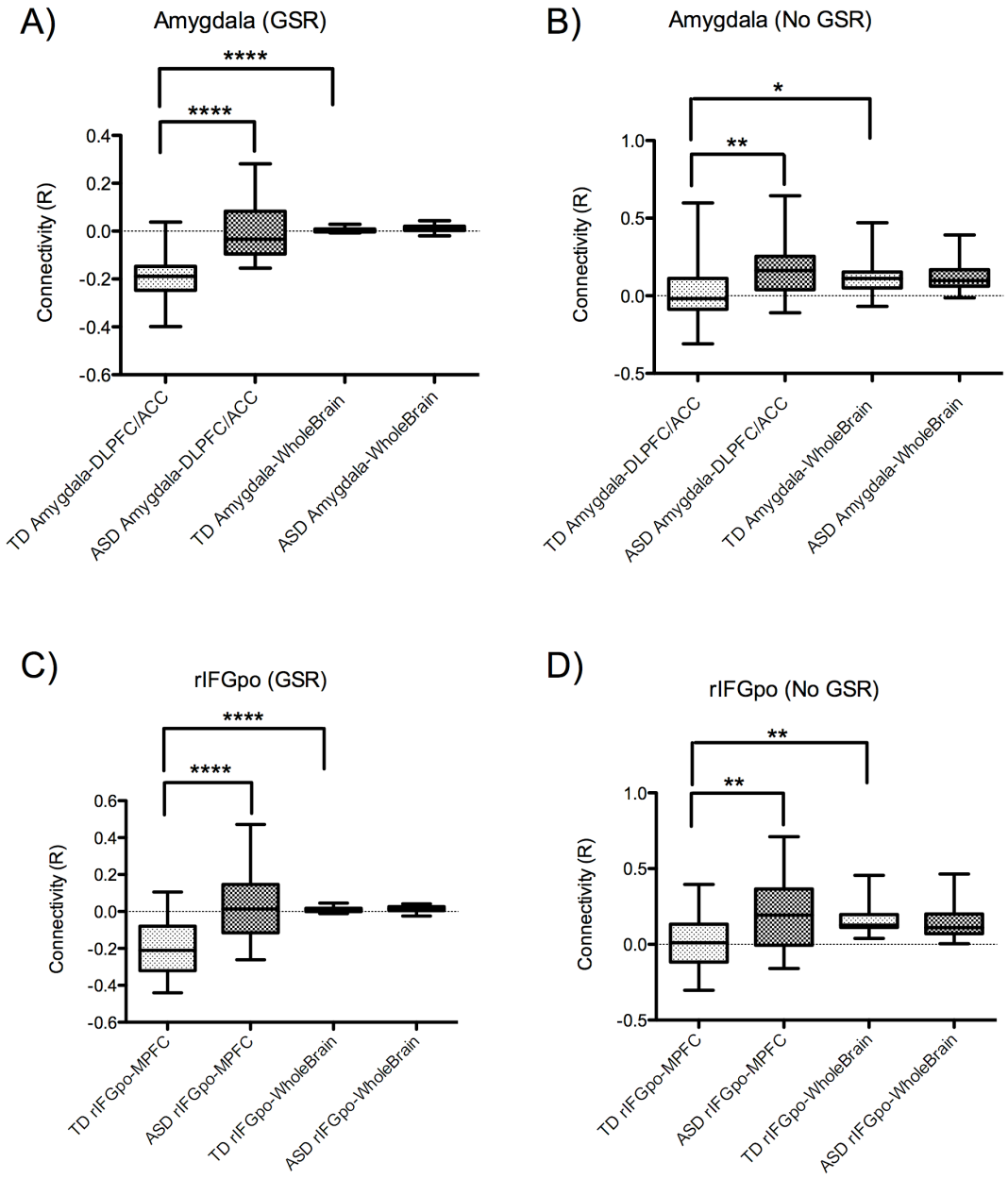

Figure 1.4. ROI analyses performed with and without global signal regression (GSR). A) Amygdala-DLPFC/ACC and Amygdala-WholeBrain connectivity with GSR for typically developing (TD) and Autism Spectrum Disorder (ASD) ASD groups. B) Amygdala-DLPFC/ACC and Amygdala-WholeBrain connectivity without GSR for TD and ASD groups. C) rIFGpo-MPFC and rIFGpo-WholeBrain connectivity with GSR for TD and ASD groups. D) rIFGpo-MPFC and rIFGpo-WholeBrain connectivity without GSR for TD and ASD groups. * $p < 0.05$, ** $p < 0.01$, *** $p < 0.001$, **** $p < 0.0001$.

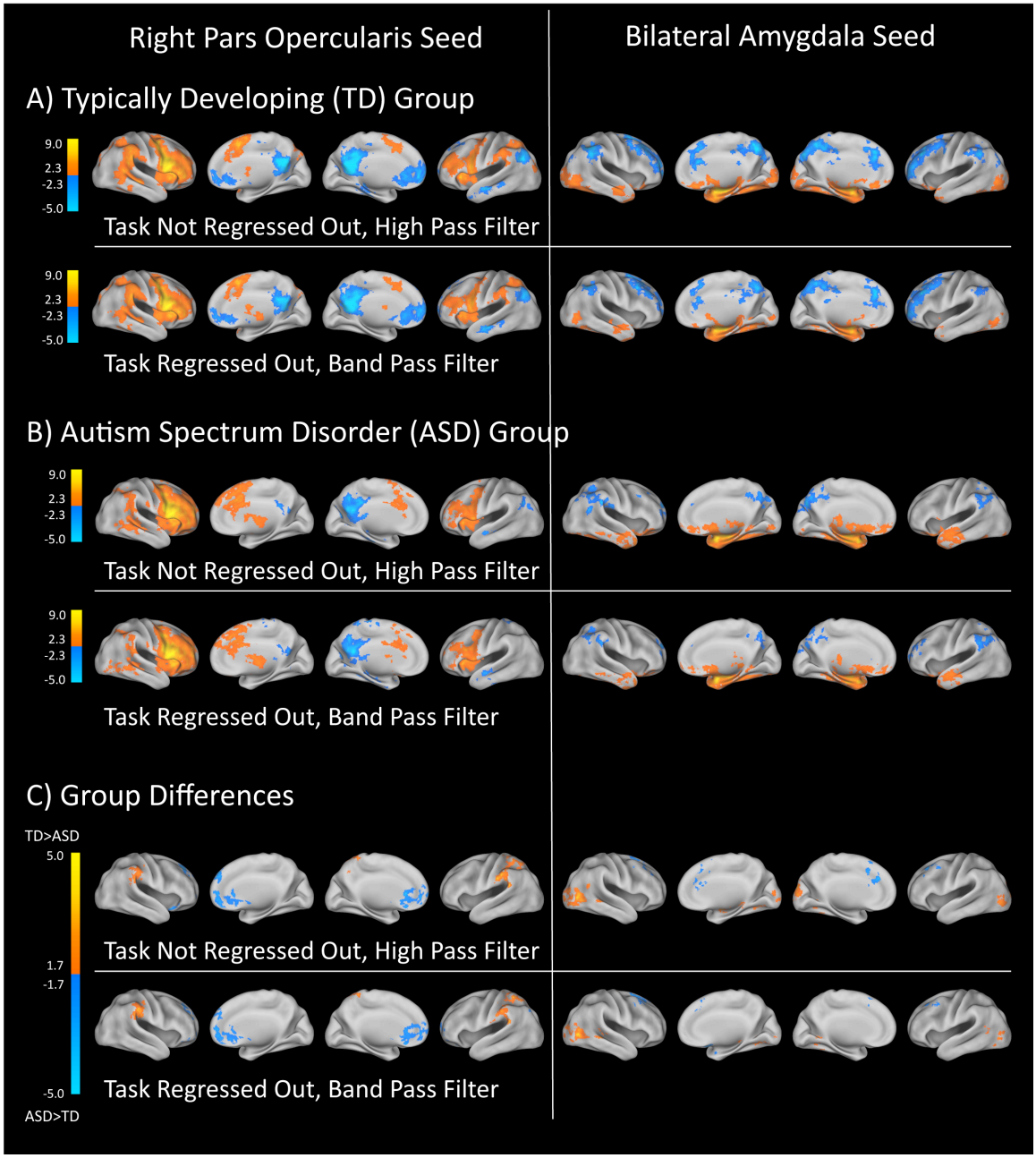

Figure 1.5. Whole brain connectivity analyses performed with or without task regression and bandpass filtering. Connectivity maps without task regression and with task regression and bandpass filtering for A) typically developing within group B) Autism Spectrum Disorder within group and C) direct between group contrasts. Z-statistics we rendered on the Inflated PALS B12 brain using CARET. Within group maps are thresholded at $Z > 2.3$ for within group maps with global signal regression, $Z > 1.7$ ($p < 0.05$) for between group contrasts, and corrected for multiple comparisons at the cluster level ($p < 0.05$).

CHAPTER 2: Altered Functional and Structural Brain Network Organization in Autism

Abstract

Structural and functional underconnectivity have been reported for multiple brain regions, functional systems, and white matter tracts in individuals with autism spectrum disorders (ASD). Although recent developments in complex network analysis have established that the brain is a modular network exhibiting small-world properties, network level organization has not been carefully examined in ASD. Here we used resting-state functional MRI (n=42 ASD, n=37 Typically Developing; TD) to show that children and adolescents with ASD display reduced short and long-range connectivity within functional systems (i.e., reduced functional integration) and stronger connectivity between functional systems (i.e., reduced functional segregation), particularly in default and higher order visual regions. Using graph theoretical methods, we show that pairwise group differences in functional connectivity are reflected in network level reductions in modularity and clustering (local efficiency), but shorter characteristic path lengths (higher global efficiency). Structural networks, generated from diffusion tensor MRI derived fiber tracts (n=51 ASD, n=43 TD), displayed lower levels of white matter integrity and modularity in ASD. TD and ASD individuals exhibited similar levels of correlation between raw measures of structural and functional connectivity (n=35 ASD, n=35 TD). However, a principal component analysis combining structural and functional network properties revealed that the balance of local and global efficiency between structural and functional networks was reduced in ASD, positively correlated with age, and inversely correlated with ASD symptom severity. Overall, our findings suggest that modeling the brain as a complex network will be highly informative in unraveling the biological basis of ASD and other neuropsychiatric disorders.

Introduction

Autism spectrum disorders (ASD) are increasingly prevalent neurodevelopmental disorders (Kim et al. 2011) characterized by atypical social behavior, including deficits in receptive and expressive language, theory of mind, and mental flexibility. Findings of functional underconnectivity between brain regions in individuals with ASD relative to matched controls have been reported as they perform a variety of cognitive tasks (see Schipul et al., 2011, for review). Multiple studies have found that task-independent (i.e., intrinsic) functional connectivity, including interhemispheric (Anderson et al., 2011a) and default mode network (DMN) connectivity is also lower in ASD (e.g., Kennedy et al., 2008). Further supporting an underconnectivity theory, diffusion tensor imaging (DTI) studies have found reductions in structural white matter integrity across most major tracts (see Vissers et al., 2011, for review).

In addition to reports of reduced functional connectivity *within* major networks (i.e., functional integration), connectivity *between* different networks (i.e. functional segregation) is altered in ASD (Rudie et al., 2011). Functional brain networks become simultaneously more integrated and segregated during typical development (e.g., Fair et al., 2009) and white matter integrity increases during development (e.g., Lebel et al., 2012), suggesting that brain networks in ASD may reflect 'immature' or aberrant developmental processes.

Despite this array of regional and systems level findings in ASD, it is unclear how these alterations might be reflected at a network level where the brain is modeled as a network of hundreds of interacting regions composing several integrated and segregated systems. Graph theory, which describes complex systems as a set of "nodes" (i.e., brain regions) and "edges" (i.e., connections between nodes), has characterized the brain as a complex network with a hierarchical modular organization consisting of several major functional communities (i.e., visual, sensorimotor, default mode, and attentional systems; see Wang et al., 2010, for review). Structural and functional brain networks exhibit robust levels of local and global efficiency (i.e.,

small-world properties; Watts and Strogatz, 1998) that can be quantitatively characterized using graph theoretical methods (Bullmore et al., 2009; Rubinov et al., 2009). Structural and functional graph theoretical studies have begun to map how local and global network properties change during development (Fair et al., 2009; Hagmann et al., 2010), aging (e.g., Meunier et al., 2009) and in diseases such as schizophrenia (e.g., Bassett et al., 2008) and Alzheimer's (e.g., Supekar et al., 2008).

In this study we sought to compare functional and structural connectivity in children and adolescents with ASD relative to typically developing (TD) children by characterizing local and global graph theoretical metrics of structural and functional networks using a recently validated 264-region functional parcellation scheme (Power et al., 2011). We sought to first compare simpler network connections and then characterize higher-level network properties including clustering, characteristic path length, small worldness and modularity. Additionally, since structural connectivity has been shown to correlate with functional connectivity (Hagmann et al., 2008; Honey et al., 2009), we wanted to determine whether structure-function correlations differed between groups and how functional and structural network properties relate to each other across development in TD and ASD individuals.

Materials and Methods

Subjects

High-functioning children and adolescents with ASD, as well as TD children and adolescents, were recruited through UCLA's Center for Autism Research and Treatment (CART) and flyers posted throughout the greater Los Angeles area. Individuals with metal implants, psychiatric or neurologic disorders, structural brain abnormalities, or known genetic conditions were excluded from participation. Informed consent and assent to participate was obtained prior to assessment according to protocols approved by the UCLA Institutional Review

Board (IRB). Verbal, performance, and overall intelligence were assessed for each participant using the Wechsler Abbreviated Scale of Intelligence (WASI; Wechsler 1991) or the full Wechsler Intelligence Scale for Children (WISC; Wechsler 1999). High-functioning children with ASD had a prior clinical diagnosis of autism based on criteria from the Diagnostic and Statistical Manual of Mental Disorders (DSM IV), which was confirmed with the Autism Diagnostic Observation Scale (ADOS-G; Lord et al., 2000) and/or Autism Diagnostic Interview (ADI-R; Lord et al., 1994).

A total of 60 individuals with ASD (52 males, 8 females) and 45 TD individuals (38 males, 7 females) were included in either the DTI, resting state or combined resting state/DTI final matched datasets (**Table 2.1**). After excluding subjects with excessive head motion, the resting state sample included 42 ASD subjects and 37 TD subjects and the DTI sample included 51 ASD subjects and 43 TD. Both structural and functional data were available for 35 ASD and 35 TD subjects. The three sets of matched groups did not significantly differ based on age, sex, mean/maximum head motion, or full-scale, verbal and performance IQ (**Table 2.1**).

Twenty-two individuals with ASD and one TD individual reported the use of one or more psychotropic medications. One TD subject was using a psychostimulant. Of the subjects in our ASD sample, 12 were taking psychostimulants, 5 were taking sympatholytics, 9 were taking atypical antipsychotics, 9 were taking selective serotonin reuptake inhibitors, 3 were taking selective norepinephrine reuptake inhibitors, 3 were taking an atypical antidepressant, and 2 were taking anticonvulsants. There were no significant differences ($ps > 0.30$) between medicated and unmedicated ASD individuals for each of the functional and structural measures described in the following sections.

MRI Data Acquisition

All resting-state fMRI and DTI scans were acquired on a Siemens 3T Trio at UCLA. A

scout localizing scan was collected to help prescribe the orientation of the scans. Next, a matched bandwidth T2-weighted high-resolution echo planar scan was acquired co-planar to the functional images, which ensures identical distortion characteristics for registration purposes (Siemens 3T Trio: TR=5000ms, TE=34ms, matrix size: 128x128, 19.2cm FoV, 36 4-mm thick slices with an in-plane voxel dimension of 1.50x1.50mm). In a single session, subjects were asked to relax and keep their eyes open while a fixation cross was displayed on a white background for 6 minutes (T2*-weighted functional images: TR=3000ms, TE=28ms, matrix size 64x64, 19.2cm FoV, 34 4-mm thick slices (no gap) with an in-plane voxel dimension of 3.0x3.0mm). The DTI sequence consisted of 32 scans with different diffusion-weighted directions (b=1000 s/mm^2), three scans with no diffusion sensitization, at b=0, and an additional six scans at b=50 s/mm^2. Other parameters were TR=9500ms, TE=87ms, GRAPPA on, FOV=256mm, with 75 slices, yielding an in-plane voxel dimension of 2x2mm with 2-mm thick axial slices, total scan time=8min 1sec.

Resting State fMRI Preprocessing

Imaging data were analyzed using FSL version 4.1.4 (FMRIB's Software Library, www.fmrib.ox.ac.uk/fsl; Smith et al., 2004) and AFNI (Analysis of Functional NeuroImages; Cox et al., 1996). Structural and functional images were skull-stripped using AFNI (3dskullstrip and 3dautomask). Functional volumes were motion corrected to the mean functional volume with MCFLIRT (Motion Correction using FMRIB's Linear Image Registration Tool) using a normalized correlation ratio cost function and sinc interpolation (Jenkinson et al., 2002). Translations and rotations in the *x*, *y*, and *z* dimensions were calculated from volume to volume and averaged to generate mean and max relative displacement values, which did not significantly differ between the final matched groups (**Table 2.1**). Subjects with a single displacement greater than 2.5 mm (13 ASD and 5 TD) were excluded prior to further analyses and not included in totals for the

final samples. Images were spatially smoothed using a Gaussian kernel of FWHM 5mm and band pass filtered (0.1 Hz > *t* > 0.01 Hz). The 6 rigid body motion parameters and average white matter (WM), cerebrospinal fluid (CSF), and global time-series and their temporal derivatives were then regressed out of the data. The WM and CSF time-series reflected signal from subject-specific regions of interest created using FAST (FSL's Automatic Segmentation Tool). Given recent concerns regarding the effect of motion in resting state fMRI connectivity (Power et al., 2012; Van Dijk et al., 2011), in addition to matching the groups by mean and maximum relative head motion, we also regressed out individual volumes with large signal intensity changes (i.e., motion spikes) by creating additional nuisance regressors that modeled individual time points with greater than half of a standard deviation change in global signal intensity.

Resting State fMRI Connectivity Matrix Construction

One major methodological hurdle in graph theory approaches to neuroimaging is how to define the nodes of the network (Wang et al., 2009; Zalesky et al., 2010; Craddock et al., 2011; Power et al., 2011). Most groups have used anatomical atlases (e.g. He et al., 2007) or individual voxels (e.g., van den Huevel et al., 2008) as nodes. However, anatomical atlases include relatively large regions that are likely to contain multiple functional regions, which can distort/obscure true properties of the network by mixing distinct signals (Butts et al., 2009; Smith et al., 2011; Craddock et al., 2011; Power et al., 2011). Conversely, voxel-wise parcellation approaches can be biased by artificially strong local connections (Power et al., 2011; 2012). A whole brain parcellation scheme was recently created based on a large meta-analysis of fMRI studies combined with whole brain functional connectivity mapping (Power et al., 2011). This set of 264 putative functional regions was shown to more accurately represent the information present in the network relative to voxelwise and atlas-based parcellation approaches. Therefore, we chose this set of 264 regions for whole brain parcellation. For each subject, 5-mm radius

spheres based on the MNI coordinates of these 264 regions (Power et al., 2011) were registered to functional space (12 DOF, affine, correlation ratio cost function) through registration from the MNI 152 template to the high-resolution echo-planar (12 DOF, affine, mutual information cost function) using FSL's Linear Image Registration Tool (FLIRT). We then correlated timeseries between each of the 264 brain regions and z-transformed correlation coefficients in order to generate 264x264 whole brain functional connectivity matrices for each subject. Graph theoretical metrics and statistics were computed with Matlab (The Mathworks, Natick, MA) using the Brain Connectivity Toolbox (Rubinov et al., 2009).

To determine the most stable number of modules, the Louvain modularity algorithm (Blondel et al., 2008) was run 100 times on the average unthresholded functional connectivity matrix. The order of nodes in the functional connectivity matrix was then reorganized based on its modular organization (**Figure 2.1A)**. In order to interrogate raw differences in connection strengths between the two groups, two-sample t-tests were performed for every z-transformed connection strength value (**Figure 2.1C**). The significance was set at $p < 0.05$, uncorrected, for these initial exploratory analyses. If there was significantly lower connectivity in a connection for the ASD or TD group (vs. the other group) that had an average correlation value below zero, it was categorized as stronger negative connectivity for that group (as opposed to stronger positive connectivity for the other group, which is mathematically equivalent). The number of connections differing between groups was assessed for each of the identified modules both for within-module positive connections and between-module negative connections (**Figure 2.1D**). Numbers of within-module positive and between-module negative connections differing between groups were compared and displayed as a function of the connection's average *z*-transformed correlation value (**Figure 2.2A**) and Euclidean distance between regions (**Figure 2.2B**).

Resting State fMRI Connectivity Graph Theoretical Analyses

As there is no rationale for using a particular cutoff for functional connectivity strength to determine whether an edge exists in a functional network, we compared local and global network properties over a range of functional connection thresholds. Thresholding a network based on correlation strength can yield different network sparsities (number of existing edges divided by number of possible edges), which influence network properties and can bias a comparison of graph metrics between groups. In fact, we found that at higher z-correlation thresholds the TD group had a higher average sparsity (**Figure 2.3A**). Therefore, we chose to equalize network sparsity between subjects by taking an equivalent percentage of the strongest positive connections for each subject and binarizing the network weights before calculating graph theoretical metrics. We examined functional network properties between 15% and 32% sparsity. The upper threshold of 32% was chosen because the weakest edge it includes corresponds to a z-transformed correlation coefficient of 0.15, which is the minimum correlation needed to be statistically significant ($p < 0.05$) across 120 volumes. At lower sparsity levels, network properties begin to break down as the network becomes fragmented. Therefore, we chose 15% sparsity (corresponding to a minimum average z-transformed correlation of 0.34) as the low end of the range based on the requirement that all individual subject graphs be fully connected (**Figure 2.3B**).

We focused on 6 global graph theoretical metrics (see Rubinov et al., 2009 for formulas of these metrics). These metrics were: *clustering coefficient* (CC), which measures how much neighbors of a node are connected to each other and is closely related to local efficiency; *characteristic path length* (CPL), which is the average number of edges needed to get from any node in the network to any other node in the network and is inversely related to global efficiency; normalized CC and CPL (*lambda* and *gamma*), which are calculated as a ratio of CC or CPL to the average CC or CPL of 100 simulated random networks with equivalent numbers of nodes and edges; *small worldness*, which is the ratio of lambda to gamma (Watts et al.,

1998); and *modularity*, which refers to the existence of subgraphs or distinct communities within the network as a whole. Modularity Q values represent the proportion of within-module edges in the network minus within-module edges calculated from a similar random network (Newman 2006). Since Q values can vary based on random differences in module assignments from run to run, Q values were averaged over 100 iterations of the algorithm. All metrics were averaged across 15% to 32% sparsities in 1% increments to generate average values for each metric. Two sample t-tests were performed on these metrics between subjects at each sparsity level and for averaged metrics (**Table 2.2**, **Figure 2.3C-H**). For each node, clustering coefficients, participation coefficients and betweenness centrality were averaged across sparsity levels for each subject and compared between groups (**Figure 2.4A**). Betweenness centrality measures how often the shortest path goes through a given node while participation coefficients reflect how much a node interacts with nodes in different communities (Guimera et al., 2005). Differences in nodal metrics are shown at more stringent (False Discover Rate: $q < 0.05$; Benjamini et al., 1995) and less stringent thresholds ($p < 0.05$, uncorrected).

Diffusion MRI Preprocessing

Subjects with excessive motion (greater than 8 volumes with motion artifacts) were not included in final samples (6 ASD, 3 TD). Additionally, individual volumes with gross motion artifacts (i.e., exceeding 2mm displacement) were identified and excluded from further analysis. MCFLIRT was used to quantify mean and maximum relative motion (**Table 2.1**); while, motion and eddy current correction was performed on the diffusion-weighted images using eddy_correct in FMRIB's Diffusion Toolbox (FDT). Dtifit was used to fit a diffusion tensor model to the data at each voxel and calculate voxelwise Fractional Anisotropy (FA) values for each subject. Whole brain deterministic tractography was then performed using the fiber assignment by continuous tracking (FACT) algorithm (Mori et al., 2002) in Diffusion Toolkit

(http://trackvis.org/dtk). Tractography was carried out propagating fibers from each voxel with a maximum turn angle of 50 degrees. Fibers were smoothed using a spline filter and fibers shorter than 5mm were excluded.

Diffusion MRI Fiber Connectivity Matrix Construction

We used the same set of 264 coordinates from Power et al. (2011) to generate 10mm radius spheres in MNI space. Dilating spheres to 10mm radii (relative to 5mm radii spheres for functional nodes) ensured inclusion of nearby white matter fibers given that nodal coordinates were centered in grey matter. These 264 masks were transformed to each subject's diffusion space (12 DOF, affine, correlation ratio cost function) through registration to the hires image (12 DOF, affine, mutual information cost function). In order to generate edges between nodes of structural networks, the number of fibers connecting each region were counted. A fiber was defined as connecting two regions if one fiber endpoint terminated within one region and the other endpoint terminated within the other region. This process was repeated using all 264 regions as seeds in order to derive a 264x264 whole brain structural connectivity matrix for each subject, using custom software written for this purpose (UCLA Multimodal Connectivity Package; http:/ /github.com/jbrown81/umcp). Additionally, average FA and mean diffusivity (MD) were calculated for each connection.

The Louvain modularity algorithm (Blondel et al., 2008) was run 100 times on the average unthresholded fiber connectivity matrix to determine the most stable number of modules. The order of nodes in the fiber connectivity matrix was reorganized based on their modular organization (**Figure 2.5A)**. Two sample t-tests ($p < 0.05$, uncorrected for initial exploratory analyses) were performed on fiber counts, FA, and MD for every connection after masking by connections that have an average of 5 or more fibers (5.75% of all possible connections; **Figure 2.5B,C**). Connections differing between groups for number of fibers and

MD were compared as a function of average fibercount and Euclidean distance.

Structural Connectivity Graph Theoretical Analyses

For structural networks, we examined the same 6 global network properties as functional networks (CC, CPL, lambda, gamma, small worldness and modularity Q values) averaged between 5% and 8.5% sparsity in 0.5% increments. A sparsity level of 5% represented the minimum sparsity level at which every subject's graph was fully connected (**Figure 2.6A**) and 8.5% represented the average unthresholded sparsity of all subjects structural matrices (**Figure 2.6B**). Two sample t-tests were performed on these metrics between subjects for averaged metrics as well as at each sparsity level.

Correlation Between Fiber Count and Functional Connectivity Strengths

Fiber counts of every connection with an average of at least 5 fibers were correlated with functional connectivity strengths for each of the 35 ASD and 35 TD subjects (**Figure 2.7**). Additionally, fiber count/functional connectivity correlations were computed for within- and between-module connections and specifically for within-module connections with lower levels of functional connectivity as identified in **Figure 2.1C**. These structure-function correlations were z transformed, then compared between groups (with two-sample t-tests).

Principal Component Analysis of Functional and Structural Network Properties

We ran an exploratory principal component analysis (PCA) on the six average functional global graph metrics and the six average structural graph global metrics across all 70 subjects with PASW Statistics 18, Release Version 18.0.3 (SPSS, Inc., Chicago, IL). Values for the first four components were computed for each subject through regression, compared between groups (two sample t-test), and correlated with chronological age after regressing out mean

relative motion (**Table 2.3; Figure 2.8A,B**). The two components that significantly differed between groups were also tested for correlation with symptom severity (as measured by the social and communication subscales of the ADOS and ADI) within the ASD group after regressing out mean relative motion and age (**Table 2.3**; **Figure 2.8C-F**).

Graph Renderings and Visualizations

Renderings were generated from scripts in the UCLA Multimodal Connectivity Package (http://github.com/jbrown81/umcp) and through the UCLA Multimodal Connectivity Database (http://umcd.humanconnectomeproject.org), which use matplotlib (http://matplotlib.sourceforge.net) and networkX (http://networkx.lanl.gov).

Results

Functional Connectivity Matrices

Over the course of 100 runs of the modularity algorithm on the average functional connectivity matrix, four communities were detected over 90% of the time. The order of nodes in the matrix was reorganized to reflect its community structure for the connectivity matrix averaged across all subjects (**Figure 2.1A)**. The four communities corresponded to visual, sensorimotor and default systems as well as a largely frontal system corresponding to the task positive control/attention network (color boxes in **Figure 2.1A** and displayed in 3D brain space in **Figure 2.1B**).

We first examined raw differences in the connectivity matrices by directly comparing correlation strengths between groups for each connection (**Figure 2.1C**) and separating differences based on within- and between-community connections. We found that the TD group exhibited 5.4 times as many stronger ($p < 0.05$, uncorrected) within-module positive connections

as the ASD group (**Figure 2.1C,D**). This was most pronounced in the default (265 (10.1%) connections stronger for TD group vs. 15 (0.5%) stronger for ASD), visual (107 (7.5%) connections stronger for TD group vs. 7 (0.5%) stronger for ASD) and sensorimotor systems (84 (2.5%) connections stronger for TD group vs. 33 (1.0%) stronger for ASD; **Figure 2.1D**, left). There were a similar number of stronger within-module connections for the attention/control network (34 (2.3%) connections stronger for TD group vs. 41 (2.3%) stronger for ASD). Additionally, the TD group exhibited 4.4 times as many stronger (p < 0.05, uncorrected) negative (i.e., weaker) between-module connections. This was most prominent for connections between other systems and the default (670 (4.8%) for TD>ASD vs. 152 (1.1%) for ASD>TD) system, but was also true for visual (383 (3.4%) for TD>ASD vs. 135 (1.2%) for ASD>TD), sensorimotor (479 (3.2%) for TD>ASD vs. 154 (1.0%) for ASD>TD), and attention (276 (2.4%) for TD>ASD vs. 165 (1.5%) for ASD>TD) systems (**Figure 2.1D**, right).

We sorted within and between-module differences as a function of average correlation strengths (**Figure 2.2A**). Connections where the TD group had stronger positive within-module connectivity tended to have higher average correlation strengths than connections where the ASD group had stronger within-module connectivity (TD = 0.26+/-0.19, ASD = 0.16+/-0.17, p = 0.0002). Between-module connections where the TD group had stronger negative connectivity were more negative than the connections where the ASD group had stronger negative connections (TD = -0.16+/-0.09, ASD = -0.08+/-0.06, p < 0.0001). We found no significant differences (all p > 0.25) for the average Euclidean distance of connections that differed between groups for stronger positive within-module connectivity or stronger negative between-module connectivity (**Figure 2.2B**).

Functional Connectivity Graph Metrics

There were group differences in nearly all graph theoretical metrics for functional networks over a range of network sparsities (**Figure 2.3**) and averaged across sparsity levels (**Table 2.2**). Clustering coefficient was significantly lower in the ASD group (**Figure 2.3C**) and although lambda was lower in the ASD group at higher sparsity levels (**Figure 2.3D**), there was only a trend for lower average gamma. Both CPL and gamma were lower in the ASD group over the entire range of sparsities (**Figure 2.3E,F**) and averaged across sparsity levels (**Table 2.2**). Both TD and ASD subjects had functional networks in the small world range (the ratio of lambda to gamma being greater than 1.2). However, small worldness was not significantly different between groups. Modularity (Q values) was significantly lower in the ASD group at every sparsity level and averaged across sparsity levels (**Figure 2.3H**).

Given the differences in global metrics for CC, CPL and modularity, we compared nodal clustering coefficients, participation coefficients (Guimera et al., 2005) and betweenness centrality measures between groups averaged over the same range of thresholds (**Figure 2.4**). We report the number of nodes with significant between-group differences ($p < 0.05$ uncorrected and FDR corrected; $q < 0.05$, $p < 0.0013$). ASD subjects had lower nodal CC in 21 visual (4 FDR: right occipital fusiform gyrus and left and right inferior lateral occipital cortex), 20 default (3 FDR: medial prefrontal cortex, ventromedial prefrontal cortex and left frontal orbital cortex), and 10 sensorimotor nodes (1 FDR: left superior parietal lobule; **Figure 2.4A**). Participation coefficients were higher for the ASD group in 26 default (3 FDR: medial prefrontal cortex and left frontal orbital cortex), 10 sensorimotor (3 FDR: left postcentral gyrus, left superior parietal lobule and brainstem) and 9 attention (0 FDR) nodes (**Figure 2.4B**). There were no differences in nodal betweenness centrality that survived FDR correction.

Structural Connectivity Matrices

The Louvain modularity algorithm detected between 8 and 10 communities for the average fiber connectivity matrix over 100 runs. Nine communities were detected in over 80% of the runs and these communities corresponded to sets of lateralized nearby brain regions (**Figure 2.5B**). The average fiber structural connectivity matrix for all TD and ASD subjects is shown in **Figure 2.5A** after reordering the nodes by community structure.

We first examined the connectivity matrices by directly comparing the number of fibers, average FA, and average MD values for each connection between groups after masking for regions that contained an average of at least 5 fibers (corresponding to 5.75% of all possible connections). We found that the ASD group had 4.2 times as many connections with significantly (p < 0.05, uncorrected) more fibers than the TD group (106 ASD>TD vs. 25 TD>ASD; **Figure 2.5C**). We also found that the ASD group had 1.6 times as many connections with lower FA (67 TD>ASD vs. 41 ASD>TD) and 6.2 times as many connections with higher MD (112 ASD>TD vs. 18 ASD>TD; **Figure 2.5D**).

The average number of fibers or Euclidean distance of the connection did not differ for connections where the ASD group had more fibers compared to connections where the TD group had more fibers (Number of fibers: TD>ASD = 30.0+/-26.6, ASD>TD = 26.3+/-25.9, p = 0.53; Euclidean distance: TD>ASD = 25.9 +/-12.8, ASD>TD = 34.8+/-26.3, p = 0.11). Connections where the TD group had higher white matter integrity (lower MD) had a higher average number of fibers than connections where the ASD group had higher white matter integrity (ASD>TD = 32.5+/-28.8, TD>ASD = 11.8+/-6.0, p = 0.003), but did not differ based on Euclidean distance (ASD>TD = 30.3+/-21.5, TD>ASD = 35.2+/-7.5, p = 0.34).

Structural Connectivity Graph Metrics

Although gamma (normalized characteristic path length) was similar for structural and functional networks (~1.2 for structural vs. ~1.1 for functional), lambda (normalized clustering coefficient) was much higher in structural networks (~5.4 for structural vs. ~2.2 for functional). Therefore, structural networks displayed higher levels of small worldness compared to functional networks in both TD and ASD groups. Measures for average structural CC, gamma, CPL, lambda and small worldness did not significantly differ between groups (**Table 2.2**). However, modularity Q values were higher in the TD group at all sparsity levels (**Figure 2.6C**). Given previous reports of modularity decreasing with age and global efficiency increasing with age in structural networks (Hagmann et al., 2010), we ran post-hoc analyses correlating these metrics with chronological age in each group. Higher modularity in the TD group was actually driven by the younger TD participants, whereby, controlling for motion, modularity was significantly negatively correlated with age in the TD group (r = -0.41, p = 0.008; **Figure 2.6D**) yet was only trending toward a negative correlation with age in the ASD group (r = -0.24, p = 0.08) although the interaction was not significant (p = 0.37). Similarly, there were no group differences for CPL or lambda, but age was negatively correlated with CPL and lambda in the TD group (controlling for motion: CPL: r = -0.34, p = 0.03; lambda r = -0.31, p = 0.04), and CPL and lambda were positively correlated with age in the ASD group (controlling for motion: CPL: r = 0.22, p = 0.12; gamma: r = 0.16, p = 0.25; **Figure 2.6F**) whereby there was a significant group by age interaction for CPL (p = 0.01) and gamma (p = 0.02).

Structure-Function Correlation

When comparing correlations between fiber counts and functional connectivity strength between groups, we found that both groups exhibited moderate, yet highly significant (all

subjects $p < 0.001$), levels of structural-functional connectivity correlations (TD $r = 0.32+/-0.03$, ASD r = 0.32+/-0.04, $p = 0.77$ for the group difference). Furthermore, there were no group differences when structure-function correlations were assessed for both within- and between-functional module connections (Within-module: TD $r = 0.28+/-0.04$, ASD $r = 0.28+/-0.05$, $p = 0.98$ for the group difference; between-module TD $r = 0.28+/-0.05$, ASD $r = 0.26+/-0.05$, $p = 0.32$ for the group difference) or specifically for within-module connections exhibiting lower levels of functional connectivity (TD $r = 0.30+/-0.12$, ASD $r = 0.31+/-0.11$, $p = 0.77$ for the group difference).

Principal Component Analysis of Structural and Functional Metrics

To identify key factors underlying correlated graph metrics and to better understand relationships between structural and functional network properties, we entered the six functional and six structural average global graph metrics for all 70 subjects into an exploratory principal component analysis. The first four components explained 88% of the variance in the data (**Table 2.3**). The first component (accounting for 33.9% of the variance) broadly weighted functional metrics positively and structural metrics negatively. This component was significantly lower in the ASD group (covarying for mean head motion, $p = 0.009$) and negatively related to symptom severity, as measured by the ADI social subscale (covarying for age and mean head motion, $r = -0.4$, $p = 0.01$; **Figure 2.8C**). The first component was also positively correlated with age in both groups (covarying for mean motion; All $r = 0.24$, $p = 0.04$, TD $r = 0.28$, $p = 0.11$, ASD $r = 0.30$, $p = 0.08$; **Figure 2.8A**). The second component weighted all functional and structural metrics positively, and although it did not differ between groups, there was a significant interaction with age (covarying for mean head motion; $p = 0.02$), whereby the second component was significantly positively correlated with age in the ASD group ($r = 0.35$, $p = 0.04$) and slightly negatively correlated with age in the TD group ($r = -0.24$, $p = 0.16$). The third

component, positively weighting functional CC/modularity and negatively weighting functional CPL, did not differ between groups. The fourth component, positively weighting structural modularity and negatively weighting structural CPL, was significantly lower in the ASD group (p = 0.007) and was negatively correlated with symptom severity as measured by the ADOS social and communication subscales (covarying for age and mean head motion, ADOS social: r = -0.46, p = 0.005, **Figure 2.8E**; ADOS communication: r = -0.36, p = 0.05, **Figure 2.8F**).

Discussion

Previous neuroimaging studies on ASD have reported reduced functional and structural connectivity both within and between specialized brain systems (Vissers et al., 2012), suggesting ASD is a network disorder (Muller et al., 2007). Here we expand upon previous findings of lower functional and structural connectivity in ASD by characterizing higher-level network properties using tools derived from the physics of complex networks (Rubinov et al., 2009). We report alterations in community organization of functional networks, as well as in the balance of local and global efficiency within and between structural and functional networks in children and adolescents with ASD relative to their typically-developing counterparts.

Functional Connectivity Alterations

We detected robust reductions in positive functional connectivity within major functional systems (i.e., functional integration) in individuals with ASD. Reduced functional connectivity was most prominent in the default system, consistent with multiple studies that have found reduced DMN connectivity in ASD (Kennedy et al., 2008; Weng et al., 2010; Assaf et al., 2010). However, we also found weaker connectivity within visual (largely secondary areas) and

sensorimotor systems, supporting more widespread alterations in functional connectivity as found by Villallobos et al. (2005), Mostofsky et al. (2009), and Anderson (2011b). Relatively few alterations were observed in the frontal attention/cognitive control network, which might reflect relatively intact cognitive skills in high-functioning individuals with ASD (Kennedy et al., 2008).

Interestingly, individuals with ASD also show reduced negative (i.e., more positive) connectivity *between* systems. Consistent with previous findings in the task positive and default mode networks in ASD (Rudie et al., 2011), weaker negative connectivity between communities suggests that specific functional systems are less distinct or functionally segregated from one another. Although there is some controversy regarding the proper interpretation of negatively correlated brain regions when using global signal regression (GSR; Murphy et al., 2009; Fox et al., 2009), anticorrelations are detected without GSR (Chang et al., 2009; Anderson et al., 2011c; Smith et al., 2012) and GSR maximizes the specificity of positive resting-state correlations in real and simulated data (Weissenbacher et al., 2009; Fox et al. et al., 2009). Interestingly, reduced negative connectivity was recently shown to be useful for diagnostic classification of autism in analyses without GSR (Anderson et al., 2011b). Therefore, although it is unclear whether widespread differences in negatively connected regions are exaggerated by GSR, differences in negative connectivity between distinct functional systems are likely important for understanding ASD neurobiology.

Although most previous functional connectivity studies of ASD have reported underconnectivity of long-range (i.e., anterior-posterior or interhemispheric) connections, it has also been widely hypothesized that ASD may be related to *overconnectivity* of short-range connections (Belmonte et al., 2004; Courchesne et al., 2005; Geschwind & Levitt et al., 2007). Previous neuroimaging studies have found increased short-range connections in neurotypical children versus adults (Fair et al., 2009; Supekar et al., 2009) but findings are somewhat mixed in individuals with ASD (Paakki et al., 2010; Shukla et al., 2010). Consistent with a recent study

(Anderson et al., 2011b) we found that even short-range functional connections are reduced in ASD. Of course, this does not exclude the possibility that local connections at the neuronal or minicolumnar level could be enhanced in ASD (Casanova et al., 2002).

In examining graph metrics of functional networks, we found that individuals with ASD had lower clustering (i.e., local efficiency), especially in nodes within the default systems and secondary visual areas. Individuals with ASD displayed a less robust modular organization (i.e., communities were less distinct) and there was a tendency for nodes in the default and sensorimotor systems to interact more with other communities as measured by higher nodal participation coefficients. Finally, we found that functional brain networks in individuals with autism had shorter average path lengths (i.e., higher levels of global efficiency) as well as normalized characteristic path lengths. Randomly connected networks tend to have short path lengths (Sporns et al., 2011) suggesting the possibility that higher global efficiency in functional networks may simply reflect a less organized or more random distribution of functional edges. This is consistent with a study finding decreased complexity or increased randomness in resting-state fMRI timeseries of individuals with ASD (Lai et al., 2010).

Previous functional graph theory studies in typical development (Supekar et al., 2009; Fair et al., 2009) did not find differences in local or global efficiency between children and adults. However, our findings in ASD are reminiscent of developmental differences, as previous developmental studies report similar differences in the integration and segregation of functional systems. Therefore, although functional networks in ASD may be 'immature' in some ways (i.e., reflect an earlier developmental stage) they may also be fundamentally different from a network perspective.

Structural Connectivity Alterations

For structural connectivity measures derived from diffusion MRI, we found reduced

integrity in short- and long-range white matter tracts in ASD in line with previous studies (e.g., Shukla 2010). We found more robust differences in MD than FA, which has been reported in several previous DTI studies (Sundaram et al., 2008; Groen et al., 2010). Interestingly, despite the fact that white matter integrity was generally reduced, we found evidence for increased fiber counts in ASD, which may relate to early reports of increased regional white matter (Herbert et al., 2004) and more recent reports of increased fiber counts in certain tracts in ASD (Pugliese et al., 2009). Although white matter integrity is lower in children compared to adults, fiber counts increase during development (Lebel et al., 2012). Therefore, like functional networks, some alterations in ASD may reflect immaturity, while other alterations are likely to reflect *aberrant* processes.

Structural networks displayed high levels of local and global efficiency in both the TD and ASD groups. Given previous reports of decreasing modularity and increasing global efficiency of structural networks with development (Hagmann et al., 2010), we examined the relationship between age and modularity/global efficiency in each group. We found that in the TD group, modularity sharply decreased with age whereas global efficiency increased with age. In the ASD group, modularity decreased at a slower rate and, contrary to findings in the TD group, global efficiency actually decreased with age. It should be noted that global efficiency in structural networks likely reflects a different underlying substrate than global efficiency in functional networks given the physical wiring costs of structural networks. Thus, despite similar levels of local and global efficiency in structural networks across both groups, it appears as though network efficiency does not appropriately shift from a more local to a more distributed pattern during development in individuals with ASD.

Relationships Between Structure and Function

When relating structural and functional connectivity, we found that measures of fiber

counts and functional connectivity strength were moderately positively correlated in both groups with no group differences regardless of whether the connections were within or between modules or whether we only included connections with lower levels of functional connectivity. This finding, in addition to the fact that we generally saw higher fiber counts, suggests that alterations in functional connectivity in ASD are not directly related to alterations in fiber organization.

Interestingly, when we extracted the principal components underlying structural and functional network properties, we found that the largest underlying factor inversely weighted structural and functional network properties. This component inversely weighted local and global efficiency (i.e., positively weighted both CC and CPL) within functional and structural networks and was positively correlated with age. Although preliminary, this finding suggests that structural networks become more globally efficient, yet less locally efficient, during development while functional networks display a relative inverse pattern. This component was reduced in ASD and inversely related to social and communicative behavior, suggesting that the balance between structural and functional network properties is related to social impairments in ASD. Further highlighting differential age-related trajectories for functional and structural network properties, the second component, which positively weighted both structural and functional metrics, decreased with age in the TD group while it increased with age in the ASD group. Finally, the fourth component, which positively weighted local and global efficiency in structural networks, was reduced in ASD and inversely related to social and communicative symptom severity. Therefore, an underlying factor positively influencing both local and global efficiency in structural networks may also relate to disrupted social behavior in ASD.

Future Directions and Conclusion

Future studies should characterize younger and/or lower functioning individuals with ASD since our findings are limited to high-functioning children and adolescents with ASD. For example, studies examining infants at high risk for ASD may be useful for developing biomarkers to aid in earlier diagnosis and treatment. Future studies may also benefit from advances in imaging acquisition (Feinberg et al., 2010), more flexible modeling approaches (Smith et al., 2012), and large-scale studies involving collaboration between institutions (Biswal et al., 2010). Additionally, comparisons with other neuropsychiatric disorders, and teasing apart underlying mechanisms such as genetic risk factors (Scott-Van Zeeland et al., 2010; Brown et al., 2011; Dennis et al., in press) will all be crucial for a more complete characterization of brain network abnormalities in ASD.

To our knowledge, this is the first study to use complex network analyses to examine both structural and functional brain networks in autism. We found significant reductions in local efficiency and modularity within several functional networks. ASD children and adolescents also displayed atypical age-related changes in the balance of local and global efficiency between structural and functional networks. Further, this imbalance was related to the severity of socio-communocative deficits in individuals with ASD. Our findings suggest that complex network modeling of structural and functional brain organization will yield a better understanding of the neural basis of ASD and other neuropsychiatric disorders. Ultimately, a more cohesive framework for understanding brain alterations in ASD may inform the design of more sophisticated diagnostic tools and targeted interventions.

Table 1. Mean, Standard Deviation and Range of Sample Descriptives

Characteristic	Typically Developing	Autism Spectrum	*p* value
Resting State (RS) Sample			
Sample Size	37.0	42.0	
Number of Females	6.0	6.0	0.81
Age	13.0+/-2.0, 9.5-17.8	13.5+/-2.4, 9.3-17.9	0.30
Verbal IQ	108.4+/11.0, 86-127	103.6+/-12.7, 79-132	0.07
Performance IQ	105.2+/-11.9, 76-129	103.5+/-14.4, 72-134	0.57
Full Scale IQ	106.8+/-10.0, 84-128	103.3+/-14.0, 79-134	0.19
Mean Relative Head Motion (mm)	0.09+/-0.07, 0.03-0.37	0.11+/-0.07, 0.04-0.37	0.33
Maximum Relative Head Motion (mm)	0.66+/-0.63, 0.10-2.46	0.83+/-0.61, 0.15-2.50	0.25
ADOS (Comm+Soc)	N/A	11.1+/-3.9, 2-19	N/A
ADI Total	N/A	47.9+/-9.8, 23-63	N/A
Diffusion Tensor Imaging (DTI) Sample			
Sample Size	43.0	51.0	
Number of Females	7.0	6.0	0.53
Age	13.1+/-2.4, 9.0-18.0	13.0+/-2.8, 8.4-18.2	0.82
Verbal IQ	108.2+/12.6, 86-131	104.3+/-13.9, 83-141	0.15
Performance IQ	105.9+/-13.2, 76-134	105.0+/-14.6, 72-135	0.74
Full Scale IQ	108.2+/-12.5, 84-134	104.1+/-13.2, 79-132	0.15
Mean Relative Head Motion (mm)	0.41+/-0.13, 0.27-0.81	0.42+/-0.11, 0.26-0.66	0.71
Maximum Relative Head Motion (mm)	1.52+/-0.69, 0.96-4.62	1.71+/-0.81, 0.90-4.86	0.23
ADOS (Comm+Soc)	N/A	10.8+/-3.6, 2-19	N/A
ADI Total	N/A	47.4+/-11.6, 16-68	N/A
DTI and RS Sample			
Sample Size	35.0	35.0	
Number of Females	6.0	5.0	0.74
Age	13.0+/-2.1, 9.5-18.0	13.4+/-2.6, 9.1-18.2	0.51
Verbal IQ	108.3+/11.5, 86-127	102.9+/-13.9, 79-132	0.08
Performance IQ	105.4+/-12.1, 76-129	105.1+/-14.5, 72-135	0.94
Full Scale IQ	107.7+/-11.0, 84-128	103.2+/-13.6, 79-132	0.13
RS Mean Relative Head Motion (mm)	0.09+/-0.07, 0.03-0.37	0.10+/-0.06, 0.04-0.29	0.38
RS Maximum Relative Head Motion (mm)	0.67+/-0.65, 0.10-2.46	0.80+/-0.57, 0.15-2.10	0.37
DTI Mean Relative Head Motion (mm)	0.39+/-0.12, 0.27-0.78	0.40+/-0.09, 0.26-0.59	0.81
DTI Maximum Relative Head Motion (mm)	1.45+/-0.59, 1.00-4.62	1.44+/-0.47, 0.90-3.17	0.99
ADOS (Comm+Soc)	N/A	11.3+/-3.8, 2-19	N/A
ADI Total	N/A	47.8+/-9.8, 23-61	N/A

Data is mean +/- standard deviation, minimum-maximum. Columns on the right display p-values for two sample t-tests for each sample characteristic except for sex, which displays p-values from a Chi square test.

Table 2. Mean and Standard Deviation of Functional and Structural Graph Metrics

Characteristic	Typically Developing	Autism Spectrum	*p* value
Functional (42 ASD vs 37 TD)			
Clustering Coeficcient	0.56 +/- 0.03	0.54 +/- 0.03	0.012
Characteristic Path Length	1.92 +/- 0.05	1.89 +/- 0.05	0.020
Lambda	2.18 +/- 0.12	2.13 +/- 0.13	0.070
Gamma	1.09 +/- 0.03	1.07 +/- 0.03	0.020
Small Worldness	2.00 +/- 0.10	1.98 +/- 0.12	0.420
Modularity (Q)	0.40 +/- 0.03	0.38 +/- 0.03	0.008
Structural (51 ASD vs 43 TD)			
Clustering Coeficcient	0.46 +/- 0.01	0.46 +/- 0.01	0.750
Characteristic Path Length	2.77 +/- 0.04	2.77 +/- 0.04	0.490
Lambda	5.44 +/- 0.23	5.39 +/- 0.19	0.270
Gamma	1.24 +/- 0.02	1.24 +/- 0.02	0.990
Small Worldness	4.38 +/- 0.16	4.33 +/- 0.13	0.120
Modularity (Q)	0.68 +/- 0.01	0.67 +/- 0.01	0.030

Data is mean +/- standard deviation. P values were generated from two-sample t-tests performed on each metric averaged over a range of sparsity thresholds

Table 3. Principal Component Analysis of Functional and Structural Network Metrics

	Component 1	Component 2	Component 3	Component 4
Functional CC	**0.863**	**0.369**	**-0.33**	-0.008
Functional CPL	**0.81**	**0.317**	**-0.486**	-0.012
Functional Lambda	**0.551**	**0.471**	**0.672**	0.047
Functional Gamma	**0.813**	**0.328**	**-0.471**	-0.013
Functional Small Worldness	0.174	**0.327**	**0.92**	0.05
Functional Modularity (Q)	**0.783**	**0.418**	**0.363**	-0.051
Structural CC	**-0.44**	**0.415**	-0.221	0.04
Structural CPL	**-0.436**	**0.656**	-0.051	**-0.604**
Structural Lambda	**-0.441**	**0.775**	-0.121	**0.329**
Structural Gamma	**-0.455**	**0.671**	-0.046	**-0.571**
Structural Small Worldness	**-0.337**	**0.648**	-0.122	**0.593**
Structural Modularity (Q)	**-0.406**	**0.373**	-0.029	**0.314**
Total Variance Explained	33.90%	25.50%	17.40%	10.50%
Relationship with Diagnosis	***b* = -0.30, *p* = 0.009**	*b* = -0.13, *p* = 0.30	*b* = 0.01, *p* = 0.95	***b* = -0.32, *p* = 0.007**
Correlation with Age (All)	***r* = 0.24, *p* = 0.04**	*r* = 0.07, *p* = 0.34	*r* = -0.02, *p* = 0.87	*r* = -0.06, *p* = 0.62
Correlation with Age (TD)	*r* = 0.28, *p* = 0.11	*r* = -0.24, *p* = 0.16	*r* = 0.09, *p* = 0.60	*r* = 0.00, *p* = 1.0
Correlation with Age (ASD)	*r* = 0.30, *p* = 0.08	***r* = 0.35, *p* = 0.04**	*r* = -0.11, *p* = 0.53	*r* = -0.09, *p* = 0.62
Correlation with ADOS social (ASD)	*r* = -0.04, *p* = 0.81	-	-	***r* = -0.36, *p* = 0.04**
Correlation with ADOS comm (ASD)	*r* = -0.06, p = 0.73	-	-	***r* = -0.46, *p* = 0.005**
Correlation with ADI social (ASD)	***r* = -0.40, *p* = 0.01**	-	-	*r* = -0.18, *p* = 0.30
Correlation with ADI comm (ASD)	*r* = -0.31, *p* = 0.08	-	-	*r* = -0.11, *p* = 0.53

Top of table displays weighting (bold indicates significant ($p < 0.05$) weight) of structural and functional metrics (Clustering (CC), Characteristic Path Lenghts (CPL), Lambda, Gamma, Small Worldness and Modularity (Q)) on each of the four principal components. Bottom of table shows regression coefficients and p values with diagnosis and pearson correlation values with age (controlling for motion), Autism Diagnostic Interview (ADI) and Autism Diagnositic Observation Scale (ADOS) social and communication subscales with each of the priniciple components (controlling for age and motion).

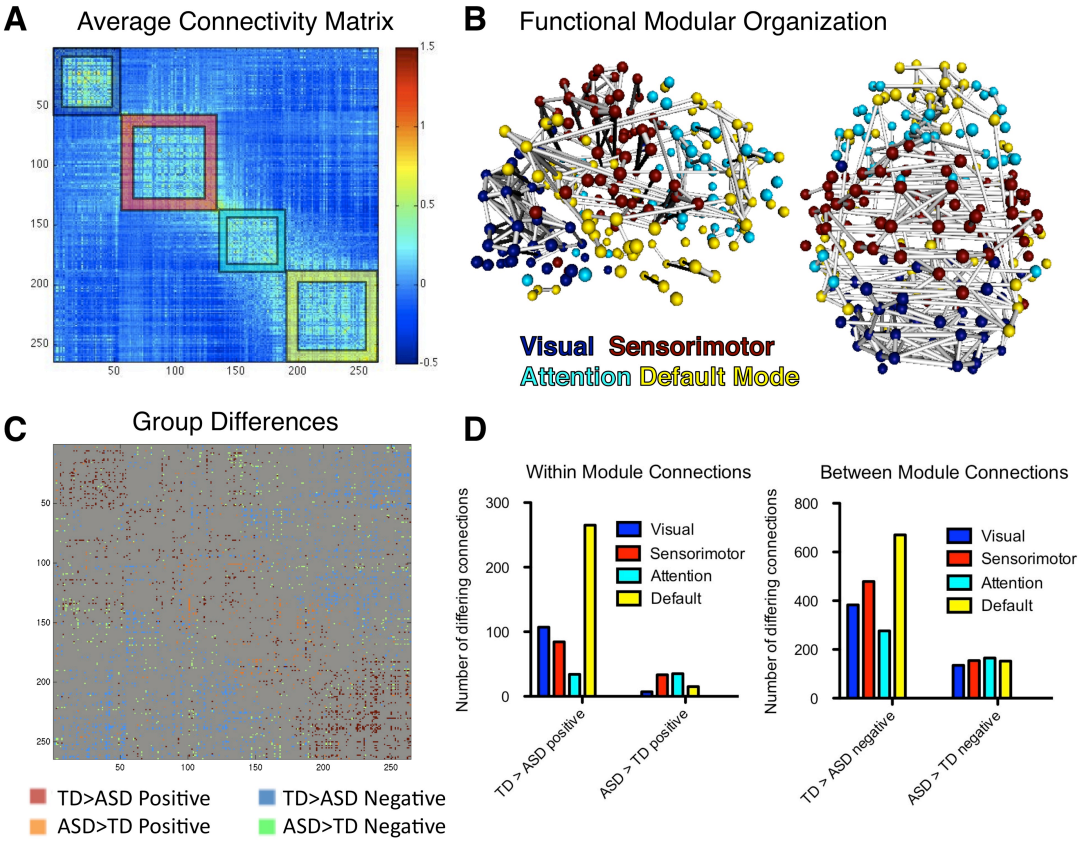

Figure 2.1. Functional network organization. (A) Average functional connectivity matrix reorganized by its modular organization with colored boxes around each of the four communities (visual=blue, sensorimotor=red, attention/control=cyan, default=yellow). (B) Three dimensional sagittal and axial views of the functional graph in anatomical space displaying top 2% of connections and nodes colored by community. (C) Functional connectivity matrix group differences (p < 0.05 uncorrected) displaying typically developing (TD) > Autism Spectrum Disorder (ASD) for positive (red), ASD>TD for positive (orange), TD>ASD for negative (blue) and ASD>TD for negative (green). (D) Numbers of TD>ASD and ASD>TD between group connections differing for within group positive connections (left) and between group negative connections (right).

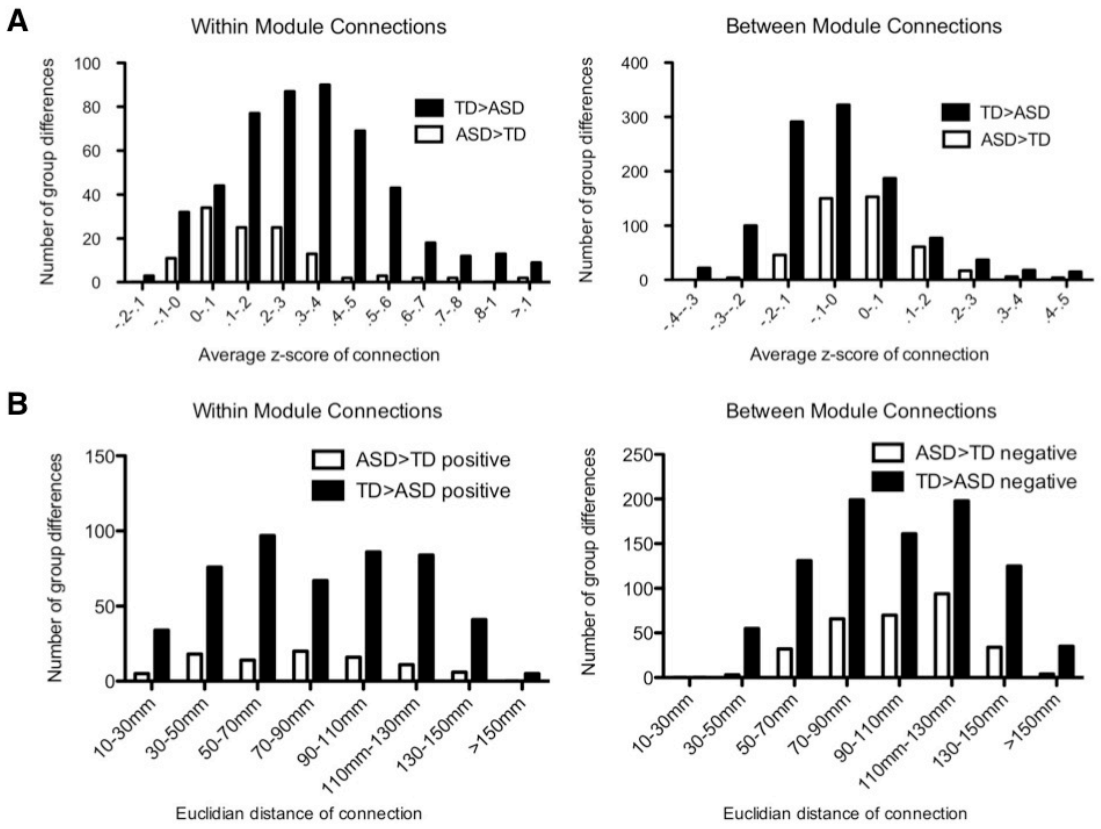

Figure 2.2. Distribution of functional connectivity differences. (A) Numbers of connections with significant group differences for typically developing (TD) > Autism Spectrum Disorder (ASD; black) and ASD>TD (white) displayed as a function of average connectivity strength across all subjects and (B) average Euclidean distance for within-module connections (left) and between-module connections (right).

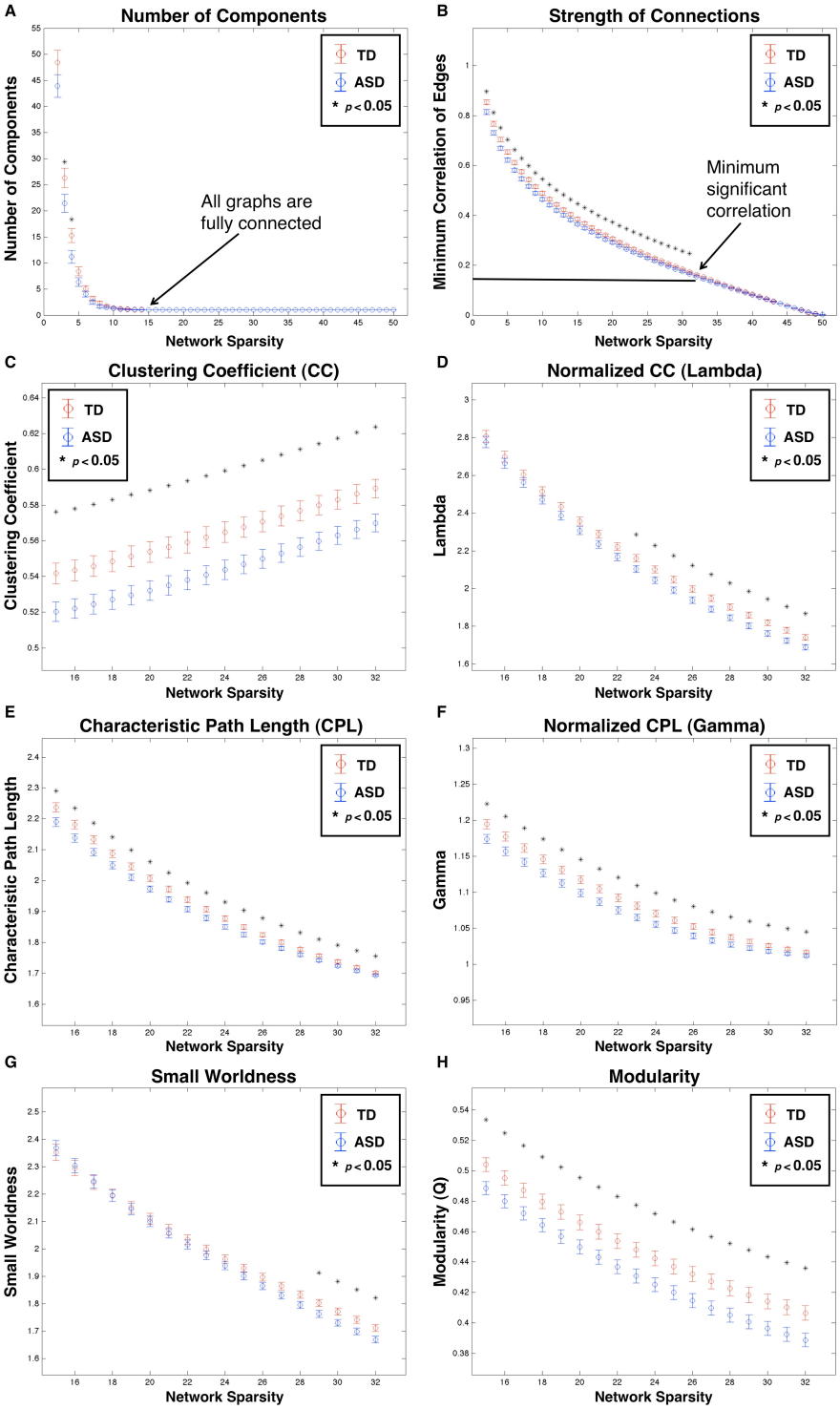

Figure 2.3. Graph theoretical metrics of functional networks. (A) Average and standard error for TD (red) and ASD (blue) number of components, (B) minimum correlation coefficient for edges, (C) clustering coefficient, (D) gamma, (E) characteristic path length, (F) lambda, (G) small worldness and (H) modularity Q values as a function of network sparsity. Number of components and minimum correlation strength are shown between 1% and 50% network

sparsity in 1% increments while other network properties are displayed between 15% and 32% network sparsity in 1% increments (equivalent to minimum correlation values of 0.34 and 0.15). Significant between group differences ($p < 0.05$) are indicated by *.

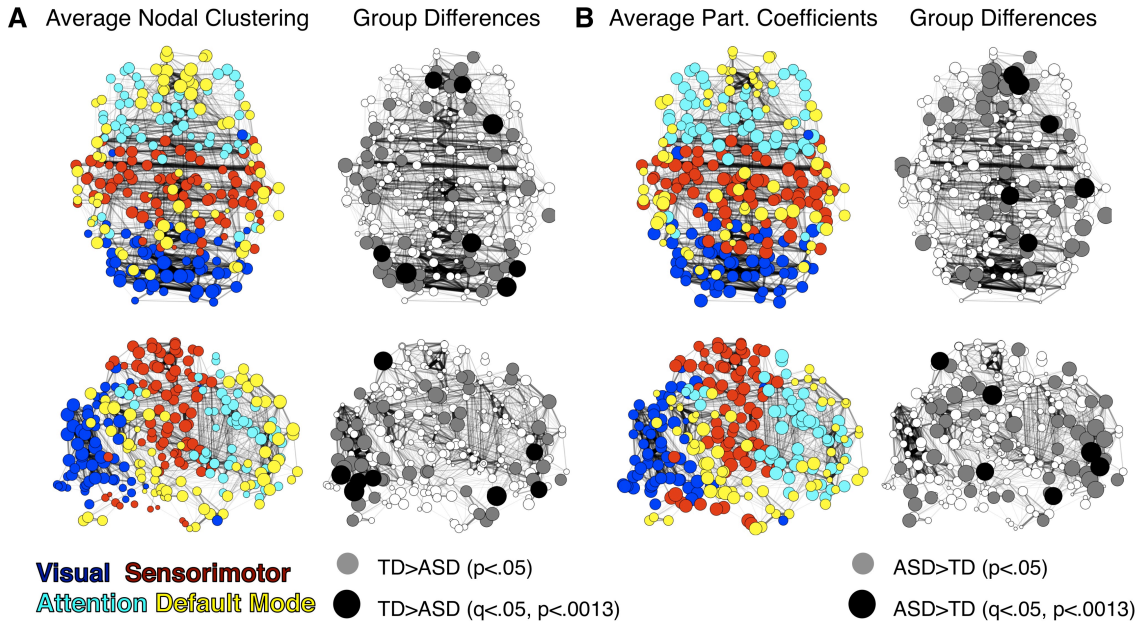

Figure 2.4. Nodal differences in clustering and participation coefficients. (A) Two dimensional axial and sagittal views of the functional graph in anatomical space displaying top 5% of connections with nodes colored by community organization (left columns) and radii proportional to average and significant between group differences ($p < 0.05$ in grey, FDR corrected $q < 0.05$ ($p < 0.0013$) in black; right column) for nodal clustering (TD>ASD) and (B) participation coefficients (ASD>TD).

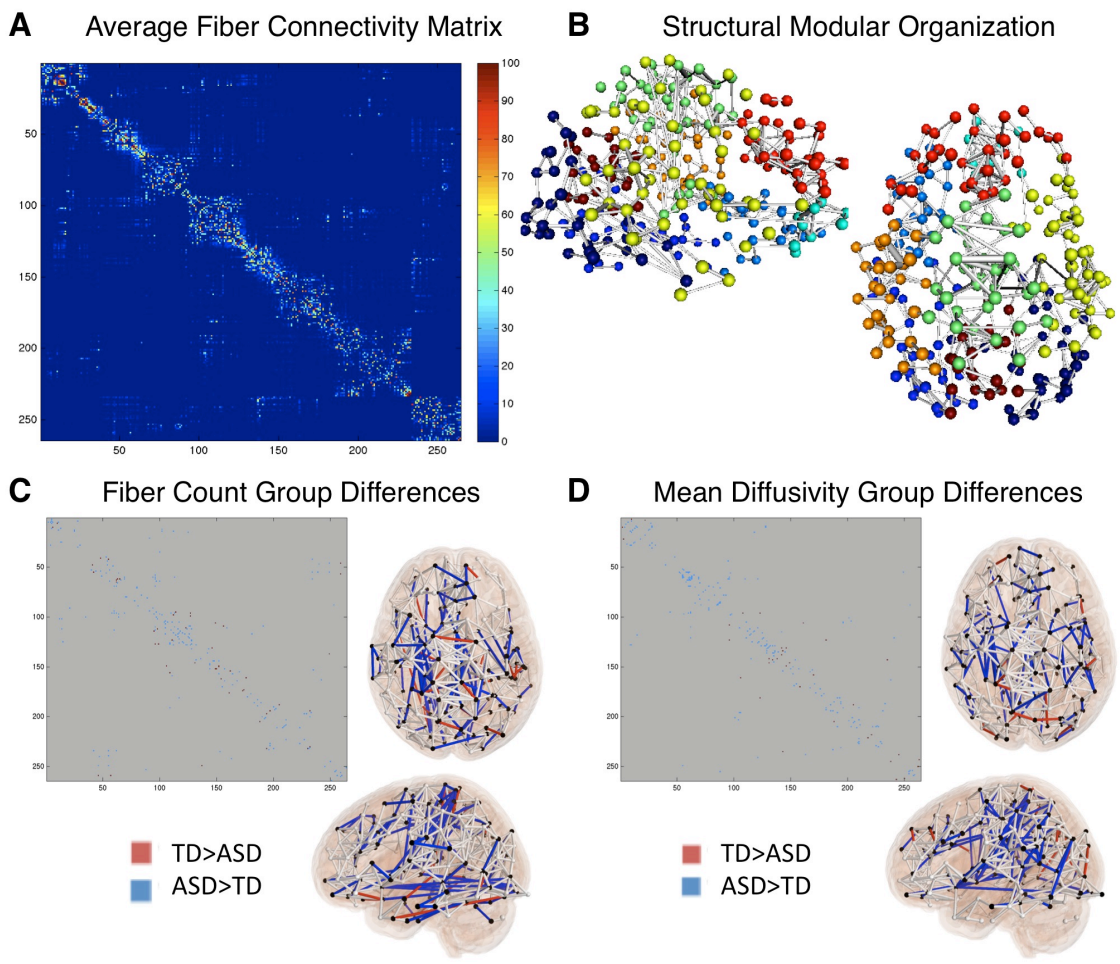

Figure 2.5. Structural network organization. (A) Average structural connectivity matrix reorganized by its modular organization. (B) Three dimensional sagittal and axial views of the structural network in anatomical space displaying top 2% of connections. (C) Structural connectivity matrix group differences ($p < 0.05$, uncorrected) displaying typically developing (TD) > Autism Spectrum Disorder (ASD) for fiber counts and (D) mean diffusivity in the connectivity matrix and in 3D brain space.

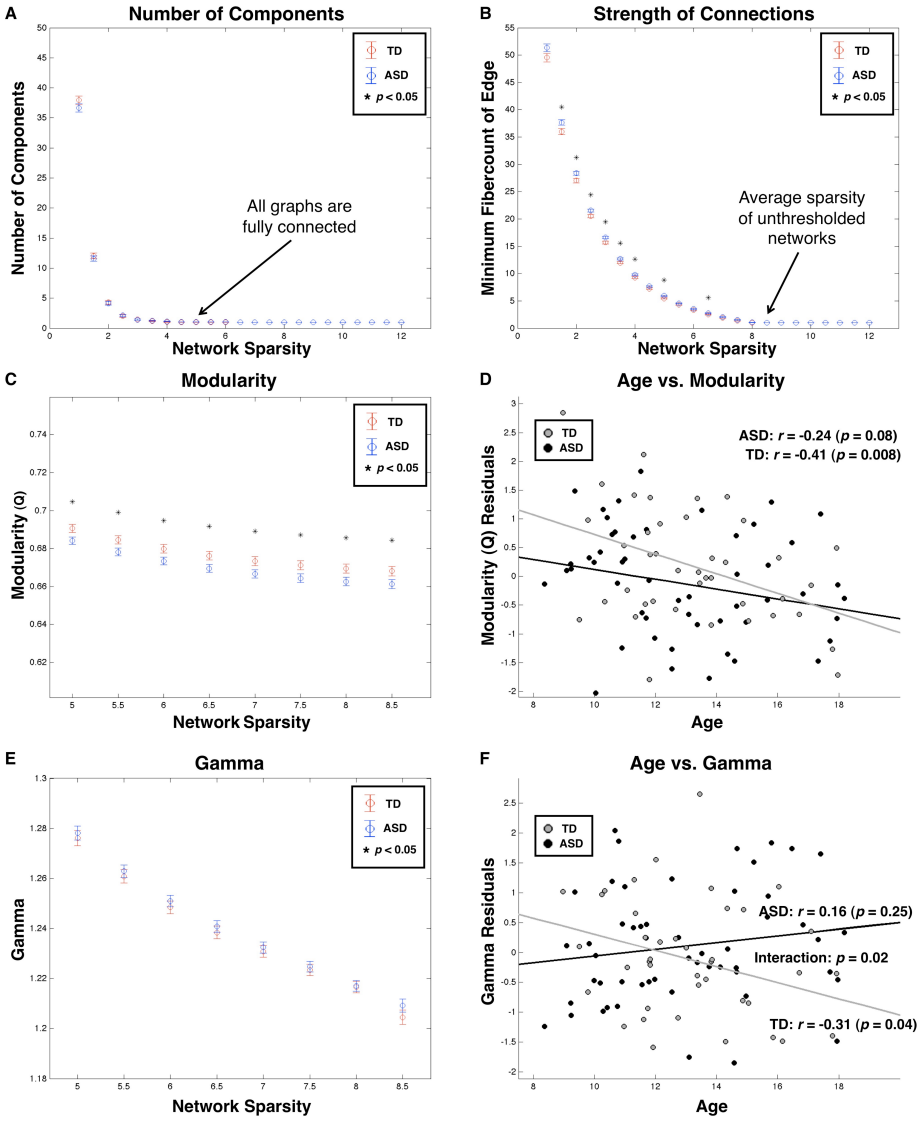

Figure 2.6. Graph theoretical metrics of structural networks. (A) Average and standard error for TD (red) and ASD (blue) number of components, (B) minimum fiber count for edges, (C) modularity Q values, (E) gamma as a function of network sparsity. Number of components and minimum correlation strength are shown between 1% and 12% network sparsity in 0.5% increments while other network properties a displayed between 5 and 8.5% sparsity in 0.5% increments. Significant between group differences ($p < 0.05$) are indicated by *. (D) Modularity and (F) gamma residuals after regressing out mean and relative values are displayed as a function of age in the TD (gray) and ASD (black) groups.

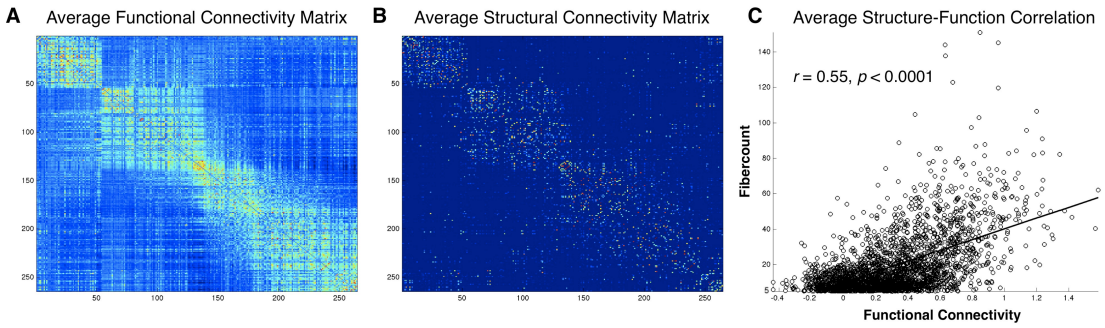

Figure 2.7. Structure-function correlations. (A) Average functional connectivity and (B) structural fiber connectivity matrices after reorganizing by modular organization for functional networks. Correlation between structure and function for group average connections with a minimum average of 5 fibers.

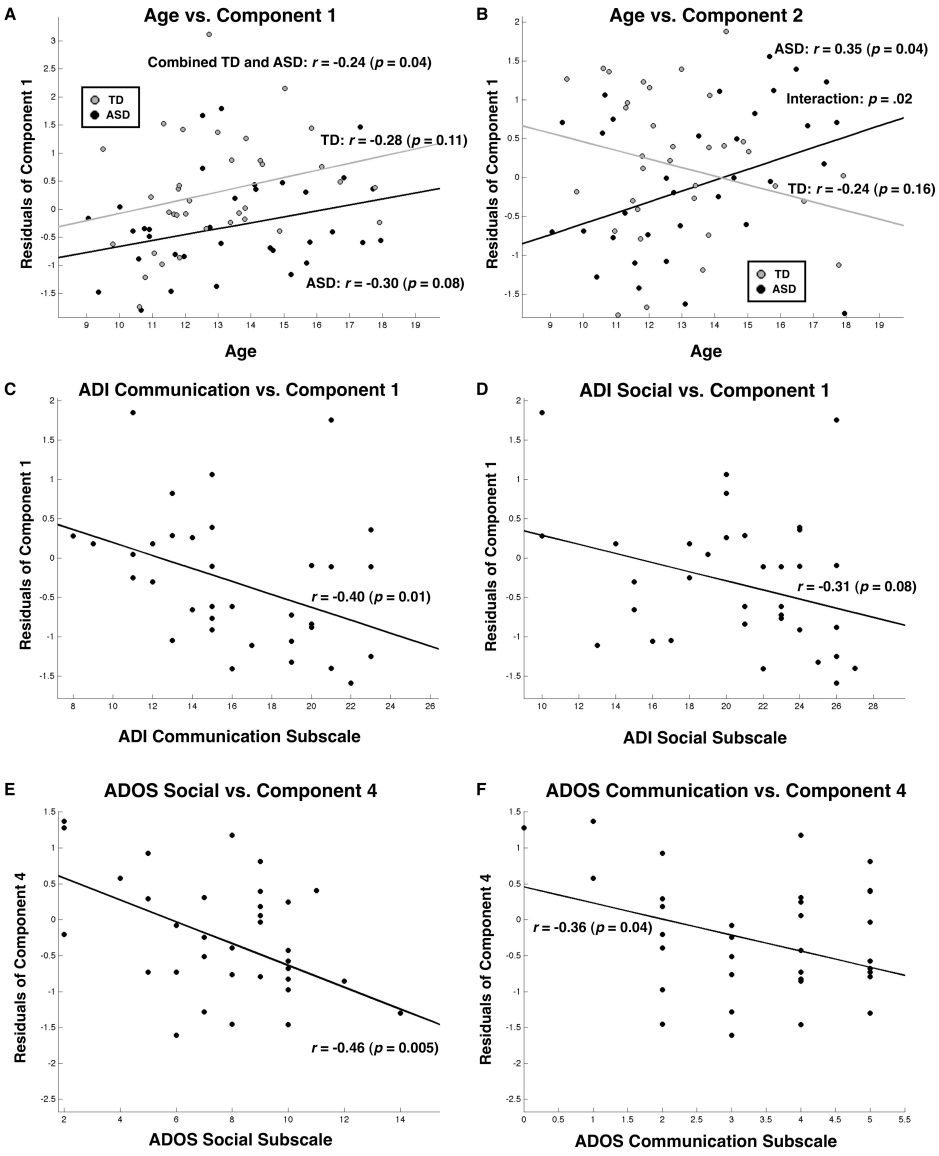

Figure 2.8. Relationships between principal components of structural and functional network properties, age and ASD symptom severity. (A) Component 1 and (B) Component 2 residuals after regressing out mean motion are displayed as a function of age in the TD (gray) and ASD (black) groups. (C) Residuals of component 1 after regressing out mean motion and age are displayed as function of the Autism Diagnostic Interview (ADI) communication and (D) social subscales. (E) Residuals of component 4 after regressing out mean motion and age are displayed as a function of the Autism Diagnostic Observation Schedule (ADOS) social and (F) communication subscales.

CHAPTER 3: Autism Risk Variant in *MET* Impacts Functional and Structural Brain Networks

Abstract

As genes that confer increased risk for autism spectrum disorder (ASD) are identified, a crucial next step is to determine how these risk factors impact brain structure and function. With three converging lines of evidence, we show for the first time that a replicated ASD risk allele in the Met Receptor Tyrosine Kinase (*MET*) gene is a potent modulator of key social brain circuitry in children and adolescents with and without ASD. *MET* risk genotype predicted atypical fMRI activation and deactivation patterns to social stimuli (i.e., emotional faces), as well as reduced functional and structural connectivity in temporo-parietal regions known to have high MET expression, particularly within the default mode network. Notably, these effects were more pronounced in individuals with ASD. These findings highlight the need to integrate genetic and neuroimaging data in order to elucidate the biological basis of complex neuropsychiatric disorders such as ASD.

Introduction

Over the past decade significant strides have been made toward understanding the genetic basis of autism spectrum disorder (ASD; see Geschwind, 2011 and State & Levitt, 2011 for review), one of the most heritable psychiatric disorders (Bailey et al., 1995; Rosenberg et al., 2009; Hallmayer et al., 2011). Yet, due to the complexities of both ASD genetic architecture and brain-behavior relationships, great challenges remain in delineating how ASD risk genes shape the circuits underlying social behavior. Brain imaging studies have demonstrated that individual variation in task-based functional MRI activation patterns, resting state functional connectivity (rs-fcMRI), and structural connectivity measures have a strong genetic component (Chiang et al., 2010; Kochunov et al., 2010; Fornito et al., 2011; Glahn et al., 2010; Koten et al., 2009) and are altered in ASD (see Di Martino et al., 2009 and Schipul et al., 2011 for review). Thus, neuroimaging endophenotypes are ideal tools for bridging the gap in our understanding of how genetic risk impacts brain circuitry. Yet, both behavioral and imaging phenotypes in ASD present significant heterogeneity, sometimes leading to discrepant findings (Müller et al., 2011). A critical question then is how genetic variability underlies phenotypic heterogeneity, and consequently, whether stratifying by common functional genetic risk factors can inform our understanding of the neurobiology of ASD.

Multiple genes encoding proteins in the ERK/PI3K signaling pathway have been implicated in syndromic and idiopathic causes of ASD (Levitt and Campbell, 2009). This pathway can be activated by receptor tyrosine kinases, including the Met Receptor Tyrosine Kinase (MET), which has been identified and replicated as an ASD risk gene (Judson et al., 2011a). In the forebrain, MET gene and protein expression is highly regulated in excitatory projection neurons during synapse formation (Judson et al., 2009; Judson et al., 2011b). MET is expressed widely in the mouse neocortex (Judson et al., 2009), but in monkeys (Judson et al., 2011b) and humans (Mukamel et al., 2011) it is limited to restricted regions of temporal,

occipital and medial parietal cortex, suggesting a role in the development of circuits underlying the processing of socially relevant information. The clinical relevance of MET cortical expression has been exemplified by post-mortem brain studies, whereby individuals with ASD displayed 50% lower levels of MET protein in superior temporal gyrus (Campbell et al., 2007), and did not display the same temporo-frontal differential expression pattern as control subjects (Voineagu et al., 2011).

Common and rare variation in *MET* has been associated with ASD across multiple independent cohorts (Pinto et al., 2010; Marshall et al., 2008; Thanseem et al., 2010; Jackson et al., 2009; Sousa et al., 2009; Campbell et al., 2008; Campbell et al., 2006). The 'C' variant of rs1858830, located in the promoter region of MET, is associated with ASD risk (Campbell et al., 2006; Campbell et al., 2008; Jackson et al., 2009). This risk allele is functional as it reduces gene transcription *in vitro* (Campbell et al., 2006) and correlates with lower levels of MET transcript and protein in the temporal cortex of healthy control subjects (Campbell et al., 2007; Heuer et al., 2011). Furthermore, this risk variant moderates the severity of social symptoms in ASD whereby individuals with ASD who carry this risk allele have more severe social and communication phenotypes than those who do not (Campbell et al., 2010).

The neurobiological correlates of the impact of reduced MET expression in humans have been recently examined in *Met* conditional knockout (*Met*-cKO) mice (Judson et al., 2009; Judson et al., 2010; Qiu et al., 2011). Neocortical pyramidal neurons in *Met*-cKO mice exhibited altered dendritic architecture and increased spine head volume (Judson et al., 2010), as well as a concomitant increase in local interlaminar excitatory drive onto corticostriatal neurons (Qiu et al., 2011). This finding of upregulated local-circuit connectivity is highly relevant as it is consistent with current theorizing regarding increased local circuit connectivity and decreased long-range connectivity of brain networks in individuals with ASD (Belmonte et al., 2004; Courchesne and Pierce, 2005; Geschwind and Levitt, 2007). Given histopathological findings of

disordered minicolumn organization (e.g., Casanova et al., 2002), it has been proposed that local over-connectivity arising from a loss of appropriate lateral inhibitory control may ultimately constrain the typical development of long-range cortical networks in ASD. MRI evidence of long-distance underconnectivity using structural and functional MRI is extensive. For example, reduced functional connectivity in distributed brain networks in ASD has been reported across a variety of cognitive tasks (e.g. Castelli et al. 2002; Just et al., 2004; Villalobos et al., 2005; Kleinhans et al., 2008) and when measuring task-independent (intrinsic) connectivity for interhemispheric (Dinstein et al., 2011; Anderson et al., 2011b) and anterior-posterior connections (Cherkassky et al., 2006; Kennedy and Courchesne, 2008; Monk et al., 2009; Weng et al., 2010; Assaf et al., 2010; Rudie et al., 2011), including the default mode network (DMN; Raichle et al., 2001). The DMN is involved in socio-emotional processing including mentalizing and empathizing, which are classically impaired in individuals with ASD. Additionally, several diffusion tensor imaging (DTI) studies have reported reduced white matter integrity of anterior-posterior and interhemispheric tracts in ASD (Barnea-Goraly et al., 2004; Alexander et al., 2007; Sundaram et al., 2008; Cheng et al., 2010; Shukla et al., 2011; Barnea-Goraly et al., 2010).

Based on the convergent genetic, clinical, and neurobiological findings regarding MET-mediated ASD risk, we hypothesized that the *MET* promoter variant would be a powerful moderator of socially relevant functional and structural neuroimaging endophenotypes. We tested this prediction by examining the relationship between *MET* risk genotype and functional activation patterns to social stimuli (i.e., emotional facial expressions), long-range DMN functional connectivity, and the integrity of major white matter tracts in which MET is highly expressed. Additionally, we hypothesized that the *MET* promoter variant would help address ASD heterogeneity by clustering a unique subset of individuals with the diagnosis, such that

individuals with ASD and *MET* risk alleles would exhibit the greatest alterations in structural and functional endophenotypes.

Results

A total of 162 children and adolescents including 75 with an ASD and 87 who were typically developing (TD) contributed data to one or more of the three neuroimaging experiments (**Table 3.1**). This included a task-based fMRI experiment involving the passive observation of emotional faces (N=144), a resting state fMRI scan (N=71), and a diffusion-weighted scan (N=84). DNA was extracted from saliva samples and the *MET* variant, rs1858830, was genotyped by direct resequencing. Individuals carried 0, 1, or 2 of the rs1858830 C "risk" alleles. There were three genotype groups: a CC homozygous risk group (30.2% of sample), a CG heterozygous risk group (49.4% of the sample), and a GG homozygous non-risk group (20.3% of the sample). Thus, the terminology (i.e., "risk" versus "non-risk" group) used hereafter refers to both TD and ASD individuals with specific *MET* genotypes. Genotypes observed Hardy-Weinberg Equilibrium ($\chi^2 = 0.001$, $p = 0.973$) and in this sample we did not observe an enrichment of the risk allele in individuals with ASD (Fisher's exact test, $p = 0.654$). However, it should be noted that our sample consisted of high functioning individuals with ASD and prior studies have shown an enrichment of the *MET* risk allele particularly in the most highly impaired individuals with ASD (Campbell et al., 2010).

In each of the three datasets, genotype groups did not differ by age, gender, head motion, IQ, or ASD diagnoses; similarly, there were no differences between diagnostic groups in age, gender, or head motion (**Table 3.1**). However, consistent with prior reports (Campbell et al., 2010), ASD homozygous risk and heterozygous risk groups had significantly higher levels of social impairment (Autism Diagnostic Observation Scale, ADOS, Lord et al., 2000, social subscale, p=0.001) than the ASD homozygous non-risk group. IQ did not differ between the

ASD homozygous non-risk group and all TD groups (homozygous risk, heterozygous risk, and homozygous non-risk) but was significantly lower in both ASD homozygous risk and heterozygous risk groups; thus, we included full scale IQ as a covariate in all analyses examining the effect of an ASD diagnosis. Additionally, given that the inheritance pattern (additive, dominant, or recessive) of the genotype effect is not clearly established, we first focused on a direct contrast between the homozygous risk (CC) and non-risk (GG) groups collapsed across diagnostic status, for all datasets. After these initial whole-brain analyses, we used the regions differing between the homozygous risk and non-risk groups as a single region of interest for analyses that included the intermediate genotype group and that were stratified by diagnostic status.

Functional Activation Patterns to Emotional Faces

We performed fMRI in a cohort of 144 children and adolescents, including 78 typically-developing (homozygous risk: N=28, heterozygous risk: N=34, homozygous non-risk: N=16) and 66 diagnosed with ASD (homozygous risk: N=15, heterozygous risk: N=39, homozygous non-risk: N=12; **Table 3.1**), during passive observation of faces displaying different emotions (angry, fearful, happy, sad, and neutral; with fixation crosses directing attention to the eye region as previously reported (Dapretto et al., 2006; Pfeifer et al., 2008; Pfeifer et al., 2011). We observed strong correlations between the *MET* risk allele and unique patterns of functional brain activity when collapsing across diagnostic category. Compared to the non-risk group (N=28), the risk group (N=43) displayed a pattern of hyperactivation and reduced deactivation in specific regions where MET is expressed in primates and humans (Mukamel et al., 2011; Judson et al., 2011b; **Figure 3.1A**, **Table 3.2**). The risk and non-risk groups both activated primary/secondary visual cortices, thalamus, and amygdala; however, the risk group activated amygdala and striatum more robustly than the non-risk group. Additionally, the non-risk group displayed a pattern of widespread deactivation (i.e., reduced activity while viewing faces vs. fixation

crosses), most prominently in midline structures of the DMN and perisylvian regions centered on primary auditory cortex. In contrast, the risk group did not deactivate these regions to the same degree as the non-risk group (**Figure 3.1A**).

To investigate the risk allele's inheritance pattern as well as the effect of an ASD diagnosis, we compared the average activity across regions differing between the risk and non-risk groups for all three genotype groups stratified into either TD or ASD subgroups. We found that the *MET* promoter variant has a differential penetrance between neurotypical and autistic individuals. Specifically, TD individuals with one risk allele showed a similar deactivation pattern to those without a risk allele (**Figure 3.1B**). In contrast, in individuals with ASD, one *MET* risk allele was sufficient to give rise to the atypical pattern of functional activity, showing less deactivation than the non-risk group. In fact, when comparing those with one risk allele, individuals with ASD exhibited significantly less deactivation in these regions compared to TD subjects.

Default Mode Network Functional Connectivity

To examine whether *MET* risk disrupts default mode network functional connectivity we used a sphere centered in the posterior cingulate (Fox et al., 2005) as a seed region for whole-brain functional connectivity analyses in rs-fcMRI data in a matched sample of 33 typically-developing and 38 children and adolescents diagnosed with ASD. In line with the functional activation results, the *MET* risk genotype significantly modulated functional connectivity such that those in the highest risk group, with two *MET* alleles (N=16) had reduced intrinsic anterior-posterior connectivity between the medial prefrontal cortex (MPFC) and the posterior cingulate cortex (PCC) compared to the non-risk group (N=16; **Figure 3.2A**, **Table 3.3**). In agreement with the functional activation analyses, the ASD heterozygous risk group (N=24) showed a pattern of functional connectivity similar to that observed in the homozygous risk group,

whereas functional connectivity in the TD heterozygous risk group (N=15) was no different than the homozygous non-risk group. Collapsed across genotype, the ASD group exhibited reduced PCC-MPFC connectivity relative to the TD group (**Figure 3.2B**). This diagnostic effect was driven by a stronger penetrance of the *MET* risk allele in the ASD group as it was only observed in risk carriers; indeed, *MET* genotype explained 1.7 times as much variance in DMN connectivity in autistic relative to neurotypical individuals.

White Matter Structural Connectivity

A third line of evidence for the impact of the *MET* risk allele was sought by examining the structural integrity of white matter tracts in a cohort of 84 children and adolescents (TD: N=38, ASD: N=46). We found that *MET* risk genotype predicted marked reductions in fractional anisotropy (FA) across several major white matter tracts known to connect the very same regions previously implicated in our functional analyses. Compared to non-risk allele homozygotes (N=19), risk allele homozygotes (N=23) displayed lower FA in multiple major tracts in temporo-parieto-occipital regions that exhibit high MET expression developmentally (i.e., splenium of the corpus callosum, superior/inferior longitudinal fasciculus, and cingulum; **Figure 3.3A**; **Table 3.4**). Consistent with the observed functional connectivity patterns, in these tracts the *MET* risk allele had a stronger impact in individuals with ASD (**Figure 3.3B**), explaining nearly twice (1.9 times) as much variance in the ASD group. More specifically, ASD heterozygous risk allele carriers (N=25) and homozygous risk allele carriers (N=12) both exhibited strong reductions in FA, whereas structural connectivity was only significantly impacted in TD homozygous risk carriers (N=11).

Correlation Between Imaging and Behavioral Measures:

Within the ASD group, we correlated scores on ADOS social subscale (Lord et al., 2000), with measures derived from the imaging analyses. Lower levels of both functional and

structural connectivity were significantly associated with higher levels of social impairment in the ASD group overall (**Figure 3.4**). However, as previously noted, there was also a direct relationship between risk genotype and increased symptom severity. Indeed, the relationship between brain circuitry and symptom severity was largely driven by the fact that individuals with ASD who have *MET* risk alleles have both increased symptom severity and impacted brain circuitry (i.e., the correlations were no longer significant when co-varying for *MET* risk genotype).

Discussion

In the present study, we used an imaging genetics approach to examine the impact of a common functional variant in *MET* on neuroimaging endophenotypes that are disrupted in ASD. We found that, irrespective of clinical diagnosis, the functional promoter *'C'* allele of *MET* alters functional activity patterns to social stimuli, long-range DMN functional connectivity, and white matter integrity in specific regions that exhibit high MET expression and subserve socially-relevant processes. This is consistent with the concept of endophenotypes, whereby a functional risk allele predisposing to a disorder could have a larger impact on disorder-relevant phenotypes than the disorder itself. Remarkably, we also found that the *MET* risk allele had a stronger impact across individuals with ASD, especially within the heterozygous risk group. Measures of structural and functional circuitry correlated with symptom severity, but this correlation was driven by the fact that *MET* risk genotype was associated with both increased symptom severity and alterations in brain circuitry. These findings suggest that *MET* genotype could be a useful means to stratify heterogeneous ASD samples.

Functional Activation Patterns

We first focused on functional activation patterns in response to the passive observation of emotional facial expressions in a large sample of 66 ASD and 78 TD subjects. The high

expression of MET in ventral temporal cortex, including the amygdala and fusiform gyrus, prompted us to test whether the C risk allele might impact activity in these regions in response to socially-relevant and affect-laden stimuli. Early studies of emotional face processing documented amydala and fusiform hypoactivation in ASD (Baron-Cohen et al. 2000; Critchley et al., 2000; Schultz et al. 2000). Later studies that better controlled for eye gaze (such as a fixation cross that directs gaze at the eyes, similar to the one used in the present study) found either no differences or hyperactivation in these regions (Hadjikani 2004; Peirce et al. 2004; Dalton et al. 2005; Monk et al. 2010). Here we found that *MET* risk genotype was associated with hyperactivation of amygdala and striatum, as well as reduced deactivation in temporal and midline neocortex. These areas comprise circuits that have the highest MET expression in developing humans and other primates (Judson et al. 2011b; Mukamel et al. 2011) and that exhibit structural and physiological dysfunction with reduced Met expression in mice (Judson et al., 2010; Qiu et al., 2011).

Overall, the risk group showed less deactivation than the non-risk group in these regions. Deactivation is a less well-characterized phenomenon in fMRI, but the DMN is known to show signal decreases in response to a variety of tasks requiring externally directed attention (Raichle et al., 2001). Interestingly, task induced DMN deactivation was shown to have a neuronal origin (Lin et al., 2011), so it may relate to intrinsic inhibitory properties of local cortical circuits. Few studies have focused on differences in deactivation in ASD, but individuals with ASD exhibit less deactivation within regions of the default mode network (Kennedy et al. 2006), consistent with our findings. The auditory cortex is also known to deactivate during visual tasks (Laurienti et al. 2002; Mozolic et al., 2008) and, in our study, the auditory cortex exhibited the strongest deactivation differences between genotype groups during this visual task. These findings of reduced deactivation of perisylvian and DMN regions in *MET* risk carriers may relate to a failure to appropriately suppress neuronal activity, perhaps through a Met-mediated

enhancement of local connectivity. Future imaging and neurophysiological studies are needed to test this hypothesis.

Functional And Structural Connectivity

The fact that *MET* risk carriers displayed altered DMN deactivation patterns further prompted us to test whether the risk allele impacts intrinsic functional connectivity in this network, particularly since DMN connectivity is consistently disrupted in ASD (Cherkassky et al., 2006; Kennedy and Courchesne, 2008; Monk et al., 2009; Weng et al., 2010; Assaf et al., 2010; Rudie et al., 2011). Indeed we found that *MET* risk carriers and individuals with ASD exhibited reductions in long-range, anterior-posterior DMN connectivity. The combination of reduced deactivation and connectivity supports the notion that the DMN is both less integrated with itself and less segregated from other neural systems in both *MET* risk carriers and individuals with ASD (Rudie et al., 2011). Additionally, these findings suggest that functional alterations in the DMN represent a trait marker shared in those with, or at risk for, ASD.

Next, we examined whether structural connectivity was altered in *MET* risk carriers, as the MET protein is highly expressed during axon outgrowth in specific white matter tracts in primates (Judson et al., 2011b). Remarkably, the presence of the *MET* risk allele was associated with even stronger disruptions in white matter integrity than having an ASD diagnosis. The effects were most pronounced in temporo-parietal regions of high MET expression and especially within the splenium, which includes fiber pathways originating from the posterior cingulate/precuneus of the DMN. This hub region, implicated in all three imaging analyses, has been characterized as the structural core of the human connectome (Hagmann et al., 2008). The combined array of imaging findings is consistent with the involvement of *MET* in multiple processes, including axon guidance and synaptogenesis, which regulate circuit development. This polymorphism may affect structure formation and ongoing synaptic function

independently. Additional work is needed to tease apart structure-function relationships with regard to both MET-mediated and ASD-general alterations in connectivity.

Finally, we found that structural and functional connectivity were related to autism symptom severity, particularly in the social domain. However, this relationship was mediated by the fact that the *MET* risk allele was associated with increased symptom severity and reduced functional and structural connectivity. This result, in combination with the finding that, across all imaging measures, TD individuals with two risk alleles exhibited more 'atypical' brain circuitry than individuals with ASD carrying no risk alleles, raises critical issues regarding the causal nature of altered connectivity findings in ASD. The idea that functional and structural alterations may at least in part reflect genetic vulnerability is also supported by recent fMRI and DTI studies showing greater similarity between individuals with ASD and their unaffected siblings than between controls and unaffected siblings (Kaiser et al., 2010; Barnea-Goraly et al., 2010; Spencer et al., 2011). Thus, these findings highlight the need for future studies to account for relevant genetic factors, such as the *MET* promoter variant, to parse the heterogeneity present in autism brain and behavioral phenotypes, and ultimately improve diagnostic or prognostic tools (Fox & Greicius 2010).

Enhanced Effect of *MET* Risk Allele in ASD

Our data suggest that the *MET* 'C' risk allele has a greater effect in individuals with ASD, likely due to the influence of other factors that shape circuits underlying social behavior. Across all three imaging measures, the neuroimaging phenotypes of the ASD intermediate-risk (heterozygote) group were similar to those observed in the high-risk (homozygote) group, whereas the neuroimaging phenotypes of the TD intermediate-risk group resembled those of the non-risk group. This is consistent with the notion that multiple genetic and/or environmental factors in ASD contribute to both disrupted MET expression and atypical circuitry in individuals

with ASD. In fact, we previously found that carriers of a common risk allele in *CNTNAP2* also display alterations in functional connectivity (Scott-Van Zeeland et al., 2010). In addition to *CNTNAP2* and *MET* modulating functional connectivity, transcription of both genes is regulated by FOXP2 (Vernes et al., 2008; Mukamel et al., 2011), which is known to pattern speech and language circuits in humans (Konopka et al., 2009). Consistent with a multiple hit model, these findings collectively indicate that in individuals with ASD, who likely have additional alterations in the MET signaling pathway, the presence of the *MET* promoter risk allele results in more severely impacted brain circuitry and social behavior.

Relevance to ASD Connectivity Theories

The converging imaging findings reported here provide a mechanistic link, through MET disruption, to the previously hypothesized relationship between altered local circuit and long-range network connectivity in ASD (Belmonte et al. 2004; Courchesne et al., 2005; Geschwind and Levitt, 2007; Qiu et al., 2011). Moreover, the present results draw a striking parallel with alterations in neuronal architecture and synaptic functioning abnormalities found in Met-disrupted mice (Judson et al., 2010; Qiu et al., 2011). Local circuit hyperconnectivity at the microcircuit level seen in conditional Met null/heterozygous mice may lead to the hyperactivation/reduced deactivation we observed in humans with *MET* risk alleles. While speculative at this point, this may in part account for the presence of enhanced visual and auditory discrimination (Baron-Cohen et al., 2009; Jones et al., 2009; Ashwin et al., 2009) or sensory over-responsivity, observed in some individuals with ASD (Ben-Sasson et al., 2007; Baranek et al., 2006). Alterations in local-circuit connectivity and/or structural connections may ultimately hinder the typical formation of long-range connectivity (Dosenbach et al., 2010) observed in both *MET* risk allele carriers and individuals with ASD.

Conclusions

To our knowledge, this is the first report showing how an ASD risk allele predisposes to ASD by affecting functional activity, connectivity and white matter tract integrity in regions involved in social cognition. These findings have a number of broad implications. First, these results reveal an enhanced penetrance of a risk allele within individuals with ASD, reflecting a novel mechanism whereby a common functional variant, in the context of other factors related to ASD etiology, has a larger effect on network structure and function than in neurotypical individuals. Second, given that differences between ASD and controls were moderated by *MET* risk genotype, and in the case of functional activity were only revealed when the cohort was stratified by *MET* genotype, these data demonstrate the power of utilizing genetic data for understanding and parsing phenotypic heterogeneity in ASD. This approach may provide a more sensitive means to identify subgroups of individuals with particular risk alleles and brain circuitry, for whom targeted treatments may be developed. Finally, expanding upon our prior findings linking a *CNTNAP2* common variant to functional connectivity (Scott-Van Zeeland et al., 2010), the discovery that the *MET* risk allele has such large effects on structural and functional brain circuitry in typical and atypical development indicates that alterations in brain networks in ASD may in part reflect genetic vulnerability, or liability, rather than causal mechanisms. Taken together, the current results indicate that considering relevant genetic factors when interpreting neuroimaging data will greatly aid in understanding, and ultimately treating, ASD and other clinically and genetically heterogeneous neuropsychiatric disorders.

Materials and Methods

Subjects

High-functioning children and adolescents with autism spectrum disorders (ASD) and typically developing (TD) children were recruited through UCLA's Center for Autism Research

and Treatment (CART) and/or flyers posted throughout the greater Los Angeles area. Individuals with metal implants or a history of neurologic, psychiatric, brain abnormalities, or known genetic conditions were excluded from participation. Informed consent and assent to participate was obtained prior to assessment under our institutional review board (IRB) approved protocols. A total of 75 individuals with ASD and 87 TD individuals were included in at least one of the three datasets detailed in **Table 3.1**. Twenty-seven individuals with ASD and 2 TD individuals reported the use of one or more psychotropic medications. One TD subject was using a psychostimulant and another reported using a selective serotonin reuptake inhibitor. Of the subjects in our ASD sample, 15 were taking psychostimulants, 5 were taking sympatholytics, 11 were taking atypical antipsychotics, 11 were taking selective serotonin reuptake inhibitors, 5 were taking selective norepinephrine reuptake inhibitors, and 1 was taking an atypical antidepressant. Although psychotropic medication usage differed as a function of diagnostic status ($\chi^2 = 30.397$, $p < 0.001$), medication usage did not differ as a function of *MET* genotype ($\chi^2 = 1.763$, $p = 0.414$), thus it is unlikely that medication usage confounds the findings of the present study.

Behavioral Measures

Verbal, performance, and overall intelligence were assessed for each participant using the *Wechsler Abbreviated Scale of Intelligence* (WASI; Wechsler 1991) or the full Wechsler Intelligence Scale for Children (WISC; Wechsler 1999). High-functioning children with ASD had a prior clinical diagnosis of autism based on criteria from the Diagnostic and Statistical Manual of Mental Disorders (DSM IV), which was confirmed with the *Autism Diagnostic Observation Scale* (ADOS-G; Lord et al., 2000) and/or *Autism Diagnosis Interview* (ADI-R; Lord et al., 1994).

Genotyping

Subjects provided saliva samples for genetic analysis. DNA was isolated from saliva using standard protocols from the OraGene Collection kit (DNA GenoTek, Ontario, Canada). Genotypes at rs1858830 were determined by direct sequencing, as described elsewhere (Campbell et al., 2007). In brief, genomic DNA was extracted from saliva specimens and 20ng was used as a template for a polymerase chain reaction (PCR) amplification of a 652bp amplicon, which includes rs1858830, using the KOD Xtreme Hot Start DNA Polymerase kit (EMD Chemicals, Gibbstown, NJ) by the manufacturer's protocol. Primer sequences were: forward primer, GATTTCCCTCTGGGTGGTG; reverse primer, CAAGCCCCATTCTAGTTTCG. Thermal cycling conditions were as follows: 94º for 2m, followed by 35 cycles of 98º for 10s then 58º for 30s then 68º for 1m, and a final extension at 68º for 7m. Agarose gel electrophoresis of the PCR product from a random sampling of reactions confirmed specific amplification of the 652 bp amplicon. A 2µl aliquot of PCR product was diluted 1:10 in water, and direct sequencing off the reverse primer was performed using a 3730xl DNA Analyzer (Applied Biosystems, Foster City, CA). Sequences were aligned to the reference sequence of the plus strand of chromosome 7 and chromatograms were visually inspected to determine genotypes using Sequencher version 4.10.1 (Gene Codes, Ann Arbor, MI). Genotypes were called while blinded to sample identity and case status, and heterozygote calls were required to have a secondary peak on the chromatogram with at least 50% the height of the primary peak.

Statistical analyses on demographics and extracted imaging measures

All statistical analyses performed on demographics and extracted activation/connectivity/FA values were conducted with PASW Statistics 18, Release Version 18.0.3 (SPSS, Inc., 2009, Chicago, IL). ANOVAs (2 diagnostic groups by 3 genotype groups) were performed for age, full scale IQ, verbal IQ, performance IQ, mean relative head motion, ADOS social, communication and repetitive/restricted subscales and chi-square tests were performed on scanner type (functional activation only) and gender for genotype and diagnostic

status groups. Tests of means were performed between the intermediate-risk genotype group (CG), risk (CC), and non-risk groups (GG) collapsed across diagnostic status, TD and ASD groups collapsed across genotype, and between TD and ASD subjects within each genotype group. Because we performed additional analyses on the mean activity/connectivity/FA in regions derived from whole brain contrast maps comparing risk and non-risk groups, we do not report the p-values generated from further tests comparing these two groups as these would be inflated.

MRI Data Acquisition

The emotional faces functional activation scans were acquired at UCLA on a Siemens 3T Trio (n=101) and Siemens 3T Allegra (n=43) MRI scanners using a 16 channel phased array coil. A similar proportion of subjects in each of the genotype groups were scanned on the two scanners (**Table 3.1**), however the diagnostic groups did differ by scanner type, thus scanner type was used as a covariate of no interest in the secondary analyses comparing activity between TD and ASD groups. All rs-fcMRI and DTI scans were acquired on a Siemens 3T Trio.

A scout localizing scan was used for graphic prescription. Next, a matched bandwidth T2-weighted high-resolution echo planar scan was acquired co-planar to the functional images ensuring identical distortion characteristics to the fMRI scan (Siemens 3T Allegra: TR=5000ms, TE=33ms, matrix size 128 by 128, 20.0cm FoV, 36 4mm thick slices with an in plane voxel dimension of 1.56x1.56mm. Siemens 3T Trio: TR=5000ms, TE=34ms, matrix size 128 by 128, 19.2cm FoV, 36 4mm thick slices with an in plane voxel dimension of 1.50x1.50mm). The emotional faces functional data acquisition consisted of 96 T2* BOLD weighted images lasting a total of 4min 54s (Siemens 3T Allegra: TR=3000ms, TE=25ms, matrix size 64 by 64, 20cm FoV, 36 4mm thick slices (no gap) with an in plane voxel dimension of 3.125x3.125mm. Siemens 3T Trio: TR=3000ms, TE=28ms, matrix size 64 by 64, 19.2cm FoV, 34 4mm thick slices (no gap)

with an in plane voxel dimension of 3.0x3.0mm). In a single resting state session, subjects were told to relax and keep their eyes open while a fixation cross was displayed on a white background for 6 minutes (T2* weighted functional images: TR=3000ms, TE=28ms, matrix size 64 by 64, 19.2cm FoV, 34 4mm thick slices (no gap) with an in plane voxel dimension of 3.0x3.0mm). Diffusion weighted scans consisted of 32 scans with diffusion weighted directions ($b=1000mm/s^2$), three scans at b=0, and an additional six scans at b=50. TR=9500ms, TE=87ms, GRAPPA on, FOV=256mm, 75 slices yielding an in plane voxel dimension of 2x2mm with 2mm thick axial slices, total scan time=8min,1s.

Functional MRI Pre-processing

Functional imaging data were analyzed using FSL version 4.1.4 (FMRIB's Software Library, www.fmrib.ox.ac.uk/fsl) (Smith et al., 2004) and AFNI (Analysis of Functional NeuroImages; Cox, 1996). Structural and functional images were skull-stripped using AFNI (3dskullstrip and 3dautomask). Functional volumes were motion corrected to the mean functional volume with MCFLIRT (Motion Correction using FMRIB's Linear Image Registration Tool) using a normalized correlation ratio cost function and sinc interpolation (Jenkinson et al., 2002). Translations and rotations in the x, y, and z dimensions were calculated from volume to volume and averaged to generate mean relative displacement values. Subjects with greater than 3mm displacement between any time were excluded prior to further analyses. Images were spatially smoothed using a Gaussian kernel of FWHM 5mm and high pass filtered ($t > 0.01$ Hz). For registration, the second functional volume was aligned to the high-resolution matched bandwidth coplanar images via an affine transformation with 6 degrees of freedom, then aligned to the standard Montreal Neurological Institute (MNI) average of 152 brains using an affine transformation with 12 degrees of freedom using FLIRT (FMRIB's Linear Image Registration Tool). After statistical analyses were performed in subject native space, this transformation

matrix was applied to contrast parameter estimate and contrast variance parameter estimate spatial maps in order to perform group level analyses in standard space.

Emotional Faces fMRI Task Design and Analysis

Participants underwent a rapid event-related fMRI paradigm in which faces with different emotional expressions were displayed (Pfeifer et al., 2011; Pfeifer et al., 2008; Dapretto et al., 2006). Subjects were asked to "just look at the expression on each face." Subjects were presented with 80-full color faces from the NimStim facial expressions stimulus set (Tottenham et al., 2009). The scan consisted of 96 events whereby each emotion (neutral, happy, sad, fearful, and angry), as well fixation crosses (null events), were presented at eye level for 2s with an average inter-trial interval of 3s. The order of events was optimized and jittered (jitter ranging from 500ms to 1500ms in 125ms increments) to maximize contrast detection efficiency (Wager and Nichols, 2003). Using FSL's FEAT (FMRI Expert Analysis Tool), time-series statistical analysis was carried out using FILM with local autocorrelation correction (Woolrich et al., 2001). The 5 sets of emotional faces and null events were modeled with a convolved double gamma HRF according to the general linear model. The contrast of all emotional faces versus null event was brought to the group level using a mixed effects analysis with FLAME (FMRIB's Local Analysis of Mixed Effects). We chose to focus on the contrast of all faces (including neutral) versus null events given that even neutral facial expressions can elicit neural responses that do not significantly differ from those elicited by other emotions. We directly compared whole-brain activation maps from the CC risk and GG non-risk groups. Whole brain Z-statistic maps for the CC>GG map were thresholded ($Z>2.3$) using correction for multiple comparisons at the cluster level ($p<0.05$) and displayed on the MNI 152 1mm standard brain (**Figure 3.1A**). Within-group maps were thresholded at $Z>1.7$ (uncorrected) for illustrative purposes.

As shown in **Table 3.1**, the three genotype groups did not differ by age, full scale IQ, verbal IQ, performance IQ, mean relative head motion, gender, or scanner type and there were no diagnostic differences in age, gender, or head motion. For further analysis, we extracted the average activity in all regions identified from the CC>GG contrast (Z>2.3, corrected) and report tests of means from a 2 by 3 factor ANOVA, covarying for Full Scale IQ and scanner type (**Figure 3.1B**).

Resting-State Data Pre-processing

In addition to all of the same pre-processing steps described above for the emotional faces functional scan, we band pass filtered (0.1 Hz > *t* > 0.01 Hz) the data and regressed out nuisance covariates, including 6 rigid body motion parameters and average white matter (WM), cerebrospinal fluid (CSF) and global time-series. The WM and CSF time-series reflected signal from subject-specific regions of interest (ROIs) created using FAST (FSL's Automatic Segmentation Tool). Additionally, volumes with large signal intensity changes (i.e. motion spikes) were modeled out by creating additional nuisance regressors that modeled individual time points with greater than a half of a standard deviation change in global signal intensity as calculated by the fsl_motion_outliers script. The residuals from the previous step were aligned to high-resolution coplanar images via an affine transformation with 6 degrees of freedom and then aligned to the standard MNI average of 152 brains using an affine transformation with 12 degrees of freedom using FLIRT.

Resting-State Data Analysis

Time-series statistical analysis was carried out according to the general linear model using FEAT, Version 5.98. In order to examine functional connectivity in the default mode network, time-series were extracted from a 5mm radius sphere in the posterior cingulate cortex centered at (-2, -39, 38), which is the peak of the combined default mode network map derived

from the conjunction of multiple DMN seeds (Fox et al., 2005). We correlated the average time series from this region with every voxel in the brain to generate connectivity maps for each subject. Individual correlation maps were converted into z-statistic maps using Fischer's *r* to *z* transformation and then combined and contrasted at the group level using the ordinary least squares method. We directly compared whole-brain activation maps from the CC risk and GG non-risk groups. Whole brain Z-statistic maps for the GG>CC map were thresholded (Z>2.3) using correction for multiple comparisons at the cluster level ($p<0.05$) and displayed on the MNI 152 1mm standard brain (**Figure 3.2A**). Within-group maps were thresholded at Z>1.7 (uncorrected) for illustrative purposes.

As shown in **Table 3.1**, the three genotype groups did not differ by full scale IQ, performance IQ, mean relative head motion, or gender and there were no diagnostic differences in age, gender, or head motion. For further analysis, we extracted the average functional connectivity Z-scores between the posterior cingulate seed and the medial prefrontal and frontal orbital regions identified from the GG>CC contrast (Z>2.3, corrected) and report tests of means from 2 by 3 factor ANOVA, covarying for age and Full Scale IQ (**Figure 3.2B**).

DTI Pre-processing and Data Analysis

We examined fractional anisotropy (FA) in major white matter tracts using FSL's Tract Based Spatial Statistics (TBSS version 1.2; Smith et al., 2006). Individual images with gross motion artifacts (exceeding 2mm displacement) were identified and removed and subjects with excessive motion (greater than 8 volumes with >2mm motion) were excluded from further analysis. Motion and eddy current correction was then applied to the diffusion weighted images with FDT (FMRIB's Diffusion Toolbox). FSL's dtifit was used to fit a diffusion tensor model to the data at each voxel. Voxelwise values of FA were calculated from tensor maps for each subject. TBSS was used to perform a whole-brain voxelwise between-group FA analysis. FA maps were

nonlinearly registered to the FMRIB58_FA 1x1x1mm MNI standard space atlas using FNIRT (FMRIB's Nonlinear Image Registration Tool). FA maps were then skeletonized and thresholded at 0.2 to minimize the effect of voxels at the edge of tracts. Skeletonized FA maps were then fed into FSL's randomise for inference testing using voxelwise permutation tests and threshold free cluster enhancement (TFCE; Smith et al., 2009). We directly compared the CC risk group and GG non-risk group skeletonized FA maps. Results are displayed at $p<0.05$, fully corrected for multiple comparisons using TFCE. Results from the voxelwise analysis on FA skeleton were expanded using tbss_fill for visualization purposes and displayed on the MNI 152 1mm standard brain (**Figure 3.3A**).

As shown in **Table 3.1**, the three genotype groups did not differ by full scale IQ, verbal IQ, performance IQ, mean relative head motion, gender, or scanner type and there were no diagnostic differences in age, gender, or head motion. For further analysis, we extracted the average FA from white matter regions identified from the GG>CC contrast ($p<0.05$, corrected) and report tests of means from 2 by 3 factor ANOVA, covarying for age and Full Scale IQ (**Figure 3.3)**

Table 3.1. Mean, standard deviation, and test statistics for MET rs1858830 genotype groups

	Typically Developing			Autism Spectrum Disorder				
Characteristic	**GG "Non Risk"**	**CG "Intermediate Risk"**	**CC "Risk"**	**GG "Non Risk"**	**CG "Intermediate Risk"**	**CC "Risk"**	***Genotype Effect***	***Diagnostic Effect***
Subjects in faces fMRI task sample								
Sample Size	16	34	28	12	39	15		
Acquired on Siemens 3T Allegra	7	18	14	0	3	1	χ^2 = 0.876, p = 0.645	χ^2 = 32.995 p < 0.001
Number of Females	5	5	6	2	2	3	χ^2 = 4.704, p = 0.095	χ^2 = 2.614, p = 0.106
Age	12.6 (2.2)	12.4 (2.4)	12.4 (1.9)	14.2 (2.9)	13.2 (2.5)	12.0 (2.7)	F(2,144) = 1.992, p = 0.140	F(1,144) = 2.320, p = 0.130
Verbal IQ	110.9 (13.4)	114.6 (10.5)	117.2 (14.3)	106.1 (15.5)	99.6 (15.3)	100.7 (7.9)	F(2,144) = 0.234, p = 0.792	F(1,144) = 24.051, p < 0.001
Performance IQ	104.9 (11.4)	110.7 (12.0)	110.9 (13.9)	106.7 (15.0)	101.6 (14.5)	98.6 (14.7)	F(2,144) = 0.038, p = 0.963	F(1,144) = 5.909, p = 0.016
Full Scale IQ	109.0 (11.9)	114.4 (10.0)	115.6 (12.0)	107.3 (16.2)	101.0 (14.5)	98.7 (9.2)	F(2,144) = 0.056, p = 0.945	F(1,144) = 21.470, p < 0.001
Mean Relative Head Motion (mm)	0.101 (0.085)	0.091 (0.057)	0.096 (0.063)	0.078 (0.055)	0.094 (0.066)	0.132 (0.125)	F(2,144) = 1.334, p = 0.267	F(1,144) = 0.123, p = 0.727
ADOS social				5.4 (2.4)	7.7 (2.3)	8.8 (2.8)	F(2,66) = 7.262, p = 0.001	
ADOS communication				2.6 (1.4)	3.2 (1.4)	3.7 (1.9)	F(2,66) = 1.863, p = 0.164	
ADOS repetitive and restricted				1.8 (1.4)	1.7 (1.7)	1.8 (1.8)	F(2,66) = 0.006, p = 0.994	
Subjects in resting-state fMRI sample								
Sample Size	9	15	9	7	24	7		
Number of Females	1	2	2	2	1	3	χ^2 = 4.976, p = 0.083	χ^2 = 0.005, p = 0.941
Age	13.9 (2.0)	12.9 (2.2)	11.5 (4.4)	14.9 (1.7)	13.5 (2.4)	12.5 (2.4)	F(2,71) = 3.693, p = 0.03	F(1,71) = 1.7, p = 0.197
Verbal IQ	101.0 (8.4)	109.07 (10.43)	111.9 (7.9)	109.7 (15.5)	100.42 (12.71)	103.9 (9.6)	F(2,71) = 0.429, p = 0.653	F(1,71) = 0.781, p = 0.380
Performance IQ	96.6 (8.9)	107.73 (7.97)	106.0 (15.79)	103.1 (15.3)	99.29 (12.29)	104.33 (18.92)	F(2,71) = 0.716, p = 0.492	F(1,71) = 0.135, p = 0.714
Full Scale IQ	99.0 (8.6)	108.53 (7.52)	109.2 (9.3)	106.3 (16.1)	100.38 (13.14)	104.3 (10.5)	F(2,71) = 0.527, p = 0.593	F(1,71) = 0.431, p = 0.514
Mean Relative Head Motion (mm)	0.079 (0.024)	0.083 (0.064)	0.093 (0.11)	0.060 (0.021)	0.11 (0.068)	0.129 (0.065)	F(2,71) = 1.637, p = 0.202	F(1,71) = 0.707, p = 0.403
ADOS social				6.1 (3.6)	7.4 (2.5)	9.1 (2.6)	F(2,38) = 3.067, p = 0.059	
ADOS communication				3.0 (1.6)	3.0 (1.4)	4.1 (0.9)	F(2,38) = 2.029, p = 0.147	
ADOS repetitive and restricted				1.6 (2.1)	1.6 (1.7)	1.7 (1.0)	F(2,38) = 0.013, p = 0.987	
Subjects in DTI sample								
Sample Size	10	17	11	9	25	12		
Number of Females	1	3	2	2	2	2	χ^2 = 0.411, p= 0.814	χ^2 = 0.128, p = 0.720
Age	14.1 (2.0)	12.8 (2.7)	12.9 (1.9)	14.0 (3.3)	13.0 (2.6)	11.8 (2.2)	F(2,84) = 2.281, p = 0.109	F(1,84) = 0.156, p = 0.694
Verbal IQ	103.4 (11.0)	107.6 (10.6)	116.0 (10.1)	107.0 (16.2)	103.0 (13.2)	104.8 (9.9)	F(2,84) = 1.472, p = .0236	F(1,84) = 2.139, p = 0.148
Performance IQ	97.2 (9.2)	107.5 (9.9)	110.5 (16.5)	105.0 (15.0)	106.6 (14.5)	101.9 (17.2)	F(2,84) = 0.877, p = 0.420	F(1,84) = 0.744, p = 0.391
Full Scale IQ	100.5 (10.0)	108.4 (8.6)	114.8 (12.6)	105.7 (18.8)	104.3 (12.8)	102.2 (11.3)	F(2,84) = 1.003, p = 0.371	F(1,84) = 1.817, p = 0.182
Volumes removed due to head motion	0.90 (1.91)	1.06 (1.48)	1.00 (2.05)	0.67 (1.32)	0.92 (1.94)	1.50 (1.98)	F(2,84) = 0.351, p = 0.705	F(1,84) = .010, p = .920
ADOS social				6.6 (3.2)	7.4 (2.5)	8.4 (2.3)	F(2,46) = 1.333, p = 0.274	
ADOS communication				2.8 (1.6)	2.9 (1.4)	3.2 (1.4)	F(2,46) = 0.210, p = 0.811	
ADOS repetitive and restricted				2.3 (2.1)	1.6 (1.7)	1.8 (1.1)	F(2,46) = 0.639, p = 0.533	

Data is mean (standard deviation). Columns on the right display F-statistics and p-values of main effects of genotype and diagnostic status from 2X3 ANOVAs for age, full scale IQ, verbal IQ, performance IQ, mean relative head motion, ADOS social, communication and repetitive/restricted subscales and χ^2-statistics and p-values for chi-square tests on scanner type (functional activation only) and gender.

Table 3.2. Peak coordinates of fMRI activation maps

	CC				GG				GG>CC			
	MNI peak (mm)			Max	MNI peak (mm)			Max	MNI peak (mm)			Max
	x	y	z	*Z*	x	y	z	*Z*	x	y	z	*Z*
Right Frontal Pole	6	64	20	4.98	26	60	-2	-6.31	8	70	14	4.49
Left Frontal Pole	-4	64	14	5.16	-20	40	42	-3.87	2	68	-4	3.61
Anterior Cingulate Gyrus	2	4	28	3.21	8	38	-6	-4.06	-6	42	20	3.49
Paracingulate Gyrus	-4	36	-16	4.06	2	34	42	-5.59	-6	32	-12	3.75
Right Middle Frontal Gyrus	34	4	62	-4.95	26	28	46	-5.68				
Left Middle Frontal Gyrus	-28	34	40	-2.92	-26	22	38	-4.89				
Right Caudate	12	10	20	-3.37	12	22	-4	-4.67	8	4	12	2.85
Subcallosal Cortex					0	16	-24	2.57				
Ventromedial Prefrontal Cortex	-4	30	-20	5.52	-4	14	-6	-4.83	4	44	-14	4.04
Left Accumbens	-8	14	-8	-2.48	-6	14	-6	-5.01				
Right Accumbens	10	10	-8	-2.74	8	14	-8	-5.67	12	20	-6	2.68
Left Caudate	-12	8	20	-3.25	-8	10	-4	-4.14	-12	-6	18	2.98
Right Putamen	30	*-12*	-10	5.66	12	10	-10	-4.65	30	-20	-2	3.13
Left Putamen	-30	-16	-8	4.29	-14	8	-10	-3.25	-30	-22	2	2.46
Left Pallidum	-20	2	2	4.00	-14	6	-6	-2.95				
Right Pallidum	20	-8	-8	4.19	14	6	-6	-4.06	20	-8	-8	2.89
Right Amygdala	18	-4	-16	6.91	20	-6	-14	4.09	48	-18	-12	3.37
Left Amygdala	-22	-6	-14	5.50	-22	-8	-10	3.55	22	-10	-12	3.10
Right Planum Polare					44	-10	-10	-4.92	50	0	0	3.22
Left Planum Polare					-44	-18	-6	-3.79	-46	-12	0	3.27
Right Heschls Gyrus	38	-20	12	2.40	36	-26	16	-3.58	52	-12	6	3.08
Right Middle Temporal Gyrus	66	-24	-22	2.38	64	-26	-10	-5.35				
Left Heschls Gyrus	-46	-24	12	2.91	-46	-28	12	-4.69	-46	-28	12	5.23
Right Planum Temporale					58	-28	16	-5.04	56	-32	14	3.63
Right Thalamus	22	-30	0	10.74	22	-30	0	7.89	20	-34	0	3.40
Left Thalamus	-18	-30	-4	9.91	-18	-30	-2	6.98	-12	-32	2	3.51
Left Planum Temporale					-46	-30	12	-4.65	-48	-28	12	4.67
Right Superior Temporal Gyrus	48	-34	8	3.19	66	-32	8	-5.41	64	-34	10	3.93
Right Supramarginal Gyrus	66	-42	18	-4.73	62	-42	12	-6.49	64	-38	10	3.63
Left Middle Temporal Gyrus	-62	2	-22	3.11	-66	-44	-4	-4.15	-56	0	-26	3.32
Left Superior Temporal Gyrus	-66	-18	-8	2.33	-66	-44	10	-4.97	-50	-12	-10	2.92
Precuneus	-2	-50	56	-5.10	4	-44	52	-7.68	0	-74	54	3.96
Left Supramarginal Gyrus	-52	-46	20	-3.57	-66	-48	10	-6.16				
Posterior Cingulate Gyrus	12	-42	40	-4.07	6	-50	40	-6.87	4	-48	18	3.55
Right Angular Gyrus	64	-48	18	-4.93	64	-50	24	-5.78	52	-46	14	3.05
Right Superior Parietal Lobule	12	-50	68	-3.98	12	-50	64	-4.85				
Left Superior Parietal Lobule	-26	-44	60	-3.96	-12	-54	66	-4.73				
Left Angular Gyrus	-56	-52	26	-3.47	-62	-54	12	-6.15				
Left Fusiform Gyrus	-12	-82	-14	8.96	-26	-80	-12	7.25	-24	-34	-22	2.73
Right Fusiform Gyrus	36	-80	-12	11.39	32	-84	-14	7.45	34	-52	-18	4.12
Lingual Gyrus	2	-88	-6	10.92	-4	-86	-2	7.74				
Right Lateral Occipital Cortex	24	-86	18	8.58	28	-88	12	6.35				
Occipital Pole/ Intracalcarine Cortex	-6	-92	-4	11.11	8	-88	8	8.47	2	-68	14	2.89
Left Lateral Occipital Cortex	-20	-84	20	7.18	-24	-90	18	5.27				

Regions are defined from the Harvard Oxford Probabilistic Atlas and are sorted anterior-posterior, based on the Y coordinate from the GG non-risk group map. Coordinates are in Montreal Neurological Institute space.

Table 3.3. Peak coordinates of default mode network connectivity maps

	CC				GG				GG>CC			
	MNI peak (mm)			Max	MNI peak (mm)			Max	MNI peak (mm)			Max
	x	y	z	Z	x	y	z	Z	x	y	z	Z
Superior Frontal Gyrus	-2	62	26	4.29	0	62	28	4.93				
Paracingulate Gyrus	0	46	0	5.06	0	54	-2	7.18	0	54	-4	3.57
Ventromedial Prefrontal Cortex	-4	18	-18	4.28	0	32	-32	2.86				
Right Frontal Orbital Cortex	38	38	12	2.49	34	30	-14	6.29	32	28	-12	4.29
Left Frontal Orbital Cortex	-28	22	-22	3.14	-36	30	-14	4.13				
Right Middle Frontal Gyrus	26	26	48	5.38	24	26	44	5.93				
Left Middle Frontal Gyrus	-28	22	48	6.65	-40	14	40	5.32				
Right Caudate	10	6	18	2.93	12	12	14	4.92				
Left Caudate	-10	6	16	2.70	-10	10	14	5.13				
Thalamus	0	-14	4	4.44	2	-14	4	5.26				
Right Middle Temporal Gyrus	66	-2	-18	5.26	72	-16	-12	3.93				
Left Middle Temporal Gyrus	-62	-32	-14	5.56	-64	-20	-14	4.56				
Right Hippocampus/Parahippocampal Gyrus	30	-30	-12	5.53	24	-30	-10	3.76				
Left Hippocampus/Parahippocampal Gyrus	-20	-38	4	5.19	-18	-32	-10	5.72				
Posterior Cingulate Gyrus	-2	-38	38	11.48	-2	-38	36	11.63				
Precuneous Cortex	0	-68	32	6.64	-6	-54	8	7.20				
Right Angular Gyrus	48	-58	38	5.35	50	-60	32	6.18				
Left Angular Gyrus	-36	-74	46	6.69	-40	-68	38	7.27				
Right Cerebellum	12	-88	-32	4.68	44	-68	-38	4.14				
Left Cerebellum	-44	-68	-44	3.95	-40	-74	-38	4.90				

Regions are defined from the Harvard Oxford Probabilistic Atlas and are sorted anterior-posterior, based on the Y coordinate from the GG group map. Coordinates are in Montreal Neurological Institute space.

Table 3.4. Tracts with reduced fractional anisotropy in the CC risk group

	MNI peak (mm)			Max	# Significant	% of Significant
	x	y	z	*corr p*	Voxels	Voxels
Splenium of Corpus Callosum	17	-40	7	0.026	1637	71.58
Body of Corpus Callosum	2	-30	21	0.026	753	24.09
Middle Cerebellar Peduncle	25	-47	-39	0.034	648	25.21
Right Posterior Corona Radiata	31	-62	19	0.028	464	56.52
Left Rentrolenticular part of Interior Capsule	-38	-33	1	0.028	431	57.47
Right Rentrolenticular part of Interior Capsule	37	-24	-3	0.028	420	56.60
Left Superior Longitudinal Fasciculus	-37	-53	12	0.032	396	28.63
Right Superior Longitudinal Fasciculus	39	-54	12	0.028	353	24.55
Right Posterior Thalamic Radiation	36	-52	12	0.028	326	28.65
Left Posterior Thalamic Radiation	-30	-54	14	0.026	307	29.38
Right Cerebral Peduncle	15	-23	-9	0.028	280	46.98
Right Posterior Limb of Interior Capsule	21	-18	-3	0.028	262	31.15
Left Cerebral Peduncle	-11	-22	-21	0.046	242	38.91
Right Corticospinal Tract	8	-22	-29	0.034	227	60.53
Left Posterior Corona Radiata	-29	-61	19	0.028	209	27.94
Left Corticospinal Tract	-10	-26	-28	0.046	180	45.92
Right External Capsule	36	-11	-13	0.028	158	11.92
Left Sagittal Striatum (Inferior Longitudinal Fasiculus)	-41	-31	-15	0.046	150	31.51
Right Fornix Cres	34	-12	-14	0.028	144	46.01
Right Superior Corona Radiata	26	-19	29	0.028	113	8.78
Left Posterior Limb of Interior Capsule	-27	-23	13	0.028	103	12.02
Pontine Crossing Tract	6	-32	-33	0.036	99	21.48
Left Superior Corona Radiata	-28	-23	19	0.032	76	5.97
Right Medial Lemniscus	6	-35	-32	0.036	67	32.37
Right Superior Cerebellar Peduncle	8	-34	-23	0.034	63	24.71
Left External Capsule	-28	-21	16	0.028	62	4.35
Right Sagittal Striatum (Inferior Longitudinal Fasiculus)	36	-12	-14	0.028	55	9.32
Left Fornix Cres	-33	-10	-16	0.048	42	10.53
Right Tapetum	32	-49	15	0.028	32	100.00
Left Cingulum Hippocampus	-17	-42	-2	0.044	13	5.08
Right Anterior Limb Interior Capsule	12	10	-4	0.048	8	1.02
Left Tapetum	-28	-52	16	0.026	7	100.00
Left Superior Cerebellar Peduncle	-5	-31	-21	0.048	6	2.63

Tracts are defined from the John Hopkins University White Matter Tractography Atlas and sorted by number (#) of significant voxels. Coordinates are in Montreal Neurological Institute space. P values are after correction form multiple comparisons.

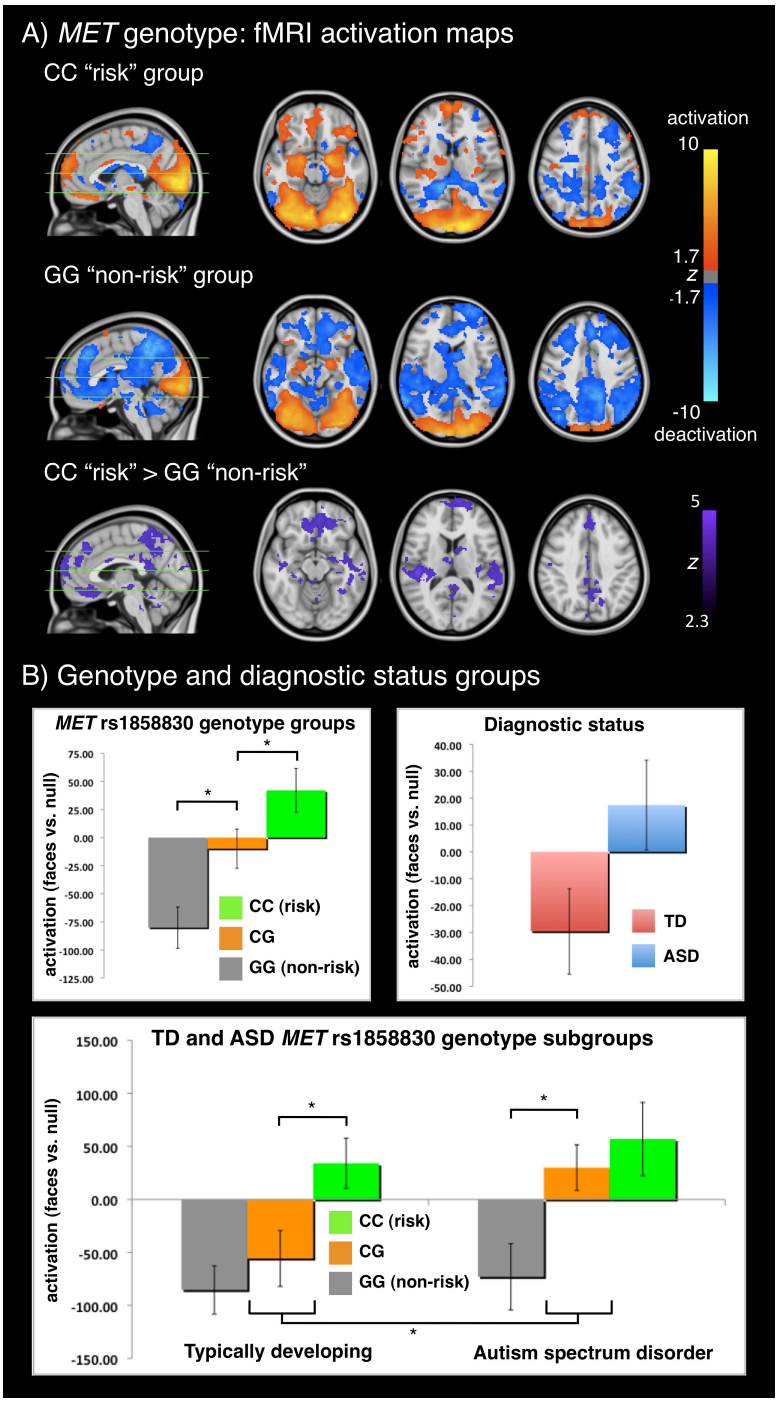

Figure 3.1. Functional MRI activation patterns to emotional faces in *MET* risk carriers. A) Within group whole-brain activation (orange) and deactivation (blue) maps for CC "risk" group, GG "non-risk" group, and between groups (risk>non-risk; purple). B) Averages and standard errors for functional activation parameter estimates from regions in risk>non-risk contrast for each genotype phenotype subgroup (Full scale IQ and MRI scanner included as covariates in 2X3 ANOVA model). *p<0.05.

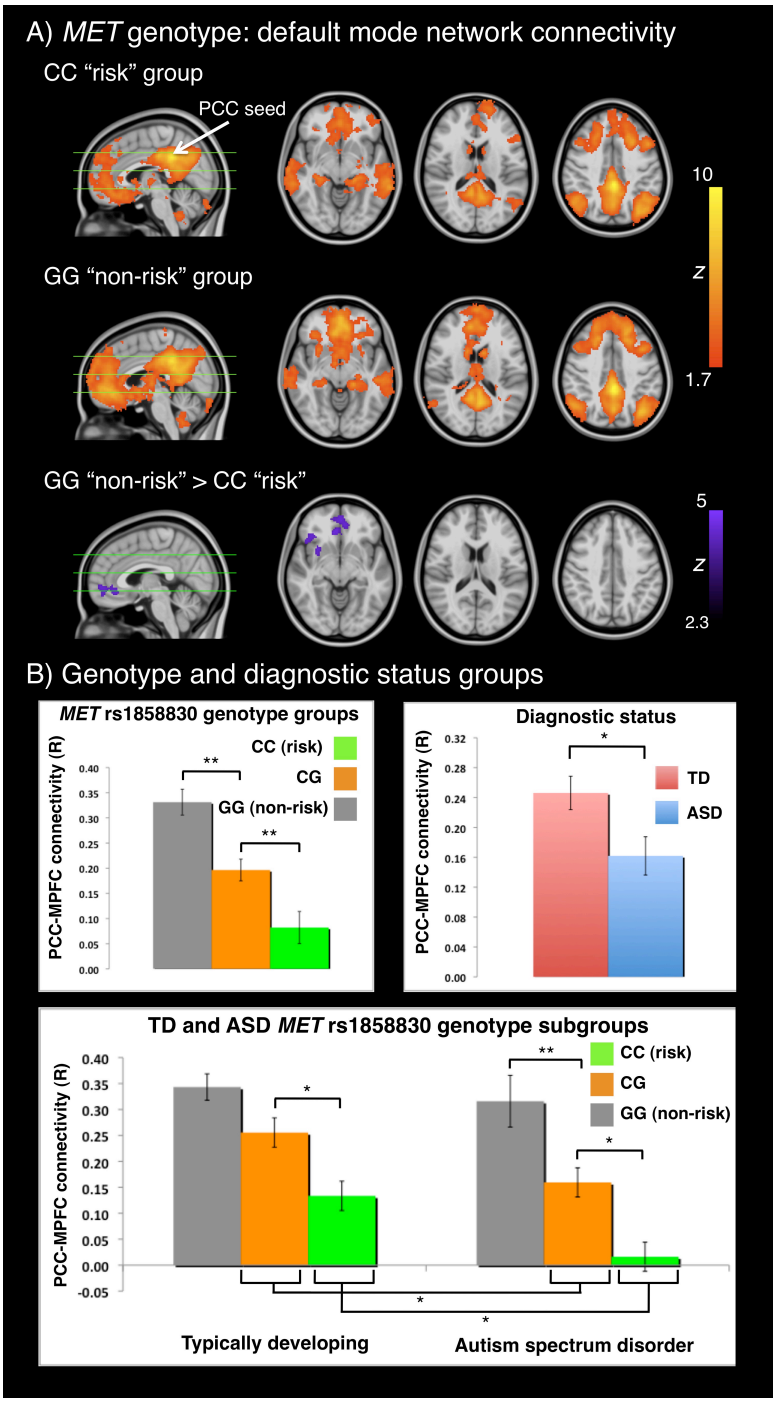

Figure 3.2. Reduced default mode network (DMN) functional connectivity in *MET* risk carriers. A) DMN connectivity within CC "risk" group, GG "non-risk" group, and between groups (risk>non-risk; purple). B) Averages and standard errors for functional connectivity between posterior cingulate seed and medial prefrontal and frontal orbital clusters from GG>CC contrast for each genotype phenotype subgroup (age and IQ included as covariates in 2X3 ANOVA). PCC = posterior cingulate cortex. *p<0.05, **p<0.01.

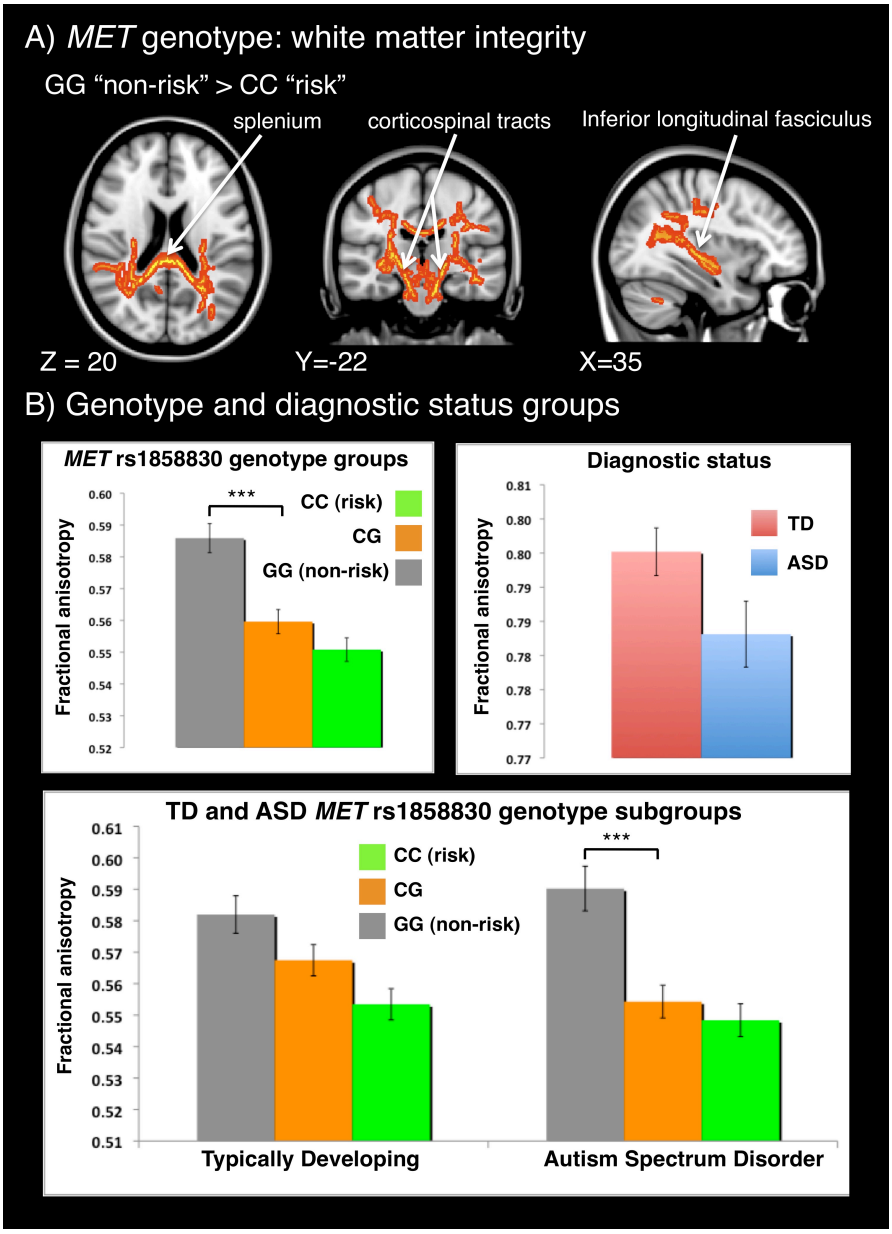

Figure 3.3. Reduced white matter integrity in *MET* risk carriers. A) Results of Tract-Based Spatial Statistics analysis comparing fractional anisotropy (FA) in GG "non-risk" group vs. CC "risk" group ($p<0.05$, corrected). B) Averages and standard errors for FA values in tracts from non-risk>risk contrast for each genotype-phenotype subgroup (age and IQ included as covariates in 2x3 ANOVA). ***$p<0.001$.

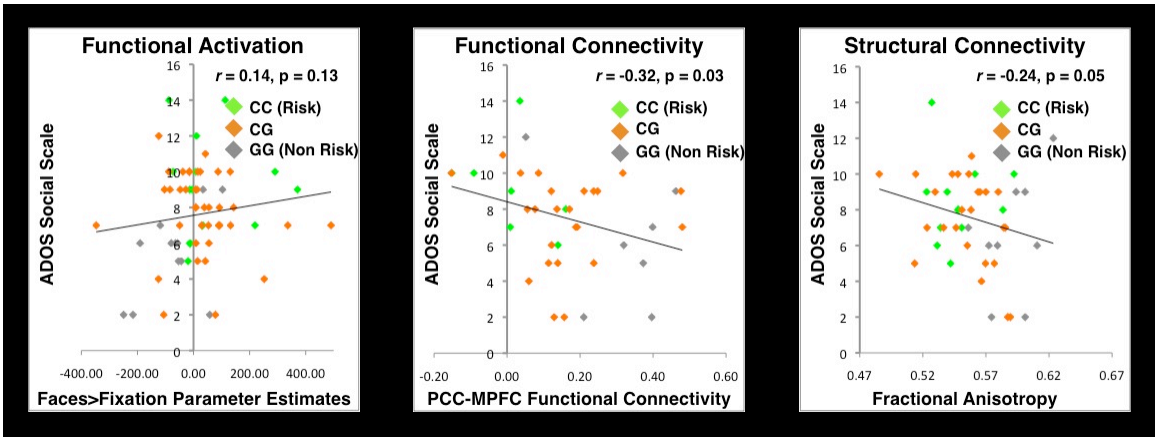

Figure 3.4. Relationship between imaging measures and social symptoms in ASD. Correlations between the social subscale of the Autism Diagnostic Observation Scale (ADOS) is shown for functional activation parameter estimates while viewing emotional faces (first column), DMN functional connectivity (second column), and white matter structural connectivity (third column). Pearson correlation coefficients shown with p-values from a 1-tailed distribution. PCC = Posterior Cingulate Cortex, MPFC = Medial Prefrontal Cortex

CONCLUSION

Autism is an incredibly complex neurodevelopmental disorder that has a growing impact on society. Although there is much we do not understand about the disorder, it is an exciting time in which research from genetics and cellular biology is starting to converge with *in vivo* neuroimaging studies, suggesting that autism is characterized by altered brain connectivity. This dissertation sought to combine the most novel and powerful data (structural, functional and genetic) and methods in order to more carefully pinpoint alterations in brain systems of individuals with ASD. Not only does this work advance how we understand brain organization in ASD but it also builds a foundation for the ultimate goal of this line of research, which is to ultimately create biomarkers that can be used as diagnostic tools to aid in the creation of targeted interventions that will focus on specific neurobiological pathways.

In the study described in the first chapter, we used a seed-based whole-brain connectivity approach to investigate connectivity of functional systems involved in processing emotional faces. We found that the amygdala was less well connected with higher-order face-processing visual areas and that anterior and posterior components of the mirror neuron system were less well connected with each other in ASD. These findings of reduced functional integration within systems are consistent with a growing body of literature reporting reduced long-range functional connectivity in multiple neural systems in ASD. We also found that there were reduced anticorrelations between bilateral amygdala and cognitive control regions as well as between mirror neuron/salience regions and the medial prefrontal cortex of the default mode network. We were thus able to show, for the first time, that there is reduced segregation between functional systems in ASD as measured by reduced negative connectivity between systems. Given that functional networks become more integrated and segregated during typical development, these findings suggested the possibility that altered brain networks in ASD may reflect an immature or delayed pattern of connectivity. Additionally, this study carefully

considered methodological concerns including task regression, global signal regression and negative correlations. Thus, this study may help explain previously conflicting reports of decreased but also increased connectivity in autism.

In the study described in the second chapter, we collected resting-state fMRI and diffusion MRI data in a large cohort of children and adolescents with ASD and matched neurotypical control subjects and used complex network modeling to examine functional and structural brain network organization. This approach was taken as we sought to address several of the limitations of the previous study, such as teasing apart the relative contributions of intrinsic connectivity as opposed to task-related connectivity, as well as the limitation of having to choose a priori seed regions. Additionally, a graph theoretical approach allowed for an expansion on previous findings of lower functional and structural connectivity in ASD by characterizing higher-level network properties. Similar to findings of our first study, we found that individuals with ASD display reduced integration *within* functional systems and reduced segregation *between* functional systems. This was true for both short- and long-range connections, which allowed us to reject a commonly stated, although imprecise, claim that local connectivity is increased in ASD, at least at the scale of several millimeters. Graph theoretical analysis of functional networks revealed significant alterations in the modular organization and efficiency of functional networks in ASD. For structural networks, we found evidence of reduced white matter integrity and atypical age-related trajectories for global efficiency. Finally, we showed that the balance of local and global efficiency between structural and functional networks varies with age and is disrupted in ASD. Further we showed that this imbalance was related to socio-communicative impairments in individuals with ASD. An issue raised by the findings described in the first chapter is the extent to which brain abnormalities observed in ASD may reflect immature or delayed connectivity, as opposed to altered connectivity that is specific to autism and/or related to compensatory mechanisms. In this study, by collecting a larger

sample and examining more measures of brain organization, we found that some aspects of brain networks in ASD reflect immaturity, whereas others reflect more *aberrant* processes. Consistent with immaturity, integration and segregation of known functional systems were reduced in ASD; however inconsistent with immaturity, we found that local connectivity, while enhanced in typical children compared to adults, was reduced in ASD. Furthermore, developmental studies have not found differences in local efficiency in modularity between children and adults; therefore, the functional network disruptions identified here are likely to be specific to the disorder. Structurally, while matter integrity was reduced in ASD and global efficiency did not increase with age, suggestive of immaturity, white matter volume was increased in ASD, which may reflect more aberrant processes. Overall, the findings of this study provide a more comprehensive framework whereby connectivity disturbances in ASD can be understood in terms of multiple interacting systems that both change across development.

In the study described in the third chapter, we sought to address how underlying genetic factors may lead to brain network abnormalities in ASD. We focused on how a functional risk allele in the Met Receptor Tyrosine Kinase gene (*MET*) affects brain circuitry, predisposes to autism, and exacerbates social deficits in individuals with autism. Prior work has established that i) *MET* exhibits the most specific neocortical expression patterns of all genes in humans, ii) a 50% reduction in MET protein dramatically alters excitatory cortical neurons, and iii) a common autism risk variant in *MET* increases the severity of social symptoms in individuals with autism. We took a multimodal approach that included analysis of complementary functional MRI, resting-state functional connectivity MRI, and diffusion tensor MRI data in a large cohort of neurotypical and autistic children and adolescents. Remarkably, not only do our results indicate that this risk allele is a potent modulator of functional and structural circuitry in specific regions where MET is expressed, but our results also highlight a novel mechanism whereby a common functional variant, in the context of other factors, can have a stronger effect on brain circuits in a

clinical cohort. Thus, this final study provides a context for how common functional variants may play a role in neuropsychiatric disorders in a field that is currently dominated by rare variant hypotheses. These findings also have widespread implications for the field of neuroimaging, indicating that alterations in brain structure/function in clinical populations may reflect markers of genetic vulnerability (rather than causal factors), thereby suggesting that future imaging studies should take genetic risk factors into consideration. Additionally, this work suggests how incorporating genetics and *in vivo* measures of neural circuitry may help uncover subgroups with disruptions in certain biological pathways. This is a crucial step for characterizing the mechanisms by which genetic risk ultimately leads to atypical social behavior in individuals with ASD and may allow for targeted treatments and interventions.

Limitations and Future Directions

All of the experiments focused on high-functioning (IQ>75) children and adolescents with ASD between the ages of 8 and 17. This was due to the current characteristics of our subject pool, difficulties in imaging children younger than eight, and the need to limit heterogeneity. The participation requirements and confounding effects of intellectual disability limited our sample to high-functioning individuals. The high proportion of males in this population (7:1) limited our investigation of female versus male alterations in ASD. These constraints limit our ability to generalize our inferences to all individuals with ASD, because differences in age, gender and intelligence may relate to different patterns of brain circuitry and genotype-phenotype relationships. In fact, it is likely that brain abnormalities are much different in very young children, as autism is not usually diagnosed until around two years and there is evidence of early brain overgrowth and premature maturation of white matter pathways in very young children with ASD. Future studies should focus on typical and atypical development of functional

and structural brain networks in even younger populations. For example, future studies examining newborn infants at high risk for ASD during natural sleep may be useful for developing biomarkers to aid in earlier diagnosis and treatment. Additionally, future experiments, including longitudinal studies, should focus on disentangling how a history of altered engagement with the environment may affect connectivity versus how early brain abnormalities may directly lead to altered connectivity patterns.

Although resting state studies minimize task-related connectivity, one limitation is that differences in covert cognition can influence connectivity patterns and may contribute to group differences. Brain networks have been shown to reconfigure during different cognitive tasks and future studies that directly compare measures of connectivity (seed based and graph theoretical) acquired during resting state and during the performance of different cognitive tasks should be useful in this respect.

There are several limitations and concerns regarding the imaging genetics approach taken in the study described in Chapter 3. Although the findings are useful in developing a more mechanistic understanding of the neurobiology of the disorder, they only provide insight about common variation in a single candidate gene. Previous work from our lab established that *CNTNAP2* modulates functional connectivity in a similar way as *MET* in typically developing individuals. Thus, future work should characterize the interaction/additive effects of multiple common and rare genetic risk variants in combination with environmental factors in the context of typical developmental processes. This is an increasingly relevant and feasible goal in a post genomic era where advances in technology and collaborative efforts are increasing the quality and quantity of both genetic and imaging data. Additionally, the contribution of genetic factors should be measured in younger ages and through longitudinal designs to further tease apart trajectories of individuals with different combinations of risk factors. Since we have shown that network alterations are present in typical individuals who simply carry risk alleles and other

studies have shown similarities between individuals with ASD and unaffected siblings, future designs should include unaffected siblings to tease apart network alterations that are simply related to genetic background from those which may be more primary.

Finally, and most importantly, future studies combining imaging data and genetics should strive to be directly relevant to clinical outcomes. There needs to be greater emphasis on characterizing the individual subjects as the findings presented here and previous studies have focused on differences at the group level. This is largely due to a low signal to noise ratio in imaging data as well as large variability due to genetic and clinical heterogeneity. Focusing on the single individual will require advanced statistical approaches such as machine learning to classify individual participants. It will also require much larger datasets (both in number of subjects and quantity of data) to better train classifiers that will only become available through large-scale studies involving collaboration between institutions.

Concluding Remarks

Autism spectrum disorder is an increasingly prevalent disorder with a large societal impact. ASD develops in the context of dramatic developmental changes in functional and structural brain organization. This thesis used a multimodal approach to characterize structural and functional brain networks in ASD in relation to both neurotypical development and genetic risk factors. We found that some aspects of altered brain organization in ASD reflect less mature patterns of connectivity whereas others reflect aberrant processes and that alterations may be partially attributable to heritable genetic factors. This work provides the foundation for future studies that will identify subgroups based on shared molecular pathways and unique neural signatures so that powerful multimodal biomarkers will eventually be used for earlier diagnosis or for developing individualized behavioral and pharmacological interventions.

REFERENCES

Autism and Developmental Disabilities Monitoring Network Surveillance Year 2008 Principal Investigators (2012). Prevalence of autism spectrum disorders - autism and developmental disabilities monitoring network, 14 sites, United States, 2008. MMWR Surveill Summ *61*, 1-19.

Adolphs, R., Sears, L., and Piven, J. (2001). Abnormal processing of social information from faces in autism. J Cogn Neurosci *13*, 232-240.

Aguirre, G.K., Zarahn, E., and D'Esposito, M. (1998). The inferential impact of global signal covariates in functional neuroimaging analyses. Neuroimage *8*, 302-06.

Alexander, A.L., Lee, J.E., Lazar, M., Boudos, R., DuBray, M.B., Oakes, T.R., Miller, J.N., Lu, J., Jeong, E.K., et al. (2007). Diffusion tensor imaging of the corpus callosum in Autism. Neuroimage *34*, 61-73.

Almeida, J.R., Versace, A., Mechelli, A., Hassel, S., Quevedo, K., Kupfer, D.J., and Phillips, M.L. (2009). Abnormal amygdala-prefrontal effective connectivity to happy faces differentiates bipolar from major depression. Biol Psychiatry *66*, 451-59.

Anderson, J.S., Druzgal, T.J., Froehlich, A., Dubray, M.B., Lange, N., Alexander, A.L., Abildskov, T., Nielsen, J.A., Cariello, A.N., et al. (2010). Decreased Interhemispheric Functional Connectivity in Autism. Cereb Cortex *21*, 1134-146.

Anderson, J.S., Druzgal, T.J., Lopez-Larson, M., Jeong, E.K., Desai, K., and Yurgelun-Todd, D. (2010). Network anticorrelations, global regression, and phase-shifted soft tissue correction. Hum Brain Mapp *32*, 919-934.

Anderson, J.S., Ferguson, M.A., Lopez-Larson, M., and Yurgelun-Todd, D. Connectivity Gradients Between the Default Mode and Attention Control Networks. Brain Connectivity

Anderson, J.S., Nielsen, J.A., Froehlich, A.L., Dubray, M.B., Druzgal, T.J., Cariello, A.N., Cooperrider, J.R., Zielinski, B.A., Ravichandran, C., et al. (2011). Functional connectivity magnetic resonance imaging classification of autism. Brain *134*, 3742-754.

Andrews-Hanna, J.R., Reidler, J.S., Huang, C., and Buckner, R.L. (2010). Evidence for the Default Network's Role in Spontaneous Cognition. J Neurophysiol *104*, 322-335.

Ashwin, E., Ashwin, C., Rhydderch, D., Howells, J., and Baron-Cohen, S. (2009). Eagle-eyed visual acuity: an experimental investigation of enhanced perception in autism. Biol Psychiatry *65*, 17-21.

Assaf, M., Jagannathan, K., Calhoun, V.D., Miller, L., Stevens, M.C., Sahl, R., O'Boyle, J.G., Schultz, R.T., and Pearlson, G.D. (2010). Abnormal functional connectivity of default mode sub-networks in autism spectrum disorder patients. Neuroimage *53*, 247-256.

Bailey, A., Le Couteur, A., Gottesman, I., Bolton, P., Simonoff, E., Yuzda, E., and Rutter, M. (1995). Autism as a strongly genetic disorder: evidence from a British twin study. Psychol Med *25*, 63-77.

Baranek, G.T., David, F.J., Poe, M.D., Stone, W.L., and Watson, L.R. (2006). Sensory Experiences Questionnaire: discriminating sensory features in young children with autism, developmental delays, and typical development. J Child Psychol Psychiatry *47*, 591-601.

Barnea-Goraly, N., Kwon, H., Menon, V., Eliez, S., Lotspeich, L., and Reiss, A.L. (2004). White matter structure in autism: preliminary evidence from diffusion tensor imaging. Biol Psychiatry *55*, 323-26.

Barnea-Goraly, N., Lotspeich, L.J., and Reiss, A.L. (2010). Similar white matter aberrations in children with autism and their unaffected siblings: a diffusion tensor imaging study using tract-based spatial statistics. Arch Gen Psychiatry *67*, 1052-060.

Baron-Cohen, S. (2002). The extreme male brain theory of autism. Trends Cogn Sci *6*, 248-254.

Baron-Cohen, S., Ashwin, E., Ashwin, C., Tavassoli, T., and Chakrabarti, B. (2009). Talent in autism: hyper-systemizing, hyper-attention to detail and sensory hypersensitivity. Philos Trans R Soc Lond B Biol Sci *364*, 1377-383.

Baron-Cohen, S., Ring, H.A., Bullmore, E.T., Wheelwright, S., Ashwin, C., and Williams, S.C. (2000). The amygdala theory of autism. Neurosci Biobehav Rev *24*, 355-364.

Baron-Cohen, S., Ring, H.A., Wheelwright, S., Bullmore, E.T., Brammer, M.J., Simmons, A., and Williams, S.C. (1999). Social intelligence in the normal and autistic brain: an fMRI study. Eur J Neurosci *11*, 1891-98.

Bassett, D.S., Bullmore, E., Verchinski, B.A., Mattay, V.S., Weinberger, D.R., and Meyer-Lindenberg, A. (2008). Hierarchical organization of human cortical networks in health and schizophrenia. J Neurosci *28*, 9239-248.

Beckmann, C.F., DeLuca, M., Devlin, J.T., and Smith, S.M. (2005). Investigations into resting-state connectivity using independent component analysis. Philos Trans R Soc Lond B Biol Sci *360*, 1001-013.

Belmonte, M.K., Allen, G., Beckel-Mitchener, A., Boulanger, L.M., Carper, R.A., and Webb, S.J. (2004). Autism and abnormal development of brain connectivity. J Neurosci *24*, 9228-231.

Ben-Sasson, A., Cermak, S.A., Orsmond, G.I., Tager-Flusberg, H., Carter, A.S., Kadlec, M.B., and Dunn, W. (2007). Extreme sensory modulation behaviors in toddlers with autism spectrum disorders. Am J Occup Ther *61*, 584-592.

Betancur, C., Sakurai, T., and Buxbaum, J.D. (2009). The emerging role of synaptic cell-adhesion pathways in the pathogenesis of autism spectrum disorders. Trends Neurosci *32*, 402-412.

Bishop, D.V., Maybery, M., Maley, A., Wong, D., Hill, W., and Hallmayer, J. (2004). Using self-report to identify the broad phenotype in parents of children with autistic spectrum disorders: a study using the Autism-Spectrum Quotient. J Child Psychol Psychiatry *45*, 1431-36.

Biswal, B., Yetkin, F.Z., Haughton, V.M., and Hyde, J.S. (1995). Functional connectivity in the motor cortex of resting human brain using echo-planar MRI. Magn Reson Med *34*, 537-541.

Biswal, B.B., Mennes, M., Zuo, X.N., Gohel, S., Kelly, C., Smith, S.M., Beckmann, C.F., Adelstein, J.S., Buckner, R.L., et al. (2010). Toward discovery science of human brain function. Proc Natl Acad Sci U S A *107*, 4734-39.

Blondel, V.D., Guillaume, J.-L., Lambiotte, R., and Lefebvre, E. (2008). Fast unfolding of communities in large networks. J Stat Mech *2008*, P10008.

Bookheimer, S.Y., Strojwas, M.H., Cohen, M.S., Saunders, A.M., Pericak-Vance, M.A., Mazziotta, J.C., and Small, G.W. (2000). Patterns of brain activation in people at risk for Alzheimer's disease. N Engl J Med *343*, 450-56.

Brown, J.A., Terashima, K.H., Burggren, A.C., Ercoli, L.M., Miller, K.J., Small, G.W., and Bookheimer, S.Y. (2011). Brain network local interconnectivity loss in aging APOE-4 allele carriers. Proc Natl Acad Sci U S A *108*, 20760-65.

Buckholtz, J.W., Sust, S., Tan, H.Y., Mattay, V.S., Straub, R.E., Meyer-Lindenberg, A., Weinberger, D.R., and Callicott, J.H. (2007). fMRI evidence for functional epistasis between COMT and RGS4. Mol Psychiatry *12*, 893-95.

Bullmore, E., and Sporns, O. (2009). Complex brain networks: graph theoretical analysis of structural and functional systems. Nat Rev Neurosci *10*, 186-198.

Butts, C.T. (2009). Revisiting the foundations of network analysis. Science *325*, 414-16.

Calhoun, V.D., Kiehl, K.A., and Pearlson, G.D. (2008). Modulation of temporally coherent brain networks estimated using ICA at rest and during cognitive tasks. Hum Brain Mapp *29*, 828-838.

Campbell, D.B., D'Oronzio, R., Garbett, K., Ebert, P.J., Mirnics, K., Levitt, P., and Persico, A.M. (2007). Disruption of cerebral cortex MET signaling in autism spectrum disorder. Ann Neurol *62*, 243-250.

Campbell, D.B., Li, C., Sutcliffe, J.S., Persico, A.M., and Levitt, P. (2008). Genetic evidence implicating multiple genes in the MET receptor tyrosine kinase pathway in autism spectrum disorder. Autism Res *1*, 159-168.

Campbell, D.B., Sutcliffe, J.S., Ebert, P.J., Militerni, R., Bravaccio, C., Trillo, S., Elia, M., Schneider, C., Melmed, R., et al. (2006). A genetic variant that disrupts MET transcription is associated with autism. Proc Natl Acad Sci U S A *103*, 16834-39.

Campbell, D.B., Warren, D., Sutcliffe, J.S., Lee, E.B., and Levitt, P. (2009). Association of MET with social and communication phenotypes in individuals with autism spectrum disorder. American Journal of Medical Genetics Part B: Neuropsychiatric Genetics *153B*, 438-446.

Carr, L., Iacoboni, M., Dubeau, M.C., Mazziotta, J.C., and Lenzi, G.L. (2003). Neural mechanisms of empathy in humans: a relay from neural systems for imitation to limbic areas. Proc Natl Acad Sci U S A *100*, 5497-5502.

Casanova, M.F., Buxhoeveden, D.P., and Brown, C. (2002). Clinical and macroscopic correlates of minicolumnar pathology in autism. J Child Neurol *17*, 692-95.

Castelli, F., Frith, C., Happé, F., and Frith, U. (2002). Autism, Asperger syndrome and brain mechanisms for the attribution of mental states to animated shapes. Brain *125*, 1839-849.

Chang, C., and Glover, G.H. (2009). Effects of model-based physiological noise correction on default mode network anti-correlations and correlations. Neuroimage *47*, 1448-459.

Cheng, Y., Chou, K.H., Chen, I.Y., Fan, Y.T., Decety, J., and Lin, C.P. (2010). Atypical development of white matter microstructure in adolescents with autism spectrum disorders. Neuroimage *50*, 873-882.

Chepenik, L.G., Raffo, M., Hampson, M., Lacadie, C., Wang, F., Jones, M.M., Pittman, B., Skudlarski, P., and Blumberg, H.P. (2010). Functional connectivity between ventral prefrontal cortex and amygdala at low frequency in the resting state in bipolar disorder. Psychiatry Res *182*, 207-210.

Cherkassky, V.L., Kana, R.K., Keller, T.A., and Just, M.A. (2006). Functional connectivity in a baseline resting-state network in autism. Neuroreport *17*, 1687-690.

Chiang, M.C., McMahon, K.L., de Zubicaray, G.I., Martin, N.G., Hickie, I., Toga, A.W., Wright, M.J., and Thompson, P.M. (2010). Genetics of white matter development: A DTI study of 705 twins and their siblings aged 12 to 29. Neuroimage *54*, 2308-317.

Courchesne, E., and Pierce, K. (2005). Why the frontal cortex in autism might be talking only to itself: local over-connectivity but long-distance disconnection. Curr Opin Neurobiol *15*, 225-230.

Courchesne, E., Carper, R., and Akshoomoff, N. (2003). Evidence of brain overgrowth in the first year of life in autism. JAMA *290*, 337-344.

Cox, R.W. (1996). AFNI: software for analysis and visualization of functional magnetic resonance neuroimages. Comput Biomed Res *29*, 162-173.

Craddock, R.C., James, G.A., Holtzheimer, P.E., Hu, X.P., and Mayberg, H.S. (2011). A whole brain fMRI atlas generated via spatially constrained spectral clustering. Hum Brain Mapp

Craig, A.D. (2009). How do you feel--now? The anterior insula and human awareness. Nat Rev Neurosci *10*, 59-70.

Critchley, H.D., Daly, E.M., Bullmore, E.T., Williams, S.C., Van Amelsvoort, T., Robertson, D.M., Rowe, A., Phillips, M., McAlonan, G., et al. (2000). The functional neuroanatomy of social behaviour: changes in cerebral blood flow when people with autistic disorder process facial expressions. Brain *123 (Pt 11)*, 2203-212.

Dalton, K.M., Nacewicz, B.M., Johnstone, T., Schaefer, H.S., Gernsbacher, M.A., Goldsmith, H.H., Alexander, A.L., and Davidson, R.J. (2005). Gaze fixation and the neural circuitry of face processing in autism. Nat Neurosci *8*, 519-526.

Dapretto, M., Davies, M.S., Pfeifer, J.H., Scott, A.A., Sigman, M., Bookheimer, S.Y., and Iacoboni, M. (2006). Understanding emotions in others: mirror neuron dysfunction in children with autism spectrum disorders. Nat Neurosci *9*, 28-30.

Dawson, G., Webb, S., Schellenberg, G.D., Dager, S., Friedman, S., Aylward, E., and Richards, T. (2002). Defining the broader phenotype of autism: genetic, brain, and behavioral perspectives. Dev Psychopathol *14*, 581-611.

Di Martino, A., Ross, K., Uddin, L.Q., Sklar, A.B., Castellanos, F.X., and Milham, M.P. (2009). Functional brain correlates of social and nonsocial processes in autism spectrum disorders: an activation likelihood estimation meta-analysis. Biol Psychiatry *65*, 63-74.

Dinstein, I., Pierce, K., Eyler, L., Solso, S., Malach, R., Behrmann, M., and Courchesne, E. (2011). Disrupted neural synchronization in toddlers with autism. Neuron *70*, 1218-225.

Dosenbach, N.U., Fair, D.A., Miezin, F.M., Cohen, A.L., Wenger, K.K., Dosenbach, R.A., Fox, M.D., Snyder, A.Z., Vincent, J.L., et al. (2007). Distinct brain networks for adaptive and stable task control in humans. Proc Natl Acad Sci U S A *104*, 11073-78.

Dosenbach, N.U., Nardos, B., Cohen, A.L., Fair, D.A., Power, J.D., Church, J.A., Nelson, S.M., Wig, G.S., Vogel, A.C., et al. (2010). Prediction of individual brain maturity using fMRI. Science *329*, 1358-361.

Eagleson, K.L., Campbell, D.B., Thompson, B.L., Bergman, M.Y., and Levitt, P. (2011). The autism risk genes MET and PLAUR differentially impact cortical development. Autism Res *4*, 68-83.

Ebisch, S.J., Gallese, V., Willems, R.M., Mantini, D., Groen, W.B., Romani, G.L., Buitelaar, J.K., and Bekkering, H. (2010). Altered intrinsic functional connectivity of anterior and

posterior insula regions in high-functioning participants with autism spectrum disorder. Hum Brain Mapp *32*, 1013-028.

Egan, M.F., Goldberg, T.E., Kolachana, B.S., Callicott, J.H., Mazzanti, C.M., Straub, R.E., Goldman, D., and Weinberger, D.R. (2001). Effect of COMT Val108/158 Met genotype on frontal lobe function and risk for schizophrenia. Proc Natl Acad Sci U S A *98*, 6917-922.

Fair, D.A., Cohen, A.L., Dosenbach, N.U., Church, J.A., Miezin, F.M., Barch, D.M., Raichle, M.E., Petersen, S.E., and Schlaggar, B.L. (2008). The maturing architecture of the brain's default network. Proc Natl Acad Sci U S A *105*, 4028-032.

Fair, D.A., Cohen, A.L., Power, J.D., Dosenbach, N.U., Church, J.A., Miezin, F.M., Schlaggar, B.L., and Petersen, S.E. (2009). Functional brain networks develop from a "local to distributed" organization. PLoS Comput Biol *5*, e1000381.

Fair, D.A., Dosenbach, N.U., Church, J.A., Cohen, A.L., Brahmbhatt, S., Miezin, F.M., Barch, D.M., Raichle, M.E., Petersen, S.E., and Schlaggar, B.L. (2007). Development of distinct control networks through segregation and integration. Proc Natl Acad Sci U S A *104*, 13507-512.

Fair, D.A., Schlaggar, B.L., Cohen, A.L., Miezin, F.M., Dosenbach, N.U., Wenger, K.K., Fox, M.D., Snyder, A.Z., Raichle, M.E., and Petersen, S.E. (2007). A method for using blocked and event-related fMRI data to study "resting state" functional connectivity. Neuroimage *35*, 396-405.

Feinberg, D.A., Moeller, S., Smith, S.M., Auerbach, E., Ramanna, S., Gunther, M., Glasser, M.F., Miller, K.L., Ugurbil, K., and Yacoub, E. (2010). Multiplexed echo planar imaging for sub-second whole brain FMRI and fast diffusion imaging. PLoS One *5*, e15710.

Fombonne E. (2003). JAMA. In *The prevalence of autism..* United States: [UNKNOWN REFERENCE TYPE]

Fornito, A., Zalesky, A., Bassett, D.S., Meunier, D., Ellison-Wright, I., Yücel, M., Wood, S.J., Shaw, K., O'Connor, J., et al. (2011). Genetic Influences on Cost-Efficient Organization of Human Cortical Functional Networks. J Neurosci *31*, 3261-270.

Fox, M.D., and Greicius, M. (2010). Clinical applications of resting state functional connectivity. Front Syst Neurosci *4*, 19.

Fox, M.D., and Raichle, M.E. (2007). Spontaneous fluctuations in brain activity observed with functional magnetic resonance imaging. Nat Rev Neurosci *8*, 700-711.

Fox, M.D., Snyder, A.Z., Vincent, J.L., Corbetta, M., Van Essen, D.C., and Raichle, M.E. (2005). The human brain is intrinsically organized into dynamic, anticorrelated functional networks. Proc Natl Acad Sci U S A *102*, 9673-78.

Fox, M.D., Zhang, D., Snyder, A.Z., and Raichle, M.E. (2009). The global signal and observed anticorrelated resting state brain networks. J Neurophysiol *101*, 3270-283.

Fransson, P. (2005). Spontaneous low-frequency BOLD signal fluctuations: an fMRI investigation of the resting-state default mode of brain function hypothesis. Hum Brain Mapp *26*, 15-29.

Fransson, P. (2006). How default is the default mode of brain function? Further evidence from intrinsic BOLD signal fluctuations. Neuropsychologia *44*, 2836-845.

Geschwind, D.H. (2011). Genetics of autism spectrum disorders. Trends Cogn Sci *15*, 409-416.

Geschwind, D.H., and Levitt, P. (2007). Autism spectrum disorders: developmental disconnection syndromes. Curr Opin Neurobiol *17*, 103-111.

Ghosh, A., Rho, Y., McIntosh, A.R., Kötter, R., and Jirsa, V.K. (2008). Noise during rest enables the exploration of the brain's dynamic repertoire. PLoS Comput Biol *4*, e1000196.

Glahn, D.C., Winkler, A.M., Kochunov, P., Almasy, L., Duggirala, R., Carless, M.A., Curran, J.C., Olvera, R.L., Laird, A.R., et al. (2010). Genetic control over the resting brain. Proc Natl Acad Sci U S A *107*, 1223-28.

Gottesman, I.I., and Gould, T.D. (2003). The endophenotype concept in psychiatry: etymology and strategic intentions. Am J Psychiatry *160*, 636-645.

Greicius, M.D., Krasnow, B., Reiss, A.L., and Menon, V. (2003). Functional connectivity in the resting brain: a network analysis of the default mode hypothesis. Proc Natl Acad Sci U S A *100*, 253-58.

Groen, W.B., Buitelaar, J.K., van der Gaag, R.J., and Zwiers, M.P. (2011). Pervasive microstructural abnormalities in autism: a DTI study. J Psychiatry Neurosci *36*, 32-40.

Guimerà, R., Mossa, S., Turtschi, A., and Amaral, L.A. (2005). The worldwide air transportation network: Anomalous centrality, community structure, and cities' global roles. Proc Natl Acad Sci U S A *102*, 7794-99.

Hadjikhani, N., Joseph, R.M., Snyder, J., and Tager-Flusberg, H. (2006). Anatomical differences in the mirror neuron system and social cognition network in autism. Cereb Cortex *16*, 1276-282.

Hadjikhani, N., Joseph, R.M., Snyder, J., and Tager-Flusberg, H. (2007). Abnormal activation of the social brain during face perception in autism. Hum Brain Mapp *28*, 441-49.

Hadjikhani, N., Joseph, R.M., Snyder, J., Chabris, C.F., Clark, J., Steele, S., McGrath, L., Vangel, M., Aharon, I., et al. (2004). Activation of the fusiform gyrus when individuals with autism spectrum disorder view faces. Neuroimage *22*, 1141-150.

Hagmann, P., Cammoun, L., Gigandet, X., Meuli, R., Honey, C.J., Wedeen, V.J., and Sporns, O. (2008). Mapping the structural core of human cerebral cortex. PLoS Biol *6*, e159.

Hagmann, P., Sporns, O., Madan, N., Cammoun, L., Pienaar, R., Wedeen, V.J., Meuli, R., Thiran, J.P., and Grant, P.E. (2010). White matter maturation reshapes structural connectivity in the late developing human brain. Proc Natl Acad Sci U S A *107*, 19067-072.

Hallmayer, J., Cleveland, S., Torres, A., Phillips, J., Cohen, B., Torigoe, T., Miller, J., Fedele, A., Collins, J., et al. (2011). Genetic Heritability and Shared Environmental Factors Among Twin Pairs With Autism. Arch Gen Psychiatry *68*, 1095-1102.

Hampson, M., Driesen, N., Roth, J.K., Gore, J.C., and Constable, R.T. (2010). Functional connectivity between task-positive and task-negative brain areas and its relation to working memory performance. Magn Reson Imaging *28*, 1051-57.

Hariri, A.R., and Weinberger, D.R. (2003). Imaging genomics. Br Med Bull *65*, 259.

Hariri, A.R., Bookheimer, S.Y., and Mazziotta, J.C. (2000). Modulating emotional responses: effects of a neocortical network on the limbic system. Neuroreport *11*, 43-48.

Hariri, A.R., Mattay, V.S., Tessitore, A., Fera, F., and Weinberger, D.R. (2003). Neocortical modulation of the amygdala response to fearful stimuli. Biol Psychiatry *53*, 494-501.

Hariri, A.R., Mattay, V.S., Tessitore, A., Kolachana, B., Fera, F., Goldman, D., Egan, M.F., and Weinberger, D.R. (2002). Serotonin transporter genetic variation and the response of the human amygdala. Science *297*, 400-03.

He, Y., Chen, Z.J., and Evans, A.C. (2007). Small-world anatomical networks in the human brain revealed by cortical thickness from MRI. Cereb Cortex *17*, 2407-419.

Herbert, M.R., Ziegler, D.A., Makris, N., Filipek, P.A., Kemper, T.L., Normandin, J.J., Sanders, H.A., Kennedy, D.N., and Caviness, V.S. (2004). Localization of white matter volume increase in autism and developmental language disorder. Ann Neurol *55*, 530-540.

Heuer, L., Braunschweig, D., Ashwood, P., Van de Water, J., and Campbell, D.B. (2011). Association of a MET genetic variant with autism-associated maternal autoantibodies to fetal brain proteins and cytokine expression. Translational Psychiatry *1*, e48.

Honey, C.J., Sporns, O., Cammoun, L., Gigandet, X., Thiran, J.P., Meuli, R., and Hagmann, P. (2009). Predicting human resting-state functional connectivity from structural connectivity. Proc Natl Acad Sci U S A *106*, 2035-040.

Horovitz, S.G., Fukunaga, M., de Zwart, J.A., van Gelderen, P., Fulton, S.C., Balkin, T.J., and Duyn, J.H. (2008). Low frequency BOLD fluctuations during resting wakefulness and light sleep: a simultaneous EEG-fMRI study. Hum Brain Mapp *29*, 671-682.

Horwitz, B., Rumsey, J.M., Grady, C.L., and Rapoport, S.I. (1988). The cerebral metabolic landscape in autism. Intercorrelations of regional glucose utilization. Arch Neurol *45*, 749-755.

Iacoboni, M. (2006). Failure to deactivate in autism: the co-constitution of self and other. Trends Cogn Sci *10*, 431-33.

Iacoboni, M., Lieberman, M.D., Knowlton, B.J., Molnar-Szakacs, I., Moritz, M., Throop, C.J., and Fiske, A.P. (2004). Watching social interactions produces dorsomedial prefrontal and medial parietal BOLD fMRI signal increases compared to a resting baseline. Neuroimage *21*, 1167-173.

Izhikevich, E.M., and Edelman, G.M. (2008). Large-scale model of mammalian thalamocortical systems. Proc Natl Acad Sci U S A *105*, 3593-98.

Jabbi, M., and Keysers, C. (2008). Inferior frontal gyrus activity triggers anterior insula response to emotional facial expressions. Emotion *8*, 775-780.

Jenkinson, M., Bannister, P., Brady, M., and Smith, S. (2002). Improved optimization for the robust and accurate linear registration and motion correction of brain images. Neuroimage *17*, 825-841.

Jenkinson, M., Bannister, P., Brady, M., and Smith, S. (2002). Improved optimization for the robust and accurate linear registration and motion correction of brain images. Neuroimage *17*, 825-841.

Jones, C.R., Happé, F., Baird, G., Simonoff, E., Marsden, A.J., Tregay, J., Phillips, R.J., Goswami, U., Thomson, J.M., and Charman, T. (2009). Auditory discrimination and auditory sensory behaviours in autism spectrum disorders. Neuropsychologia *47*, 2850-58.

Jones, T.B., Bandettini, P.A., Kenworthy, L., Case, L.K., Milleville, S.C., Martin, A., and Birn, R.M. (2010). Sources of group differences in functional connectivity: an investigation applied to autism spectrum disorder. Neuroimage *49*, 401-414.

Judson, M.C., Amaral, D.G., and Levitt, P. (2010). Conserved Subcortical and Divergent Cortical Expression of Proteins Encoded by Orthologs of the Autism Risk Gene MET. Cereb Cortex *21*, 1613-626.

Judson, M.C., Bergman, M.Y., Campbell, D.B., Eagleson, K.L., and Levitt, P. (2009). Dynamic gene and protein expression patterns of the autism-associated met receptor tyrosine kinase in the developing mouse forebrain. J Comp Neurol *513*, 511-531.

Judson, M.C., Eagleson, K.L., and Levitt, P. (2011). A new synaptic player leading to autism risk: Met receptor tyrosine kinase. J Neurodev Disord *3*, 282-292.

Judson, M.C., Eagleson, K.L., Wang, L., and Levitt, P. (2010). Evidence of cell-nonautonomous changes in dendrite and dendritic spine morphology in the met-signaling-deficient mouse forebrain. J Comp Neurol *518*, 4463-478.

Just, M.A., Cherkassky, V.L., Keller, T.A., and Minshew, N.J. (2004). Cortical activation and synchronization during sentence comprehension in high-functioning autism: evidence of underconnectivity. Brain *127*, 1811-821.

Just, M.A., Cherkassky, V.L., Keller, T.A., Kana, R.K., and Minshew, N.J. (2007). Functional and anatomical cortical underconnectivity in autism: evidence from an FMRI study of an executive function task and corpus callosum morphometry. Cereb Cortex *17*, 951-961.

Kaiser, M.D., Hudac, C.M., Shultz, S., Lee, S.M., Cheung, C., Berken, A.M., Deen, B., Pitskel, N.B., Sugrue, D.R., et al. (2010). Neural signatures of autism. Proc Natl Acad Sci U S A *107*, 21223-28.

Kana, R.K., Keller, T.A., Cherkassky, V.L., Minshew, N.J., and Just, M.A. (2006). Sentence comprehension in autism: thinking in pictures with decreased functional connectivity. Brain *129*, 2484-493.

Kana, R.K., Keller, T.A., Cherkassky, V.L., Minshew, N.J., and Just, M.A. (2009). Atypical frontal-posterior synchronization of Theory of Mind regions in autism during mental state attribution. Soc Neurosci *4*, 135-152.

Kana, R.K., Keller, T.A., Minshew, N.J., and Just, M.A. (2007). Inhibitory control in high-functioning autism: decreased activation and underconnectivity in inhibition networks. Biol Psychiatry *62*, 198-206.

Kanner, L., and others (1943). Autistic disturbances of affective contact. Nervous child *2*

Kelly, A.M., Di Martino, A., Uddin, L.Q., Shehzad, Z., Gee, D.G., Reiss, P.T., Margulies, D.S., Castellanos, F.X., and Milham, M.P. (2009). Development of anterior cingulate functional connectivity from late childhood to early adulthood. Cereb Cortex *19*, 640-657.

Kelly, A.M., Uddin, L.Q., Biswal, B.B., Castellanos, F.X., and Milham, M.P. (2008). Competition between functional brain networks mediates behavioral variability. Neuroimage *39*, 527-537.

Kennedy, D.P., and Courchesne, E. (2008). Functional abnormalities of the default network during self- and other-reflection in autism. Soc Cogn Affect Neurosci *3*, 177-190.

Kennedy, D.P., and Courchesne, E. (2008). The intrinsic functional organization of the brain is altered in autism. Neuroimage *39*, 1877-885.

Kennedy, D.P., Redcay, E., and Courchesne, E. (2006). Failing to deactivate: resting functional abnormalities in autism. Proc Natl Acad Sci U S A *103*, 8275-280.

Kim, Y.S., Leventhal, B.L., Koh, Y.J., Fombonne, E., Laska, E., Lim, E.C., Cheon, K.A., Kim, S.J., Kim, Y.K., et al. (2011). Prevalence of Autism Spectrum Disorders in a Total Population Sample. Am J Psychiatry

Kleinhans, N.M., Richards, T., Sterling, L., Stegbauer, K.C., Mahurin, R., Johnson, L.C., Greenson, J., Dawson, G., and Aylward, E. (2008). Abnormal functional connectivity in autism spectrum disorders during face processing. Brain *131*, 1000-012.

Kochunov, P., Glahn, D.C., Lancaster, J.L., Winkler, A.M., Smith, S., Thompson, P.M., Almasy, L., Duggirala, R., Fox, P.T., and Blangero, J. (2010). Genetics of microstructure of cerebral white matter using diffusion tensor imaging. Neuroimage *53*, 1109-116.

Konopka, G., Bomar, J.M., Winden, K., Coppola, G., Jonsson, Z.O., Gao, F., Peng, S., Preuss, T.M., Wohlschlegel, J.A., and Geschwind, D.H. (2009). Human-specific transcriptional regulation of CNS development genes by FOXP2. Nature *462*, 213-17.

Koshino, H., Carpenter, P.A., Minshew, N.J., Cherkassky, V.L., Keller, T.A., and Just, M.A. (2005). Functional connectivity in an fMRI working memory task in high-functioning autism. Neuroimage *24*, 810-821.

Koten, J.W., Wood, G., Hagoort, P., Goebel, R., Propping, P., Willmes, K., and Boomsma, D.I. (2009). Genetic contribution to variation in cognitive function: an FMRI study in twins. Science *323*, 1737-740.

Lai, M.C., Lombardo, M.V., Chakrabarti, B., Sadek, S.A., Pasco, G., Wheelwright, S.J., Bullmore, E.T., Baron-Cohen, S., and Suckling, J. (2010). A shift to randomness of brain oscillations in people with autism. Biol Psychiatry *68*, 1092-99.

Laurienti, P.J., Burdette, J.H., Wallace, M.T., Yen, Y.F., Field, A.S., and Stein, B.E. (2002). Deactivation of sensory-specific cortex by cross-modal stimuli. J Cogn Neurosci *14*, 420-29.

Lebel, C., Gee, M., Camicioli, R., Wieler, M., Martin, W., and Beaulieu, C. (2012). Diffusion tensor imaging of white matter tract evolution over the lifespan. Neuroimage *60*, 340-352.

Lebel, C., Walker, L., Leemans, A., Phillips, L., and Beaulieu, C. (2008). Microstructural maturation of the human brain from childhood to adulthood. Neuroimage *40*, 1044-055.

Le Couteur, A., Bailey, A., Goode, S., Pickles, A., Robertson, S., Gottesman, I., and Rutter, M. (1996). A broader phenotype of autism: the clinical spectrum in twins. J Child Psychol Psychiatry *37*, 785-801.

LeDoux, J.E. (2000). Emotion circuits in the brain. Annu Rev Neurosci *23*, 155-184.

Lee, J.E., Bigler, E.D., Alexander, A.L., Lazar, M., DuBray, M.B., Chung, M.K., Johnson, M., Morgan, J., Miller, J.N., et al. (2007). Diffusion tensor imaging of white matter in the superior temporal gyrus and temporal stem in autism. Neurosci Lett *424*, 127-132.

Leslie, K.R., Johnson-Frey, S.H., and Grafton, S.T. (2004). Functional imaging of face and hand imitation: towards a motor theory of empathy. Neuroimage *21*, 601-07.

Levitt, P., and Campbell, D.B. (2009). The genetic and neurobiologic compass points toward common signaling dysfunctions in autism spectrum disorders. J Clin Invest *119*, 747-754.

Lin, P., Hasson, U., Jovicich, J., and Robinson, S. (2011). A neuronal basis for task-negative responses in the human brain. Cereb Cortex *21*, 821-830.

Lord, C., Risi, S., Lambrecht, L., Cook, E.H., Leventhal, B.L., DiLavore, P.C., Pickles, A., and Rutter, M. (2000). The autism diagnostic observation schedule-generic: a standard

measure of social and communication deficits associated with the spectrum of autism. J Autism Dev Disord *30*, 205-223.

Lord, C., Rutter, M., and Le Couteur, A. (1994). Autism Diagnostic Interview-Revised: a revised version of a diagnostic interview for caregivers of individuals with possible pervasive developmental disorders. J Autism Dev Disord *24*, 659-685.

Marshall, C.R., Noor, A., Vincent, J.B., Lionel, A.C., Feuk, L., Skaug, J., Shago, M., Moessner, R., Pinto, D., et al. (2008). Structural variation of chromosomes in autism spectrum disorder. Am J Hum Genet *82*, 477-488.

Meunier, D., Achard, S., Morcom, A., and Bullmore, E. (2009). Age-related changes in modular organization of human brain functional networks. Neuroimage *44*, 715-723.

Meyer-Lindenberg, A., Kolachana, B., Gold, B., Olsh, A., Nicodemus, K.K., Mattay, V., Dean, M., and Weinberger, D.R. (2008). Genetic variants in AVPR1A linked to autism predict amygdala activation and personality traits in healthy humans. Mol Psychiatry *14*, 968-975.

Mizuno, A., Villalobos, M.E., Davies, M.M., Dahl, B.C., and Müller, R.A. (2006). Partially enhanced thalamocortical functional connectivity in autism. Brain Res *1104*, 160-174.

Monk, C.S., Peltier, S.J., Wiggins, J.L., Weng, S.J., Carrasco, M., Risi, S., and Lord, C. (2009). Abnormalities of intrinsic functional connectivity in autism spectrum disorders(,). Neuroimage *47*, 764-772.

Monk, C.S., Weng, S.J., Wiggins, J.L., Kurapati, N., Louro, H.M., Carrasco, M., Maslowsky, J., Risi, S., and Lord, C. (2010). Neural circuitry of emotional face processing in autism spectrum disorders. J Psychiatry Neurosci *35*, 105-114.

Mori, S., and van Zijl, P.C. (2002). Fiber tracking: principles and strategies - a technical review. NMR Biomed *15*, 468-480.

Mostofsky, S.H., Powell, S.K., Simmonds, D.J., Goldberg, M.C., Caffo, B., and Pekar, J.J. (2009). Decreased connectivity and cerebellar activity in autism during motor task performance. Brain *132*, 2413-425.

Mozolic, J.L., Joyner, D., Hugenschmidt, C.E., Peiffer, A.M., Kraft, R.A., Maldjian, J.A., and Laurienti, P.J. (2008). Cross-modal deactivations during modality-specific selective attention. BMC Neurol *8*, 35.

Mukamel, Z., Konopka, G., Wexler, E., Osborn, G.E., Dong, H., Bergman, M.Y., Levitt, P., and Geschwind, D.H. (2011). Regulation of MET by FOXP2, Genes Implicated in Higher Cognitive Dysfunction and Autism Risk. J Neurosci *31*, 11437-442.

Mundy, P., Sullivan, L., and Mastergeorge, A.M. (2009). A parallel and distributed-processing model of joint attention, social cognition and autism. Autism Res *2*, 2-21.

Munson, J., Dawson, G., Abbott, R., Faja, S., Webb, S.J., Friedman, S.D., Shaw, D., Artru, A., and Dager, S.R. (2006). Amygdalar volume and behavioral development in autism. Arch Gen Psychiatry *63*, 686-693.

Murphy, K., Birn, R.M., Handwerker, D.A., Jones, T.B., and Bandettini, P.A. (2009). The impact of global signal regression on resting state correlations: are anti-correlated networks introduced? Neuroimage *44*, 893-905.

Müller, R.A. (2007). The study of autism as a distributed disorder. Ment Retard Dev Disabil Res Rev *13*, 85-95.

Müller, R.A., Shih, P., Keehn, B., Deyoe, J.R., Leyden, K.M., and Shukla, D.K. (2011). Underconnected, but How? A Survey of Functional Connectivity MRI Studies in Autism Spectrum Disorders. Cereb Cortex

Nacewicz, B.M., Dalton, K.M., Johnstone, T., Long, M.T., McAuliff, E.M., Oakes, T.R., Alexander, A.L., and Davidson, R.J. (2006). Amygdala volume and nonverbal social impairment in adolescent and adult males with autism. Arch Gen Psychiatry *63*, 1417-428.

Newman, M.E.J. (2006). Modularity and community structure in networks. Proceedings of the National Academy of Sciences *103*, 8577.

Newschaffer, C.J., Croen, L.A., Daniels, J., Giarelli, E., Grether, J.K., Levy, S.E., Mandell, D.S., Miller, L.A., Pinto-Martin, J., et al. (2007). The epidemiology of autism spectrum disorders. Annu Rev Public Health *28*, 235-258.

Nishitani, N., Avikainen, S., and Hari, R. (2004). Abnormal imitation-related cortical activation sequences in Asperger's syndrome. Ann Neurol *55*, 558-562.

Noonan, S.K., Haist, F., and Müller, R.A. (2009). Aberrant functional connectivity in autism: evidence from low-frequency BOLD signal fluctuations. Brain Res *1262*, 48-63.

Oberman, L.M., and Ramachandran, V.S. (2007). The simulating social mind: the role of the mirror neuron system and simulation in the social and communicative deficits of autism spectrum disorders. Psychol Bull *133*, 310-327.

Paakki, J.J., Rahko, J., Long, X., Moilanen, I., Tervonen, O., Nikkinen, J., Starck, T., Remes, J., Hurtig, T., et al. (2010). Alterations in regional homogeneity of resting-state brain activity in autism spectrum disorders. Brain Res *1321*, 169-179.

Pelphrey, K.A., and Carter, E.J. (2008). Brain mechanisms for social perception: lessons from autism and typical development. Ann N Y Acad Sci *1145*, 283-299.

Pezawas, L., Meyer-Lindenberg, A., Drabant, E.M., Verchinski, B.A., Munoz, K.E., Kolachana, B.S., Egan, M.F., Mattay, V.S., Hariri, A.R., and Weinberger, D.R. (2005). 5-HTTLPR polymorphism impacts human cingulate-amygdala interactions: a genetic susceptibility mechanism for depression. Nat Neurosci *8*, 828-834.

Pfeifer, J.H., Iacoboni, M., Mazziotta, J.C., and Dapretto, M. (2008). Mirroring others' emotions relates to empathy and interpersonal competence in children. Neuroimage *39*, 2076-085.

Pfeifer, J.H., Masten, C.L., Moore, W.E., Oswald, T.M., Mazziotta, J.C., Iacoboni, M., and Dapretto, M. (2011). Entering adolescence: resistance to peer influence, risky behavior, and neural changes in emotion reactivity. Neuron *69*, 1029-036.

Phillips, M.L., Drevets, W.C., Rauch, S.L., and Lane, R. (2003). Neurobiology of emotion perception I: The neural basis of normal emotion perception. Biol Psychiatry *54*, 504-514.

Pierce, K., and Courchesne, E. (2000). Exploring the neurofunctional organization of face processing in autism. Arch Gen Psychiatry *57*, 344-46.

Pierce, K., Haist, F., Sedaghat, F., and Courchesne, E. (2004). The brain response to personally familiar faces in autism: findings of fusiform activity and beyond. Brain *127*, 2703-716.

Pierce, K., Müller, R.A., Ambrose, J., Allen, G., and Courchesne, E. (2001). Face processing occurs outside the fusiform 'face area' in autism: evidence from functional MRI. Brain *124*, 2059-073.

Popa, D., Popescu, A.T., and Paré, D. (2009). Contrasting activity profile of two distributed cortical networks as a function of attentional demands. J Neurosci *29*, 1191-1201.

Power, J.D., Barnes, K.A., Snyder, A.Z., Schlaggar, B.L., and Petersen, S.E. (2011). Spurious but systematic correlations in functional connectivity MRI networks arise from subject motion. Neuroimage *59*, 2142-154.

Power, J.D., Cohen, A.L., Nelson, S.M., Wig, G.S., Barnes, K.A., Church, J.A., Vogel, A.C., Laumann, T.O., Miezin, F.M., et al. (2011). Functional network organization of the human brain. Neuron *72*, 665-678.

Pugliese, L., Catani, M., Ameis, S., Dell'Acqua, F., Thiebaut de Schotten, M., Murphy, C., Robertson, D., Deeley, Q., Daly, E., and Murphy, D.G. (2009). The anatomy of extended limbic pathways in Asperger syndrome: a preliminary diffusion tensor imaging tractography study. Neuroimage *47*, 427-434.

Qiu, S., Anderson, C.T., Levitt, P., and Shepherd, G.M. (2011). Circuit-specific intracortical hyperconnectivity in mice with deletion of the autism-associated met receptor tyrosine kinase. J Neurosci *31*, 5855-864.

Raichle, M.E., MacLeod, A.M., Snyder, A.Z., Powers, W.J., Gusnard, D.A., and Shulman, G.L. (2001). A default mode of brain function. Proc Natl Acad Sci U S A *98*, 676-682.

Raznahan, A., Pugliese, L., Barker, G.J., Daly, E., Powell, J., Bolton, P.F., and Murphy, D.G. (2009). Serotonin transporter genotype and neuroanatomy in autism spectrum disorders. Psychiatr Genet *19*, 147-150.

Rizzolatti, G., and Fabbri-Destro, M. (2010). Mirror neurons: from discovery to autism. Exp Brain Res *200*, 223-237.

Roffman, J.L., Weiss, A.P., Goff, D.C., Rauch, S.L., and Weinberger, D.R. (2006). Neuroimaging-genetic paradigms: a new approach to investigate the pathophysiology and treatment of cognitive deficits in schizophrenia. Harv Rev Psychiatry *14*, 78-91.

Rosenberg, R.E., Law, J.K., Yenokyan, G., McGready, J., Kaufmann, W.E., and Law, P.A. (2009). Characteristics and concordance of autism spectrum disorders among 277 twin pairs. Arch Pediatr Adolesc Med *163*, 907-914.

Roy, A.K., Shehzad, Z., Margulies, D.S., Kelly, A.M., Uddin, L.Q., Gotimer, K., Biswal, B.B., Castellanos, F.X., and Milham, M.P. (2009). Functional connectivity of the human amygdala using resting state fMRI. Neuroimage *45*, 614-626.

Rubinov, M., and Sporns, O. (2009). Complex network measures of brain connectivity: Uses and interpretations. Neuroimage *52*, 1059-069.

Rudie, J.D., Shehzad, Z., Hernandez, L.M., Colich, N.L., Bookheimer, S.Y., Iacoboni, M., and Dapretto, M. (2012). Reduced Functional Integration and Segregation of Distributed Neural Systems Underlying Social and Emotional Information Processing in Autism Spectrum Disorders. Cereb Cortex *22*, 1025-037

Schipul, S.E., Keller, T.A., and Just, M.A. (2011). Inter-regional brain communication and its disturbance in autism. Front Syst Neurosci *5*, 10.

Schölvinck, M.L., Maier, A., Ye, F.Q., Duyn, J.H., and Leopold, D.A. (2010). Neural basis of global resting-state fMRI activity. Proc Natl Acad Sci U S A *107*, 10238-243.

Schultz, R.T. (2005). Developmental deficits in social perception in autism: the role of the amygdala and fusiform face area. Int J Dev Neurosci *23*, 125-141.

Schultz, R.T., Gauthier, I., Klin, A., Fulbright, R.K., Anderson, A.W., Volkmar, F., Skudlarski, P., Lacadie, C., Cohen, D.J., and Gore, J.C. (2000). Abnormal ventral temporal cortical activity during face discrimination among individuals with autism and Asperger syndrome. Arch Gen Psychiatry *57*, 331-340.

Schumann, C.M., Barnes, C.C., Lord, C., and Courchesne, E. (2009). Amygdala enlargement in toddlers with autism related to severity of social and communication impairments. Biol Psychiatry *66*, 942-49.

Scott-Van Zeeland, A.A., Abrahams, B.S., Alvarez-Retuerto, A.I., Sonnenblick, L.I., Rudie, J.D., Ghahremani, D., Mumford, J.A., Poldrack, R.A., Dapretto, M., et al. (2010). Altered Functional Connectivity in Frontal Lobe Circuits Is Associated with Variation in the Autism Risk Gene CNTNAP2. Sci Transl Med *2*, 56ra80.

Seeley, W.W., Menon, V., Schatzberg, A.F., Keller, J., Glover, G.H., Kenna, H., Reiss, A.L., and Greicius, M.D. (2007). Dissociable intrinsic connectivity networks for salience processing and executive control. J Neurosci *27*, 2349-356.

Shehzad, Z., Kelly, A.M., Reiss, P.T., Gee, D.G., Gotimer, K., Uddin, L.Q., Lee, S.H., Margulies, D.S., Roy, A.K., et al. (2009). The resting brain: unconstrained yet reliable. Cereb Cortex *19*, 2209-229.

Shih, P., Shen, M., Ottl, B., Keehn, B., Gaffrey, M.S., and Müller, R.A. (2010). Atypical network connectivity for imitation in autism spectrum disorder. Neuropsychologia *48*, 2931-39.

Shukla, D.K., Keehn, B., and Müller, R.A. (2010). Regional homogeneity of fMRI time series in autism spectrum disorders. Neurosci Lett *476*, 46-51.

Shukla, D.K., Keehn, B., and Müller, R.A. (2010). Tract-specific analyses of diffusion tensor imaging show widespread white matter compromise in autism spectrum disorder. J Child Psychol Psychiatry

Shukla, D.K., Keehn, B., Smylie, D.M., and Müller, R.A. (2011). Microstructural abnormalities of short-distance white matter fiber tracts in autism spectrum disorder. Neuropsychologia

Smith, S.M., and Nichols, T.E. (2009). Threshold-free cluster enhancement: addressing problems of smoothing, threshold dependence and localisation in cluster inference. Neuroimage *44*, 83-98.

Smith, S.M., Fox, P.T., Miller, K.L., Glahn, D.C., Fox, P.M., Mackay, C.E., Filippini, N., Watkins, K.E., Toro, R., et al. (2009). Correspondence of the brain's functional architecture during activation and rest. Proc Natl Acad Sci U S A *106*, 13040-45.

Smith, S.M., Jenkinson, M., Johansen-Berg, H., Rueckert, D., Nichols, T.E., Mackay, C.E., Watkins, K.E., Ciccarelli, O., Cader, M.Z., et al. (2006). Tract-based spatial statistics: voxelwise analysis of multi-subject diffusion data. Neuroimage *31*, 1487-1505.

Smith, S.M., Jenkinson, M., Woolrich, M.W., Beckmann, C.F., Behrens, T.E., Johansen-Berg, H., Bannister, P.R., De Luca, M., Drobnjak, I., et al. (2004). Advances in functional and structural MR image analysis and implementation as FSL. Neuroimage *23 Suppl 1*, S208-219.

Smith, S.M., Miller, K.L., Moeller, S., Xu, J., Auerbach, E.J., Woolrich, M.W., Beckmann, C.F., Jenkinson, M., Andersson, J., et al. (2012). Temporally-independent functional modes of spontaneous brain activity. Proc Natl Acad Sci U S A

Smith, S.M., Miller, K.L., Salimi-Khorshidi, G., Webster, M., Beckmann, C.F., Nichols, T.E., Ramsey, J.D., and Woolrich, M.W. (2010). Network modelling methods for FMRI. Neuroimage

Spencer, M.D., Holt, R.J., Chura, L.R., Suckling, J., Calder, A.J., Bullmore, E.T., and Baron-Cohen, S. (2011). A novel functional brain imaging endophenotype of autism: the neural response to facial expression of emotion. Translational Psychiatry *1*, e19.

Sporns, O. (2011). The non-random brain: efficiency, economy, and complex dynamics. Front Comput Neurosci *5*, 5.

State, M.W., and Levitt, P. (2011). The conundrums of understanding genetic risks for autism spectrum disorders. Nat Neurosci

Stein, J.L., Hua, X., Morra, J.H., Lee, S., Hibar, D.P., Ho, A.J., Leow, A.D., Toga, A.W., Sul, J.H., et al. (2010). Genome-wide analysis reveals novel genes influencing temporal lobe structure with relevance to neurodegeneration in Alzheimer's disease. Neuroimage

Stein, J.L., Wiedholz, L.M., Bassett, D.S., Weinberger, D.R., Zink, C.F., Mattay, V.S., and Meyer-Lindenberg, A. (2007). A validated network of effective amygdala connectivity. Neuroimage *36*, 736-745.

Stevens, M.C. (2009). The developmental cognitive neuroscience of functional connectivity. Brain Cogn *70*, 1-12.

Stevens, M.C., Pearlson, G.D., and Calhoun, V.D. (2009). Changes in the interaction of resting-state neural networks from adolescence to adulthood. Hum Brain Mapp *30*, 2356-366.

Sundaram, S.K., Kumar, A., Makki, M.I., Behen, M.E., Chugani, H.T., and Chugani, D.C. (2008). Diffusion tensor imaging of frontal lobe in autism spectrum disorder. Cereb Cortex *18*, 2659-665.

Supekar, K., Menon, V., Rubin, D., Musen, M., and Greicius, M.D. (2008). Network analysis of intrinsic functional brain connectivity in Alzheimer's disease. PLoS Comput Biol *4*, e1000100.

Supekar, K., Musen, M., and Menon, V. (2009). Development of large-scale functional brain networks in children. PLoS Biol *7*, e1000157.

Supekar, K., Uddin, L.Q., Prater, K., Amin, H., Greicius, M.D., and Menon, V. (2010). Development of functional and structural connectivity within the default mode network in young children. Neuroimage *52*, 290-301.

Thanseem, I., Nakamura, K., Miyachi, T., Toyota, T., Yamada, S., Tsujii, M., Tsuchiya, K.J., Anitha, A., Iwayama, Y., et al. (2010). Further evidence for the role of MET in autism susceptibility. Neurosci Res *68*, 137-141.

Tottenham, N., Tanaka, J.W., Leon, A.C., McCarry, T., Nurse, M., Hare, T.A., Marcus, D.J., Westerlund, A., Casey, B.J., and Nelson, C. (2009). The NimStim set of facial expressions: judgments from untrained research participants. Psychiatry Res *168*, 242-49.

Turner, K.C., Frost, L., Linsenbardt, D., McIlroy, J.R., and Müller, R.A. (2006). Atypically diffuse functional connectivity between caudate nuclei and cerebral cortex in autism. Behav Brain Funct *2*, 34.

Uddin, L.Q., and Menon, V. (2009). The anterior insula in autism: under-connected and under-examined. Neurosci Biobehav Rev *33*, 1198-1203.

Uddin, L.Q., Davies, M.S., Scott, A.A., Zaidel, E., Bookheimer, S.Y., Iacoboni, M., and Dapretto, M. (2008). Neural basis of self and other representation in autism: an FMRI study of self-face recognition. PLoS One *3*, e3526.

Uddin, L.Q., Iacoboni, M., Lange, C., and Keenan, J.P. (2007). The self and social cognition: the role of cortical midline structures and mirror neurons. Trends Cogn Sci *11*, 153-57.

Uddin, L.Q., Supekar, K., and Menon, V. (2010). Typical and atypical development of functional human brain networks: insights from resting-state FMRI. Front Syst Neurosci *4*, 21.

van den Heuvel, M.P., Stam, C.J., Boersma, M., and Hulshoff Pol, H.E. (2008). Small-world and scale-free organization of voxel-based resting-state functional connectivity in the human brain. Neuroimage *43*, 528-539.

Van Dijk, K.R., Hedden, T., Venkataraman, A., Evans, K.C., Lazar, S.W., and Buckner, R.L. (2010). Intrinsic functional connectivity as a tool for human connectomics: theory, properties, and optimization. J Neurophysiol *103*, 297-321.

Van Dijk, K.R., Sabuncu, M.R., and Buckner, R.L. (2012). The influence of head motion on intrinsic functional connectivity MRI. Neuroimage *59*, 431-38.

Vernes, S.C., Newbury, D.F., Abrahams, B.S., Winchester, L., Nicod, J., Groszer, M., Alarcón, M., Oliver, P.L., Davies, K.E., et al. (2008). A functional genetic link between distinct developmental language disorders. N Engl J Med *359*, 2337-345.

Villalobos, M.E., Mizuno, A., Dahl, B.C., Kemmotsu, N., and Müller, R.A. (2005). Reduced functional connectivity between V1 and inferior frontal cortex associated with visuomotor performance in autism. Neuroimage *25*, 916-925.

Vissers, M.E., Cohen, M.X., and Geurts, H.M. (2012). Brain connectivity and high functioning autism: a promising path of research that needs refined models, methodological convergence, and stronger behavioral links. Neurosci Biobehav Rev *36*, 604-625.

Voineagu, I., Wang, X., Johnston, P., Lowe, J.K., Tian, Y., Horvath, S., Mill, J., Cantor, R.M., Blencowe, B.J., and Geschwind, D.H. (2011). Transcriptomic analysis of autistic brain reveals convergent molecular pathology. Nature

Wager, T.D., and Nichols, T.E. (2003). Optimization of experimental design in fMRI: a general framework using a genetic algorithm. Neuroimage *18*, 293-309.

Wang, A.T., Dapretto, M., Hariri, A.R., Sigman, M., and Bookheimer, S.Y. (2004). Neural correlates of facial affect processing in children and adolescents with autism spectrum disorder. J Am Acad Child Adolesc Psychiatry *43*, 481-490.

Wang, A.T., Lee, S.S., Sigman, M., and Dapretto, M. (2007). Reading affect in the face and voice: neural correlates of interpreting communicative intent in children and adolescents with autism spectrum disorders. Arch Gen Psychiatry *64*, 698-708.

Wang, J., Wang, L., Zang, Y., Yang, H., Tang, H., Gong, Q., Chen, Z., Zhu, C., and He, Y. (2009). Parcellation-dependent small-world brain functional networks: a resting-state fMRI study. Hum Brain Mapp *30*, 1511-523.

Wang, J., Zuo, X., and He, Y. (2010). Graph-based network analysis of resting-state functional MRI. Front Syst Neurosci *4*, 16.

Watts, D.J., and Strogatz, S.H. (1998). Collective dynamics of 'small-world' networks. Nature *393*, 440-42.

Wechsler D. 1999. Wechsler Abbreviated Scale of Intelligence. San Antonio, Texas: Psychological Corporation.

Weissenbacher, A., Kasess, C., Gerstl, F., Lanzenberger, R., Moser, E., and Windischberger, C. (2009). Correlations and anticorrelations in resting-state functional connectivity MRI: a quantitative comparison of preprocessing strategies. Neuroimage *47*, 1408-416.

Welchew, D.E., Ashwin, C., Berkouk, K., Salvador, R., Suckling, J., Baron-Cohen, S., and Bullmore, E. (2005). Functional disconnectivity of the medial temporal lobe in Asperger's syndrome. Biol Psychiatry *57*, 991-98.

Weng, S.J., Wiggins, J.L., Peltier, S.J., Carrasco, M., Risi, S., Lord, C., and Monk, C.S. (2010). Alterations of resting state functional connectivity in the default network in adolescents with autism spectrum disorders. Brain Res *1313*, 202-214.

Whitfield-Gabrieli, S., Thermenos, H.W., Milanovic, S., Tsuang, M.T., Faraone, S.V., McCarley, R.W., Shenton, M.E., Green, A.I., Nieto-Castanon, A., et al. (2009). Hyperactivity and hyperconnectivity of the default network in schizophrenia and in first-degree relatives of persons with schizophrenia. Proc Natl Acad Sci U S A *106*, 1279-284.

Woolrich, M.W., Ripley, B.D., Brady, M., and Smith, S.M. (2001). Temporal autocorrelation in univariate linear modeling of FMRI data. Neuroimage *14*, 1370-386.

Zalesky, A., Fornito, A., Harding, I.H., Cocchi, L., Yücel, M., Pantelis, C., and Bullmore, E.T. (2010). Whole-brain anatomical networks: does the choice of nodes matter? Neuroimage *50*, 970-983.